HAPTIC INTERFACE FOR VIRTUAL REALITY BASED LAPAROSCOPIC SURGERY TRAINING ENVIRONMENT

THÈSE N° 1734 (1997)

PRÉSENTÉE AU DÉPARTEMENT DE MICROTECHNIQUE

ÉCOLE POLYTECHNIQUE FÉDÉRALE DE LAUSANNE

POUR L'OBTENTION DU GRADE DE DOCTEUR ÈS SCIENCES TECHNIQUES

PAR

Roger BAUMANN

Dipl. El.-Ing. ETH
Master of Science in Computer and Systems Engineering,
Rensselaer Polytechnic Institute, USA
originaire de Pratteln (BL)

acceptée sur proposition du jury:

Prof. R. Clavel, directeur de thèse
Prof. M. Bergamasco, corapporteur
Prof. H. Bleuler, corapporteur
Dr J.-F. Cuttat, corapporteur
Prof. G. Hirzinger, corapporteur

Lausanne, EPFL
1997

Preface

This thesis describes research performed during my activity as research assistant between 1994 and 1997 at the Institut de Microtechnique of the Ecole Polytechnique Fédérale de Lausanne (EPFL). Many people have contributed to this work; it is a great pleasure to thank them here.

In particular, I wish to thank my advisor Professor Reymond Clavel for his confidence and support, for many helpful suggestions and ideas, and the conscientious correction of the manuscript. Moreover, I would like to thank the members of my doctoral committee, Professor Massimo Bergamasco of the Scuola Superiore Santa Anna in Pisa, Italy, Professor Gerd Hirzinger of the Deutsche Forschungsanstalt für Luft- und Raumfahrt (DLR) at Oberpfaffenhofen, Germany, and Professor Hannes Bleuler of the Institut de Microtechnique for accepting the co-examination and their interest in my work, as well as Dr. Jean-François Cuttat from the Centre Hospitalier Universitaire Vaudois (CHUV) for his valuable advise in the medical domain.

I wish to acknowledge also Dominique Glauser, the leader of this project until January of this year, for his fruitful critique and many suggestions as well as his logistical support. Thanks also to Charles Baur, the group leader of the graphics team for his commitment to this project.

The most heartfelt thanks I owe Willy Maeder, our *maître de construction*, not only for the innumerable hours he spent on the mechanical construction of the *Panto-Scope*, but also for the time and effort he devoted to many valuable discussions, his continuous technical support, and friendship. Likewise I wish to acknowledge Marc Epitaux for his help and efforts on the actuation and transmission of the translational degree of freedom, and Didier Guzzoni for his fruitful collaboration in bringing the haptic feedback system together with the graphical simulation environment.

Abstract

Force reflecting manual man-machine interfaces can provide the operator with useful kinesthetic information in teleoperation tasks and virtual reality applications. They allow the user to reach into worlds otherwise not haptically perceivable, or to acquire understanding of natural phenomena involving forces and torques for which visual representations are inappropriate. Education, training, tele- and micro-manipulation, scientific visualization, and entertainment are only a few potential application areas where force reflecting devices may demonstrate their efficiency in the near future.

This thesis contributes to the development of a novel force reflecting interface for minimally invasive surgery simulation. The envisioned training environment aims at replacing and extending today's limited and unsatisfactory surgery training possibilities by combining interactive graphical organ simulation and computer generated haptic feedback. Force reflecting mechanisms shall be installed inside an artificial patient in order to exert forces and torques on the surgical instruments manipulated by the surgeon, thus simulating force feedback from the encountered virtual organic tissues.

Based on an investigation of minimally invasive surgical procedures the most stringent requirements for the force reflecting system have been determined. They can be traced back to two fundamental demands expressed by the surgeons: realistic force reflection and realistic visual appearance. Realistic force reflection implies a mechanical setup which allows for sufficient displacement ranges and output force capability in four degrees of freedom. In order to achieve realistic visual appearance, all mechanisms providing force feedback need to be completely hidden below the skin of the artificial patient. These specifications, together with the constraints related to the capabilities of the human sensorimotor system, have served as guidelines for the design of a novel hybrid parallel-serial spherical remote-center-of-motion force reflecting

Résumé

Les interfaces homme-machine à retour d'efforts peuvent procurer à l'opérateur des informations utiles dans des tâches de téléopération ou des applications de réalité virtuelle. Elles permettent à l'utilisateur de s'immerger dans des mondes qui ne sont normalement pas perceptibles avec le sens tactile, ou d'acquérir une compréhension des phénomènes naturels impliquant des forces et des moments dont la représentation visuelle serait non-appropriée. L'éducation, l'entraînement, la télé- et la micro-manipulation, la visualisation scientifique ainsi que les divertissements ne sont que quelques applications potentielles où des systèmes à retour de forces pourraient prouver leur efficacité dans le futur proche.

Cette thèse contribue au développement d'une nouvelle interface à retour de forces pour la simulation de la chirurgie mini-invasive. L'environnement d'entraînement envisagé a pour but de remplacer et étendre les possibilités d'entraînement de chirurgie actuelles limitées et insuffisantes, par la combinaison d'une simulation graphique interactive d'organes et d'un retour de forces généré par ordinateur. Des mécanismes à retour d'efforts seront installés dans un patient artificiel afin d'exercer des forces et des moments sur les instruments chirurgicaux manipulés par les chirurgiens, simulant ainsi les interactions entre les outils chirurgicaux et les organes.

En s'appuyant sur une analyse des procédures mini-invasives, les demandes les plus importantes pour le système à retour d'efforts ont été déterminées. Parmi celles-ci on peut distinguer deux requêtes fondamentales exprimées par les chirurgiens: le réalisme du retour d'efforts et le réalisme de l'apparence visuelle du patient artificiel. Un retour de forces réaliste implique une construction mécanique avec un volume de travail suffisant, capable d'exercer des forces assez grandes en quatre degrés de liberté. Afin d'atteindre une apparence visuelle réaliste, tous les mécanismes à retour de forces doi-

Zusammenfassung

Kraftrückgekoppelte Mensch-Maschine Schnittstellen können dem Bediener im Bereich der Teleoperation und virtuellen Realität nützliche kinesthetische Informationen liefern. Sie erlauben dem Anwender in Welten einzutauchen, die üblicherweise über den Tastsinn nicht wahrnehmbar sind, und fördern das Verständnis natürlicher Phänomene, welche visuell kaum dargestellt werden können. Ausbildung, Training, Tele- und Mikromanipulation, wissenschaftliche Darstellungen und Unterhaltung sind nur einige wenige potentielle Anwendungsgebiete in denen kraftrückgekoppelte Systeme in naher Zukunft zum Einsatz kommen könnten.

Die vorliegende Arbeit leistet einen Beitrag zur Entwicklung einer neuen kraftrückgekoppelten Benutzeroberfläche für die Simulation von minimal-invasiven chirurgischen Eingriffen. Die angestrebte Trainingsumgebung soll durch den kombinierten Einsatz interaktiver graphischer Organdarstellungen und computergeneriertem Kraftfeedback die heute vorhandenen, weitgehend unzureichenden und unbefriedigenden Trainingsmöglichkeiten ersetzen und erweitern. Kraftfeedback-Manipulatoren sollen in einem künstlichen Patienten installiert werden, um Kräfte und Momente auf die vom Chirurgen manipulierten Instrumente auszuüben, und damit die Wechselwirkung zwischen den Organen und den Instrumenten zu simulieren.

Die wichtigsten Anforderungen an das Kraftrückkopplungssystem wurden an Hand eines Studiums von minimal-invasiven chirurgischen Eingriffen ermittelt. Dabei lassen sich zwei grundsätzliche Forderungen der Chirurgen unterscheiden: die realistische Wiedergabe von Kräften und das realistische Aussehen des künstlichen Patienten. Realistische Kraftrückkopplung bedingt einen mechanischen Aufbau, der über einen hinreichend großen Arbeitsbereich verfügt und genügend hohe Kräfte in vier Freiheitsgraden ausüben kann. Um ein realistisches Erscheinungsbild des Simulators zu gewähr-

Contents

Terminology

The domains of virtual reality and virtual tactile and force feedback technology are relatively new. Even within the technical community, many terms relating to these fields are often used interchangeably and may lead to confusion. This section is intended as a brief glossary of terms relevant to the fields of virtual reality, virtual haptic feedback, and human sensory perception.

Virtual reality:

> Computer generated interactive environment presented to a user such that he feels *immersed* or *present* within the simulation [Burdea and Coiffet, 1994]. The aim of virtual reality is to generate realistic three-dimensional visual, audio, and tactile stimuli to the operator. Synonymous to *artificial reality*, *virtual environment*, and *virtual world*.

Presence:

> A state of accepting the ambient sensory information as the physical surroundings. *Virtual presence* is experienced by a person when sensory information generated only by a computer and associated display devices compels a feeling of being present in an environment other than the one the person is actually in [Sheridan, 1992a].

Proprioception:

> Sense of limb dynamics and body posture mediated by muscle receptors sensing muscle contractions and tensions. Proprioception describes sensation that is caused by stimuli arising within the organism, while *exteroception* pertains to sensation that results from external inputs from the environment [Webster, 1996].

Notation

In the derivation of the geometric and kinematic models and the discussion of the control algorithms we will make use of scalars, vectors, matrices, and coordinate frames. The notation used in this thesis follows common practice and is largely based on the textbook by Paul [1981].

Vectors are denoted by lower case bold face characters, matrices are denoted by upper case bold face characters, and scalars by italic characters. Coordinate frames are denoted by upper case script characters, and functions are written in normal case font. For example:

scalars	q, η, ρ, A
vectors	$\mathbf{p}$, $\mathbf{n}$, $\mathbf{f}$
matrices	$\mathbf{T}$, $\mathbf{R}$
coordinate frames	$\mathcal{O}$, $\mathcal{P}$, $\mathcal{T}$
functions	sin, cos, Rot, Trans

Leading superscripts describe the defining coordinate frame of a point vector or transformation matrix. For example, ${}^{\mathcal{A}}\mathbf{p}$ represents a position vector in coordinate frame $\mathcal{A}$, and ${}^{\mathcal{A}}\mathbf{R}_{\mathcal{B}}$ is a rotation matrix comprised of the unit vectors of frame $\mathcal{B}$ expressed in frame $\mathcal{A}$. Trailing superscripts indicate the transpose or inverse of a matrix. For example, $\mathbf{T}^{\mathrm{T}}$ is the transpose of $\mathbf{T}$, and $\mathbf{T}^{-1}$ is the inverse of $\mathbf{T}$.

Subscripts refer to individual components of coordinate frames, vectors, and matrices, or indicate which coordinate system a vector, matrix, or variable is belonging to. For example, the vector $\mathbf{p}$ has the components p_x, p_y, and p_z, the vector ${}^{\mathcal{A}}\mathbf{p}_{\mathcal{B}org}$ denotes the origin of the frame $\mathcal{B}$ expressed in coordinates of frame $\mathcal{A}$, and $\mathbf{x}_{\mathcal{A}}$ is the base vector in x-direction of the frame $\mathcal{A}$. Note that sub- and superscripts may be omitted for base vectors represented in their defining frame, thus ${}^{\mathcal{A}}\mathbf{x}_{\mathcal{A}} = \mathbf{x}$.

1.2 Motivation

The evolution of minimally invasive surgery within the last ten years has profoundly changed the surgical approach to a wide variety of diseases. Following the principle of minimal intervention, laparoscopic surgery requires only three to five small incisions for the insertion of endoscopic surgical instruments and an endoscopic miniature camera into the abdominal cavity. The benefits of minimally invasive surgery are manifold. In comparison with traditional surgery, the patient's discomfort and surgical trauma as well as potential complications occurring after surgery are drastically reduced. Moreover, the time a patient has to stay in hospital and the rehabilitation period are shortened. In this way, both direct health-care costs and indirect costs in lost worker productivity can be lowered.

The principle of minimal access to the area of intervention, however, leads to a number of disadvantages for the surgeon. The direct manual operation at free visible organs is no longer possible. Much of the surgeon's manipulative freedom, usually available in open surgery, is lost, and his sense of touch and dexterity are severely reduced due to the use of long and rigid instruments. Moreover, today's laparoscopic surgery is usually performed under monoscopic conditions. Thus, the notion of depth is lost in executing the operation while looking at the endoscopic image displayed on a video monitor.

As a matter of fact, minimally invasive surgery requires the surgeons to be familiar with a new form of hand-eye coordination. These skills are not intuitive, and the optimization of the surgical procedures requires extensive training and experimentation before they can actually be applied in real operations. Today's training possibilities, however, are not satisfactory. Training on existing devices or on cadavers and anesthetized animals either lacks sufficient realism, or is too expensive and overly restricted in number. These drawbacks call for alternative means of laparoscopic surgery training. The emergence of powerful, affordable computers, combined with scientific advances in mathematical modeling and simulation techniques as well as robotics, offers training possibilities that let the surgeon develop the necessary skills and practice operations without limiting the number of repetitions necessary to master the procedure. A learning tool including haptic feedback as well as visual feedback would allow novice surgeons to train gestures and optimize surgical procedures in a realistic, safe, and efficient way, without any danger for the patient and ethical or political limitations.

to achieve real-time interactivity, linear elasticity models of the organic tissues are used which allow for partial pre-computation of deformations. Texture mapping and force reflection have not been integrated yet.

A laparoscopic surgery training system including force reflection is being developed by Asano et al. [1997] in Japan. The system integrates two six-degree-of-freedom force reflecting manipulators (based on Iwata's Haptic Master, see chapter 2) providing force feedback on both hands. The organ force models are based on viscous-elastic deformable surfaces. For a realistic graphical simulation the virtual organs are texture mapped with real images.

In Switzerland, the Eidgenössische Technische Hochschule (ETH) in Zurich is addressing the simulation of gynecological laparoscopy [Székely, 1996]. The project focuses on the photorealistic rendering of patient anatomy and the volumetric elasto-mechanical modeling of organs providing realistic real-time deformations. The range of applications shall be limited to diagnostic procedures, thus avoiding the need for the simulation of tissue cutting and bleeding. For force reflection, the force feedback system discussed in this thesis shall be employed.

First commercial laparoscopic simulators have been developed by Ixion, Inc. [Hon, 1996]. The PreCeptor™ laparoscopic surgery simulator, realized for Ethicon Endo Surgery, Inc., provides three-dimensional organ representations with real-image texturing and basic haptic feedback. In a more recent development, Ixion has attacked also the simulation of the endoscopic exploration of the gastro-intestinal tract.

The large number of articles related to the subject of surgery simulation shows the tremendous interest in this topic at various technical and medical research institutes all over the world. While some of the aforementioned systems have convincingly demonstrated the concept of virtual reality based surgery training, most existing trainers are lacking sufficient realism, and are still far away from truly immersive simulation. Most research and development into virtual reality technology focuses on visual aspects such as photorealistic rendering and real-time deformations, thereby largely ignoring the physical aspects of interaction. The simulation of tactile and force information is addressed only by a few research groups. The majority of the current surgery simulation systems that include force reflection make use of the commercially available force feedback devices from Immersion, Inc. [1995] and SensAble Devices, Inc. [1996] (see chapter 2).

1.5 Contributions

The primary contribution of the research described in this thesis is the design and realization of a force reflecting manual man-machine interface for virtual reality based minimally-invasive surgery simulation, and its connection to the respective graphical simulation environment.

In particular, this includes:

1. Determination of the *specific requirements* applicable to the development of a force reflecting manipulator system for laparoscopic surgery simulation. Specifications are formulated with respect to the manipulator's mechanical design as well as the related control aspects.

2. Design of a *novel four-degree-of-freedom, hybrid parallel-serial, spherical, remote-center-of-motion mechanical structure*, named *PantoScope*, which is employed as force feedback manipulator. The direct and inverse geometric models, instantaneous kinematics and statics, special configurations and usable workspace are derived.

3. Integration and implementation of an *implicit force control strategy* for the control of the four-degree-of-freedom force reflecting manual man-machine interface including gravity and friction compensation for wide dynamic range. A *supervisory control scheme* for the connection of the haptic interface to the visual simulation environment and the organ impedance models is proposed.

4. Implementation of several *dynamic force models*, such as springs, dampers, and virtual walls, which allowed the *experimental verification and evaluation* of the proposed mechanical design and control concept.

5. Realization of a *multi-processor control system* for the concurrent control of three four-degree-of-freedom force reflecting manipulators.

In the course of this work a *four-degree-of-freedom prototype system* has been realized, and coupled to the graphical simulation environment concurrently developed at the Institut de Microtechnique. In this way, the validity of the proposed approach to laparoscopic surgery simulation could be demonstrated[1].

---

[1]This thesis deals exclusively with the development of the force reflecting manipulator system and an appropriate control scheme. The development of realistic *organic tissue models* was not part of this effort.

virtual hard surfaces and organic tissue will be evaluated with respect to the realism of their perception.

Chapter 8, finally, summarizes the contributions of this thesis and recommends future directions.

In recent years, haptic feedback systems have gained increasing importance for the further development of virtual reality technology. In 1965 already, Ivan Sutherland, a well-known pioneer of computer graphics, envisioned an 'ultimate display' to a virtual world including haptic feedback [Sutherland, 1965]. Since then, the interest in force and tactile feedback for virtual reality applications has lead to the development of numerous haptic devices, ranging from tactile displays to force reflecting joysticks and sophisticated force feedback arm and hand exoskeletons.

This chapter is intended to provide an overview on the current state of the art on haptic feedback technology for virtual reality environments. The most important force reflecting systems will be described together with key parameters such as available workspace, maximum output forces and torques, position resolution, system bandwidth, and inherent friction. For a more detailed description of today's research efforts on force reflection in various institutions all over the world the reader is referred to [Burdea, 1996].

2.2 Master Arms

Master arms have originally been developed for bilateral master-slave teleoperation systems, where the user controls a mechanical master which transmits the position and force commands to a remote slave for interaction with a remote or hazardous environment. Some of these devices have later been adapted for use in virtual reality applications. Teleoperation master arms are often heavy and bulky and are therefore generally less suitable for use as haptic interfaces to virtual environments.

One of the best known virtual reality applications using a teleoperation master arm is the GROPE project that has been pursued for more than 20 years at the University of North Carolina at Chapel Hill. Stimulated by Ivan Sutherland's vision of an ideal virtual reality interface, Frederick Brooks, Jr. and his colleagues envisioned already in 1967 the development of a haptic display for the simulation of molecular docking forces [Brooks et al., 1990]. Insufficient computing power, however, prevented them for many years to reach this goal. In 1988 finally, Ouh-young et al. [1988] presented **GROPE-III** which was comprised of a six-degree-of-freedom Argonne E-3 Remote Manipulator [Goertz, 1964] combined with a large screen visual display for the graphical representation (figure 2.1). However, the inherent friction, which accounted for 20% of peak actuation force, and the high inertia of the Argonne Master Arm severely limited force resolution and bandwidth.

decoupled arm inertia, low friction, and high structural stiffness. Brushless direct drive dc motors were chosen as actuators. The force feedback loop is closed at 1 kHz [Adachi et al., 1995].

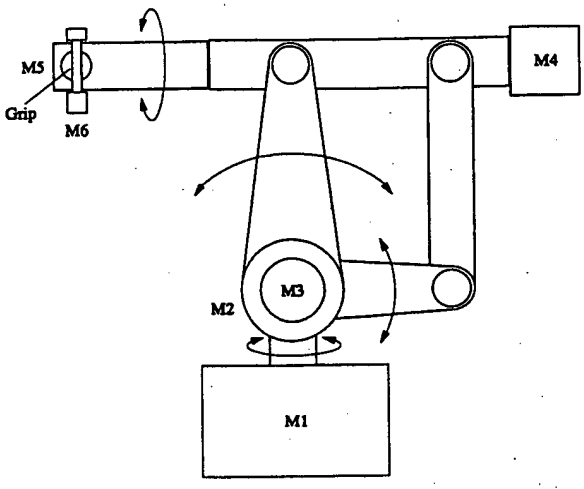

Figure 2.2: Structure of SPICE (adapted from [Adachi et al., 1995]).

At the National Institute of Bioscience and Human Technology in Japan, Yokoi et al. [1994] developed a **Cartesian manipulator** for force reflection. This device is comprised of three orthogonal Cartesian axes and three orthogonal revolute axes providing a total of six degrees of freedom. In contrast to the master arms discussed previously, the Cartesian manipulator is equipped with a force-torque sensor in the wrist for admittance control. The force feedback electro-mechanical bandwidth is limited to 4 Hz. Resonance problems leading to vibrations have been reported.

A more recent design is the **Five-Bar-Linkage Force Reflecting Interface** developed at the University of Waterloo, Canada [Ching and Wang, 1997]. This direct drive manipulator consists of a gravity balanced planar linkage structure with three degrees of freedom. The force control loop is executed at 200 Hz.

2.3 Joysticks

Joysticks are the most prevalent form of haptic interfaces. Joysticks have been used for many years both as computer interfaces and input devices for entertainment applications. It is therefore not surprising that numerous joystick-based systems incorporating force reflection have been realized in recent years. Most of these systems are prototypes for research purposes, but also a few commercial products have evolved.

Another simple two-degree-of-freedom force reflecting joystick is the **EXOS Powerstick™** developed by EXOS, Inc. This commercial device provides a sustained maximum force of 2.2N in a 60° conical workspace. Friction is approximately 0.18N, corresponding to 8% of the maximum force output [Burdea, 1996].

At **Queen's University**, Kingston, Canada, Ellis et al. [1993] have realized a three-degree-of-freedom Cartesian joystick with low inertia and damping, high structural stiffness, and high dynamic range. Their device is comprised of a parallel x-y Cartesian positioning mechanism onto which a rotary stage is mounted. It has a workspace of 15×15 cm. Low inertia brushed dc motors are used as actuators, while Teflon-coated steel cables ensure minimal friction transmission. Maximum open-loop force output of the x-y-stage is 56N with friction accounting for about 3%. A six-axes force-torque sensor is used to measure interaction forces between the mechanism and the human operator which allows to compensate for unmodeled dynamics. With the force control loop running at 1200Hz, the perceived static friction could be reduced by approximately 75%. The first structural resonance frequency is about 90Hz.

Commercial force feedback joysticks are also developed by Immersion, Inc. [1995]. The Impulse Engine™ product line features a variety of haptic interfaces with one to three degrees of freedom force feedback for medical simulation, entertainment, and education. The **Laparoscopic Impulse Engine™**, depicted in figure 2.4, aims at the simulation of laparoscopic surgical procedures and is therefore probably more relevant to this thesis than any other system discussed so far. The Laparoscopic Impulse

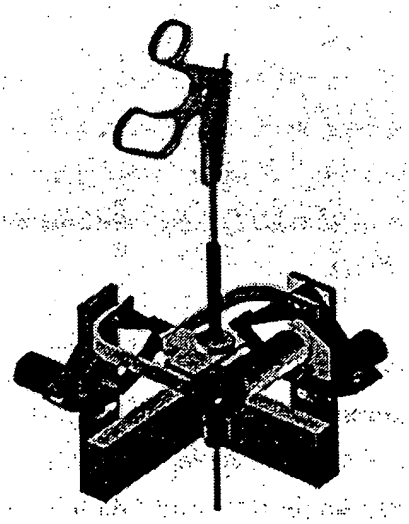

Figure 2.4: Laparoscopic Impulse Engine [Immersion, Inc., 1995].

A six-degree-of-freedom haptic interface has been developed by Nissho Electronics, Corporation in Japan [Nissho, 1995] based on an earlier prototype by Iwata at the University of Tsukuba [Iwata, 1990]. The **Haptic Master™**, shown in figure 2.6, consists of a triangular motion platform which is connected to the base by three sets of pantograph link mechanisms. Each pantograph is driven by three dc motors in a redundant actuation scheme, providing for a maximum static force at the handle of 69N. The motion platform has a 40cm diameter spherical workspace. The simulation runs at a force control bandwidth of 50Hz.

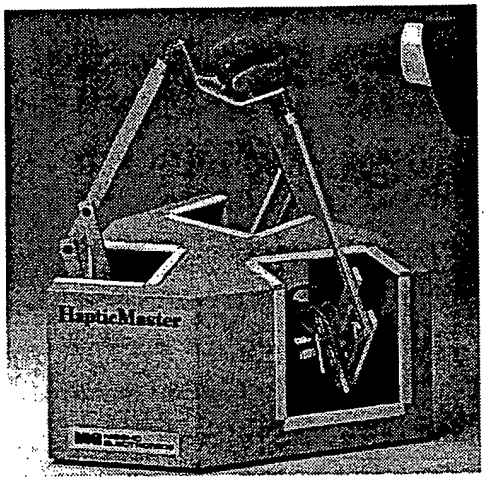

Figure 2.6: Nissho Haptic Master [VR News, 1995].

The **PER-Force** hand controller produced by Cybernet Systems, Inc. [1995] is another commercial haptic interface (figure 2.7). This six-degree-of-freedom force reflecting joystick consists of a serial x-y-z Cartesian platform and three orthogonal revolute axes. The three linear axes each have a motion range of 10 cm, both the yaw and pitch rotational axes provide a range of 90°, and the roll axis allows motion within an angle of 180°. The PER-Force joystick is actuated by six brushless dc motors that produce up to 53 N of translational force and 4.5Nm peak torque. Friction is approximately 0.5N.

A completely friction free mechanism has been realized at the University of British Columbia [Salcudean and Vlaar, 1994]. This magnetically levitated six-degree-of-freedom device, known as the **UBC Maglev Joystick**, has previously been used as master manipulator and slave end-effector in a course-fine motion control teleoperation system [Salcudean et al., 1995]. The device has six Lorentz actuators, arranged in a star configuration with 120° symmetry. Each actuator consists of a flat coil immersed in the

pantograph arm with a fingertip thimble-gimbal support (figure 2.8). The PHANToM provides six degrees of freedom, of which only the three translations are actuated. The gimbal orientation is passive and allows the user's finger tip to assume any comfortable orientation. The workspace of the PHANToM is $8 \times 17 \times 25$ cm, in which a position resolution of 0.07mm is achieved. The maximum continuous output force of 1.5N is delivered by three brushed dc motors. Peak output force capability is 10N, backdrive friction is less than 0.1N. Transmissions are realized through cables and pulleys with an elegant reduction mechanism that meshes two motor capstans with a single cable. The PHANToM is now sold by SensAble Devices, Inc. [SensAble Devices, 1996]. SensAble Devices considers 1kHz the minimum possible update frequency in order to achieve smooth force simulation. No data on the mechanical bandwidth is available.

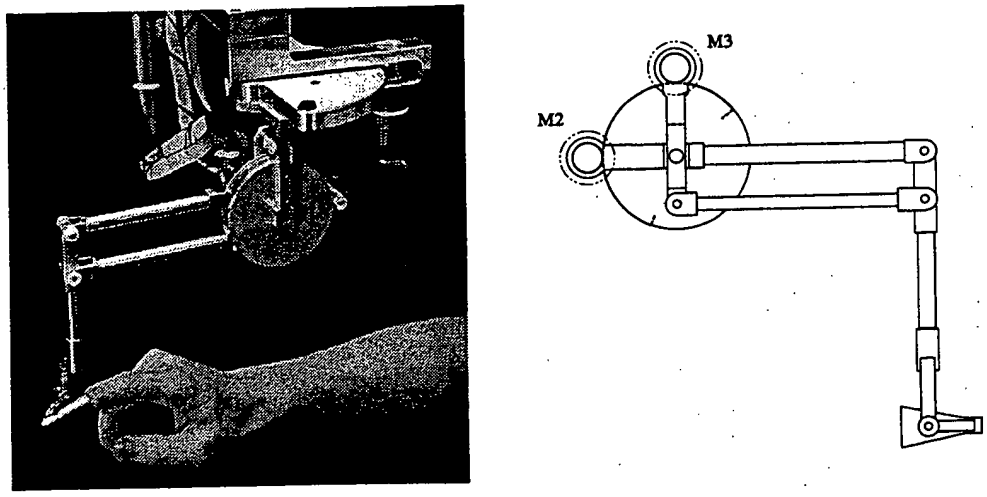

Figure 2.8: (a) PHANToM haptic interface [SensAble Devices, Inc., 1996], (b) cable transmission principle (adapted from [Massie and Salisbury, 1994]).

A six-degree-of-freedom pen-based force display has been developed at the **University of Tsukuba** [Iwata, 1993]. The system is based on two three-degree-of-freedom pantograph linkage manipulators which are connected to both ends of a pen-shaped handgrip (figure 2.9b). The resulting compact and lightweight structure, depicted in figure 2.9a, provides for a spherical workspace of 44cm diameter. A maximum force output of 5N and a position accuracy of 2mm have been reported. The force display has been integrated with a Silicon Graphics Indigo workstation. The sampling rate of the force feedback device and graphics display is 10Hz.

4.8Nm, respectively. However, the large Coulomb friction in the actuators masks small forces and impedes precise motions. In addition, jerky motion due to the low force update rate of 10Hz has been reported.

At the Tokyo Institute of Technology, Ishii and Sato developed the **SPIDAR** system (SPace Interface Device for Artificial Reality) [Ishii and Sato, 1993]. Similar to the Touchy-Feely, the initial prototype of SPIDAR had four strings attached to a thimble worn on the user's index finger (figure 2.10a). Strings passed through fulcrums at the vertices of a cubic support structure and rotary encoders on the motor shafts measured cable length with a resolution of 0.5mm. Subsequently, the SPIDAR system was modified to allow feedback on both the thumb and the index finger. The resulting system, depicted in figure 2.10b, has eight strings, and the tension in each string can be controlled by an electrical motor exerting forces of up to 4N. Occasional interference among the strings has been reported, but is not considered a significant limitation. The SPIDAR II system has a spherical workspace of 30cm diameter and is integrated with a graphic workstation. The refresh rate of force generation has been reported to be 100Hz; the graphics update rate is 10Hz [Ishii and Sato, 1994a].

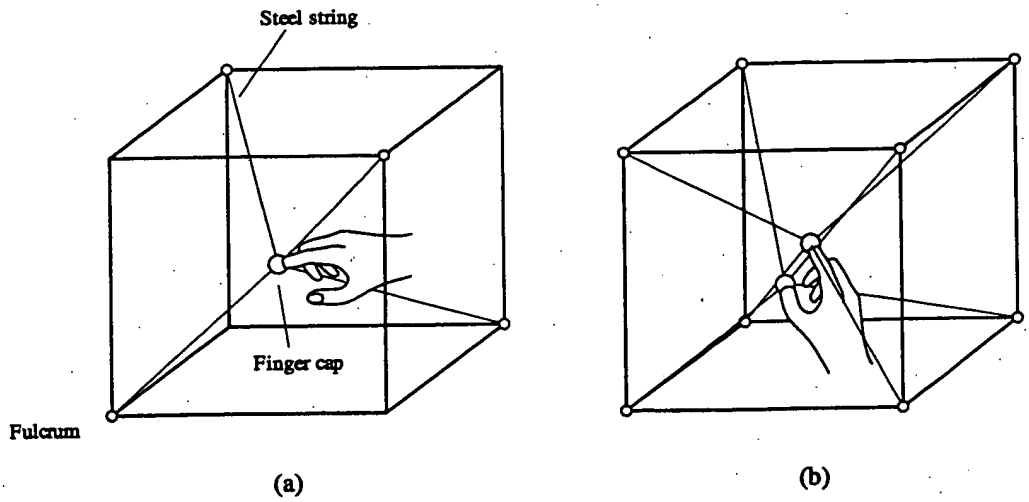

Figure 2.10: (a) SPIDAR-I; (b) SPIDAR-II (adapted from [Ishii and Sato, 1994b]).

Other string based force feedback devices that use the same basic principle as the SPIDAR system have been proposed by Kawamura et al. [1995] and Morizono et al. [1997] for virtual sports training.

Figure 2.12: SARCOS non-portable force feedback exoskeleton [Burdea, 1996].

Hand exoskeletons are haptic interfaces that measure hand movements and apply forces to the user's individual fingers and wrist. As with arm exoskeletons, portable and non-portable systems are distinguished. Portable hand masters are grounded on the user's forearm or palm. Non-portable systems include desktop grounded or otherwise supported exoskeletons.

In order to reduce weight, many portable hand exoskeletons rely on remote actuation via strings and pulleys or transmission sheaths. The actuators are placed remotely from the hand, either on the forearm or on the user's back. Examples are the **LRP Hand Master** (figure 2.13) designed at the Laboratoire de Robotique de Paris, France [LRP, 1997], and the **ARTS Hand Force Feedback System** developed at the Scuola Superiore Santa Anna in Italy [Bergamasco, 1992, 1997].

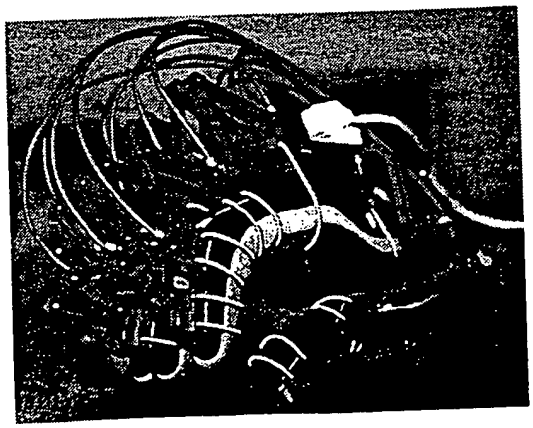

Figure 2.13: LRP Hand Exoskeleton [LRP, 1997].

Figure 2.15: PemRAM motion platform [Burdea, 1996].

2.8 Conclusions

This chapter has reviewed various haptic interface devices. In recent years, a large number of force feedback systems ranging from master arms and desktop force reflecting interfaces such as joysticks, pen- and string-based systems, to complete arm and hand exoskeletons as well as personal motion platforms have been developed for a wide variety of applications. Table 2.1 summarizes the most important characteristics of the discussed devices, and may serve as reference for the haptic interface system described in this thesis.

In our discussion we have focused on kinesthetic interfaces. Aside from hand masters with *force feedback*, a number of *tactile feedback* systems have been developed. Tactile feedback stimulates the cutaneous receptors in the skin of the user and provides information on the surface texture and geometry of virtual objects. As opposed to force reflection, tactile feedback does not address the operator's muscles and can therefore not prevent him from 'grasping through' an object. For a detailed review of tactile feedback systems the reader is referred to [Shimoga, 1993b].

ticular attention shall be paid to the laparoscopic resection of the gallbladder which has been chosen as benchmark for our prototype surgery simulation system.

3.2.1 Laparoscopic Surgery

Laparoscopy is the minimally invasive intervention at the abdomen and is always performed following the same basic procedure. In accordance with the principle of minimal intervention, the incisions are limited to three to five small holes in the abdominal wall for the insertion of tube-like devices, called *trocars*. These trocars serve as guideways for the subsequent introduction of the laparoscopic camera and instruments. As the surgeon has no direct vision of the surgical site, the laparoscopic microcamera is indispensable for the visualization of the operation taking place inside the abdominal cavity. The image of the laparoscopic camera is usually displayed on a video monitor. Figure 3.1 shows a typical configuration for a minimally invasive surgical intervention.

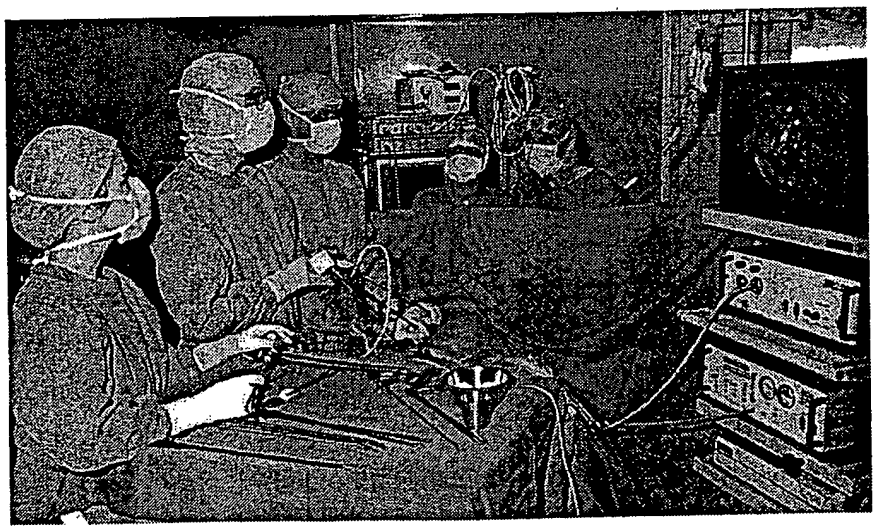

Figure 3.1: Minimally invasive surgical intervention [Wolf, 1994].

Every laparoscopic intervention begins with the induction of the *pneumoperitoneum*. For this purpose, a Veress needle is inserted at the umbilicus and connected to an insufflation unit. The intra-abdominal insufflation of gas raises the abdominal wall and increases the volume of the intraperitoneal space. The needle is then retracted and the first trocar is inserted (figure 3.2a). The insertion is done blindly, and care has to be taken not to injure any underlying organs. The introduction of the trocar is facilitated by the trocar shaft which fits precisely into the sleeve (figure 3.2b). After the perforation of

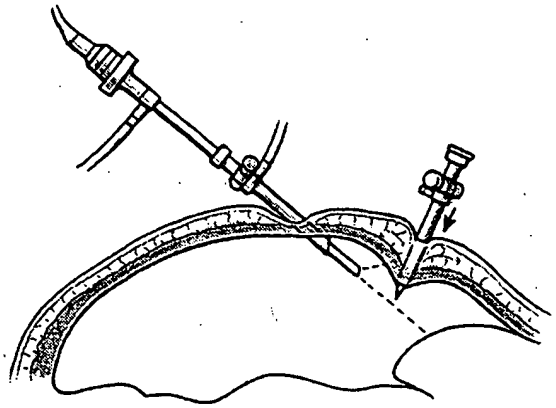

Figure 3.4: Insertion of additional trocars [Klaiber et al., 1993].

The additional trocars serve for the insertion of the laparoscopic instruments, such as grasping forceps, scissors, hook-electrodes, clip applicators, or suction-irrigation tubes which allow to lift and move organs, to dissect one organ from another, to cut tissues, to irrigate the intervention site, or to remove blood and secretions from the abdominal cavity. Figure 3.5 depicts a grasping forceps.

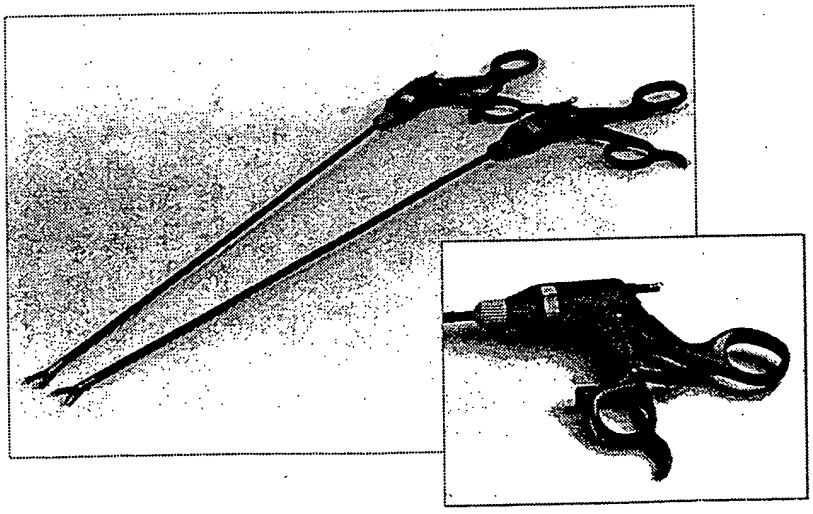

Figure 3.5: Grasping forceps.

Due to the fixed entrance points in the abdominal wall, the range of motion of the camera and tools is always restricted to the pivoting about the entrance points and the translational and rotational movement with respect to the trocars. Usually there is one instrument used with each trocar, and instruments are exchanged only rarely in order to minimize the escape of insufflation gas and safe time.

fourth trocar is introduced to the upper left of the umbilicus (site 4) and has a diameter of 10mm for the passage of the working instruments, such as the hook electrode, scissors, and the clip applicator. In the ideal case, the portals form a semicircle around the gallbladder. Yet, the exact location varies slightly from patient to patient. In any case, when placing the trocars, care has to be taken to allow sufficient distance between the sites of insertion to ensure that the instruments do not interfere with each other. The sites must also be far enough away from the gallbladder to allow for an adequate radius of action.

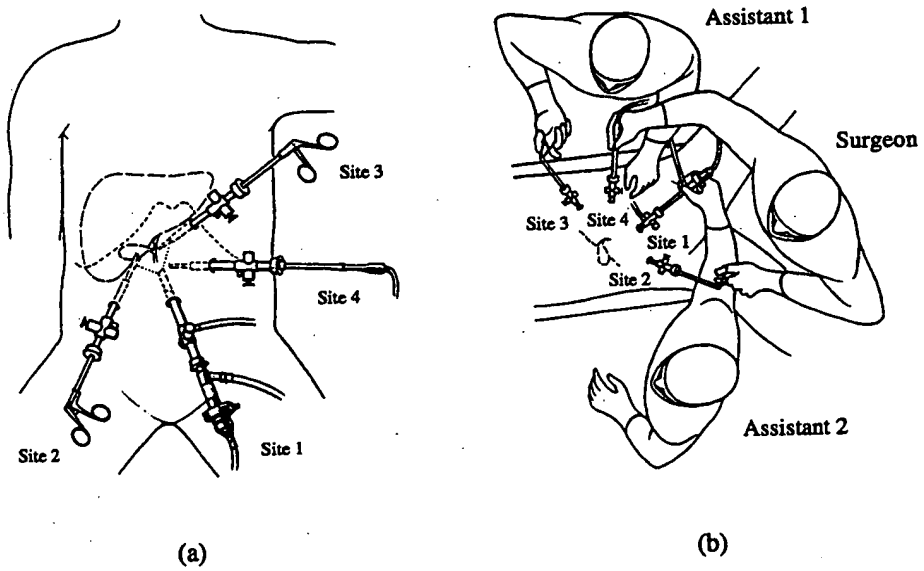

Figure 3.7: (a) Puncture sites and (b) operating technique for cholecystectomy (European method) [Klaiber et al., 1993].

The surgeon grasps the gallbladder by means of the grasping forceps using his left hand (figure 3.7b, site 2), and manipulates the working instruments with his right hand (site 4). The first assistant, standing to the left of the patient, operates the suction-irrigation tube (site 3) with his right hand. With the left hand he manipulates the trocar sleeve valves. A second assistant controls the laparoscopic camera (site 1), and at times holds the grasping forceps (site 2) when the surgeon requires his left hand for other maneuvers.

For a more detailed discussion of laparoscopic cholecystectomy and other minimally invasive surgical procedures, the reader is referred to two very comprehensive books by Klaiber et al. [1993] and Cuschieri et al. [1992].

Thus, there are strong reasons for developing surgery trainers which allow for more realistic training than can be performed with today's phantoms. In this context, the technological advances in virtual reality based simulation techniques offer a tremendous opportunity to the efficient and safe education and training of laparoscopic procedures without any danger for the patient and/or ethical or political limitations.

3.3 Simulator Requirements

In collaboration with the surgical department of the Centre Hospitalier Universitaire Vaudois (University Hospital of Lausanne), the most stringent requirements associated with the laparoscopic surgery simulator, and in particular the force feedback system, have been determined from a medical as well as a technical point of view [Baumann and Cuttat, 1995].

3.3.1 A Surgeon's Point of View

- The surgery trainer needs to be as realistic as possible with respect to its visual appearance and the forces reflected from the virtual organic tissues. The simulator should therefore resemble a human body and dispose of a surface similar to the human skin. The laparoscopic instruments manipulated by the surgeon should approximate real instruments. The surgeon shall be able to work under the same conditions as in a real laparoscopic intervention.

- Depending on the operation to be simulated, two to four instruments are required, all of which may interact with gastro-intestinal organs. The laparoscopic camera is normally not in contact with organic tissue. Therefore, forces and torques on the camera can be neglected in the simulation.

- The simulator should be applicable to any laparoscopic intervention. Thus, the trocar configuration should be easily adjustable in order to be adapted to different types of operations. As a general rule, the trocars are located on a circle of 20cm diameter around the cite of intervention; the distance between the different entrance points into the body varies from about 80 to 200mm. In rare cases, this distance can decrease to a minimum of 50mm.

- During the simulation, the surgeon should be able to use the majority of the current 5, 7, 10, and 12mm diameter laparoscopic tools. More particular manipulations employing larger diameter instruments do not need to be simulated.

- Every instrument inserted into the mannequin through an actuated trocar shall have four degrees of freedom:
  - Orientation of the instrument with respect to the entrance point into the artificial body. It shall be possible to move the instrument within a vertically oriented conic workspace with 100° opening angle.
  - Axial translation of the instrument with respect to the trocar sleeve. The instrument shall be inserted into the mannequin by approximately 200mm with a range of motion of ±50mm.
  - Rotation of the instrument about its longitudinal axis of n times 360°.

  Small translational movements of the trocar pivot point shall be neglected as such movements are very restricted due to the taut abdominal wall. Fixed entrance points are therefore assumed.

- To have the force feedback structures remain at all times completely below the skin of the mannequin, the working envelope of each manipulator is restricted to a hemisphere with respect to the entrance point of the attached trocar into the artificial body. Each mechanical system must allow the user to pivot the respective trocar about this virtual center of motion. In addition, care has to be taken to avoid any interference of the force reflecting mechanisms with each other or the instruments; while allowing a minimum distance of 80mm between the trocar entrance points. Interference among instruments like in a real intervention is permitted.

- The maximum appearing forces and torques have been determined experimentally in collaboration with surgeons [Cuttat, 1994] and are listed in table 3.1.

	Pivoting about entry point	Translation pulling	Translation pushing	Rotation about tool axis
Normal	2.0Nm	10N	7N	-
Maximum	2.6Nm	15N	10N	0.05Nm

Table 3.1: Approximate forces and torques on the surgical instruments during a normal laparoscopic intervention.

- The position of the trocars shall be fixed during the simulation of a specific intervention; their configuration should, however, be adaptable to the operation to be simulated.

4 Human Haptic Perception and Related Design Issues

Things which we see are not by themselves what we see. ... It remains completely unknown to us what the objects may be by themselves and apart from the receptivity of our senses. We know nothing but our manner of perceiving them.

Immanuel Kant

4.1 Introduction

In the previous chapter the demands on the force feedback system have been discussed in terms of freedom of motion, workspace, maximum output forces, and geometric constraints. So far, nothing has been said about design issues determining the quality of the human operator's illusion of feel. Mechanical quantities such as the manipulator's inherent friction, apparent inertia, stiffness, and maximum backlash, as well as control parameters such as the bandwidth of position sensing and force control are of fundamental importance for the performance of a haptic man-machine interface.

In performing manipulative tasks in a virtual world, the operator is physically manipulating the haptic device, which in turn stimulates his tactile and kinesthetic sensory systems. Hence, haptic interfaces have two basic functions: to measure the position and movement of the user's hand, and to display virtual (or remote) contact forces back to the operator. High quality force feedback can only be achieved by a proper match between the performance of the device and the human operator's haptic abilities. Basic understanding of the biomechanical, sensorimotor, and cognitive capabilities of the human haptic system is therefore critical for proper design specification of force reflecting interfaces.

feedback is available, users often fail to differentiate compliance of the contacted environment from the deformation of the soft tissues of the finger pads.

Vibration sensing resolution and bandwidth

Physiological studies have shown that the detection threshold for vibrotactile stimulation is below 1 μm in amplitude [Howe and Kontarinis, 1993]. According to Sharpe [1988] the human skin's vibratory perceptors can sense frequencies of up to 5-10 kHz with a range of maximum sensitivity of 40Hz to 400Hz [Eberhardt et al., 1994]. In the vicinity of 300Hz vibrations with an amplitude as low as 0.1 μm can be detected [Kokjer, 1987][Bolanowsky et al., 1988].

Force control bandwidth

While our sensory system can perceive vibrotactile stimuli up to several kilohertz, the maximum bandwidth with which the human fingers can apply force and motion commands is only on the order of 5-10Hz [Brooks, 1990]. Yet, the minimum bandwidth with which the human fingers demand force input signals to be represented for meaningful kinesthetic perception is generally reported to be 20-30 Hz [Shimoga, 1993a] [Tan et al., 1994]. The human high-level force compliance control loop has a considerably lower bandwidth of only about 1-2Hz. Hogan [1989] found that the human's impedance parameters do not change until more than 1200ms have elapsed if unexpected instability or load is applied. Shimoga [1992] in his review paper summarized the above findings as depicted in figure 4.1.

4.3 Design Issues

The fidelity of a force reflecting manipulator system is characterized by its ability to accurately generate a wide range of dynamic behaviors. At one extreme the interface should be able to appear mechanically invisible, i.e. the device should exert no external forces on the user moving through free virtual space. At the other extreme, the interface should behave as if it were infinitely stiff, or infinitely resistive, so that it could immobilize the human operator's arm hitting a virtual wall.

Available actuator, sensor, material, and computer technology will ultimately determine the degree to which these criteria can be met. Yet, perfect backdriveability and infinite stiffness are not indispensable. The limitations of the human haptic system can be exploited to create a convincing and immersive illusion of feel, even under the

Force resolution

In order for the human operator to perceive the forces displayed by the haptic interface as smoothly varying, the force resolution of the device should match or exceed human sensing resolution. Srinivasan and Chen [1993] claim that haptic interfaces need to have a force resolution of at least 0.01 N in order to make full use of human haptic capabilities. Rosenberg [1995b] specifies a minimum torque resolution of 3 mNm.

Force control bandwidth

The effective force control bandwidth is one of the most important parameters determining the quality of a force feedback system. An exceedingly low control bandwidth leads to destabilizing, 'punch-like' actuation in response to fast hand movements, thus seriously degrading haptic simulations. Sufficiently high data sampling rates and low update latencies are therefore important. As discussed previously, the force feedback signals must be presented to the human operator at at least 20-30 Hz. In order to achieve satisfactory performance, the control loop sampling frequency must be about 10 to 20 times the minimum necessary bandwidth [Brooks, 1990]. Thus the minimum force update rate must not be less than 300 Hz - a result which has been validated on a one-degree-of-freedom test-bed.

Force smoothness

The ability to sense vibrations in frequency ranges well above 300 Hz represents an extremely tight constraint on haptic interface design, and requires careful attention to all aspects of hardware design, actuator selection, and control software. A significant level of vibration is greatly corrupting haptic fidelity and can quickly destroy the sense of presence in the virtual environment. Sources of vibrations such as cogging torques, ripple torques, backlash, and noise-prone transmission elements, as well as sensor quantization, inadequate sensor resolution, etc. should therefore be avoided or minimized.

Backdriveability

The operator must be able to move the force reflecting manipulator in virtual space. For this to be possible, the haptic device must be mechanically backdriveable. The drive train must therefore employ relatively low gear ratios, and transmission elements such as harmonic drives or lead screws are hardly applicable. Force feedback control is only marginally successful in making a non-backdriveable manipulator appear backdriveable [Millman and Colgate, 1991].

Position bandwidth

The position bandwidth refers to the bandwidth of the haptic device's positional tracking and represents the update rate of position information in the virtual image. Experiences from teleoperation suggest a minimum bandwidth of 10-15Hz, approximately matching the motion control bandwidth of the human arm [Sharpe, 1988][Fischer et al., 1990].

Stiffness

Another important metric for the performance of a force-reflecting interface is the maximum stiffness it is capable of representing. Compliance in the links, joints, or transmissions, or low stiffness of the force control loop due to low resolution sensors and actuators reduces the bandwidth of the system, and may cause closed loop instabilities when force sensors and actuators are non-collocated [Millman and Colgate, 1991].

4.4 Conclusions

In this chapter various aspects of human perception and sensorimotor control have been discussed. Force and position sensing resolution, stiffness perception, the ability to sense vibrations, and force and motion control bandwidth have been studied from the literature. This has allowed to derive quantitative criteria on the most important mechanical and electrical design issues for efficient and realistic force simulation. The most severe constraints are the demand for high dynamic range and therefore low apparent friction, high structural and control bandwidth, and very low force ripple. A summary of the relevant parameters is provided in table 4.1.

When comparing the above specifications with the characteristics of the force reflecting joysticks discussed in chapter 2, it is obvious that none of them is truly suitable to our application. Besides non-appropriate degrees of freedom and insufficient motion ranges, most systems do not provide for sufficient force capacity or suffer from exceedingly high inherent friction. Bandwidth limitations are another frequently encountered problem.

5 Manipulator Design and Implementation

One real robot is worth a thousand simulated robots.

Rodney A. Brooks

5.1 Introduction

In chapters 3 and 4, we have determined the requirements of the haptic interface system and defined quantitative performance criteria. We are now ready to start the discussion of the mechanical design and implementation of our novel hybrid parallel-serial mechanism, named *PantoScope*, which allows to provide force feedback on the spherical movement of a surgical instrument about a fixed virtual pivot, and on the translational and rotational movements along and about its longitudinal axis.

In the following section we will address the design of spherical remote-center-of-motion manipulators and introduce a number of possible solutions. The advantages and disadvantages of the different alternatives will be discussed, and the motivation for the choice of the *PantoScope* concept will be presented. Subsequently, we will derive the kinematics and statics of the *PantoScope* structure and investigate its singular configurations and usable workspace. Then, the choice of the employed actuators and transmission principles will be explained based on the previously discussed design specifications. Finally, we will detail the mechanical implementation of the developed concepts and evaluate the system with respect to the requirements defined in chapter 4.

Bending planar mechanisms with only revolute joints around a sphere results in the spherical two-link mechanism [Asada and Cro Granito, 1985] and its extensions to parallel spherical four- and five-bar-linkages [Artobolevski, 1975]. An extensive discussion of these mechanisms together with their kinematic and dynamic optimization is provided in [Yang and Zhishang, 1983] and [Ouerfelli and Kumar, 1994].

Another interesting parallel drive mechanism, which is based on three spherical two-link arms, has been introduced by Asada and Cro Granito [1985]. This structure has been further developed by Gosselin who analyzed different topologies [Gosselin et al., 1989, 1992a, 1992b, 1993] and named the solution with three orthogonal driving axes *Agile Eye* [Gosselin and Hamel, 1994]. The same structure has been investigated by Craver and Tesar [1990], Takeda et al. [1993], and Alizade et al. [1994].

Following the second design principle of displacing the center of rotation of a general spherical structure by means of a pantograph linkage leads to the *Roticulator* mechanism proposed by Mosher [1985]. The *Roticulator* is a planar pantograph structure comprised of two parallelograms which allow to orient the end-effector about the center of a virtual sphere.

The combination of two pantograph drive linkages into a parallel mechanism leads to a novel spherical remote-center-of-motion design: the *PantoScope* structure, depicted in figure 5.1 [Baumann et al., 1996a, 1997]. The two kinematic drive chains connect the end-effector to the common base. They comprise only revolute joints and

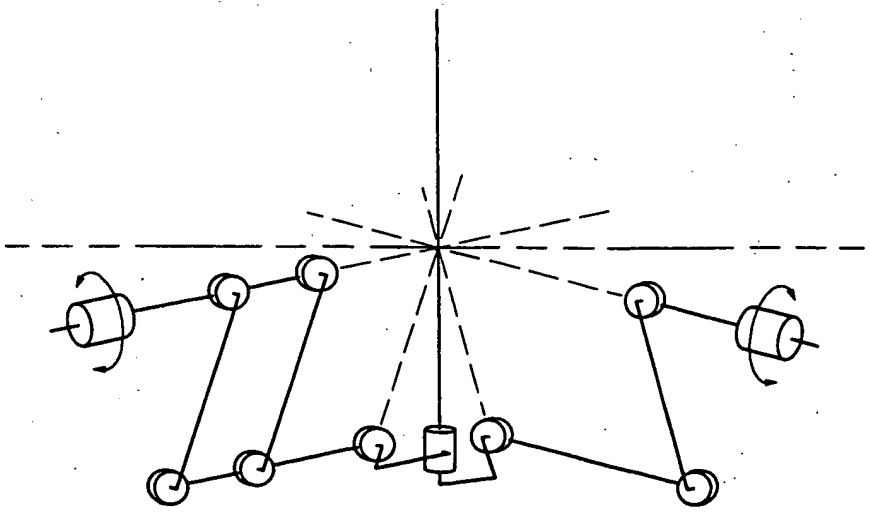

Figure 5.1: The PantoScope structure.

Classification			Solutions			
Principle	DoF	Loops	#	Diagram	Description	Variations
'Bend' a planar mechanism around a sphere	2	0	1	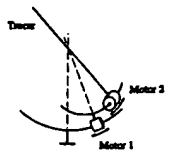	PP *Spherical Cartesian Manipulator* [Taylor et al., 1992]	
			2	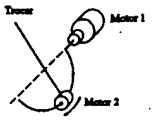	RP *Spherical Cylindrical Manipulator* [Gayed et al., 1987]	
			3	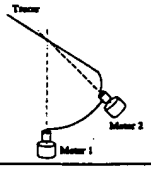	RR *Spherical Two-Link-Mechanism* [Asada et al., 1985]	
		1	4	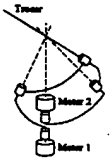	(RRR)/(RR) *Four-Bar-Linkage* [Artobolevski, 1975], [Yang et al., 1983]	To avoid static over-determination, replace in one chain an R joint by an S joint, and an R joint by an (RP) joint.
			5	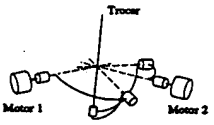	(RRR)/(RR) *Five-Bar-Linkage* [Artobolevski, 1975], [Ouerfelli et al., 1994]	To avoid static over-determination, replace in one chain an R joint by an S joint, and an R joint by an (RP) joint.
		2	6	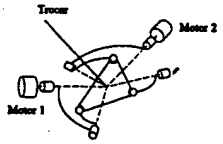	[2(RRS)]/(RS) [Gosselin et al., 1992]	
	3		7	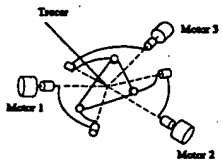	3(RRS) *Agile Eye* [Gosselin et al., 1989], [Gosselin et al., 1994]	With collinear axes [Asada et al., 1985]; with coplanar axes [Gosselin et al., 1992]; with orthogonal axes [Gosselin et al., 1993].
Displace the center of rotation by a pantograph linkage	2	2	8	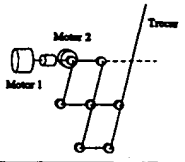	R(RR/RRR/RR) *Roticulator* [Mosher, 1985]	To avoid static over-determination, replace in each parallelogram an R joint with an S joint, and an R joint with an U joint.
			9	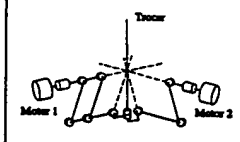	[R(RR/RR)RR]/(RRRR) *PantoScope* [Baumann et al., 1996] [Baumann et al., 1997]	To avoid static over-determination, replace in each parallelogram an R joint with an S joint, and an R joint with an U joint.
	3	5	10	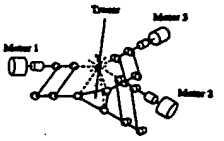	3[R(RR/RR)S] *Argos* [Vischer, 1996], [Vischer et al., 1997]	To avoid static over-determination, replace in each parallelogram an R joint with an S joint, and an R joint with an U joint.

with $n=10$, $g=11$, $l=2$, and $f_i=1$ for all joints, yields the mobility $m=-1$. This result conflicts with the expected two degrees of freedom of a spherical structure. Why this inconsistency? Obviously, the freedoms of the joints in the pantograph drive chain are not independent, as their axes are not by any means generally oriented. In order to guarantee perfect operation, care has to be taken to ensure precise parallelism of these four joint axes. Alternatively, one of the revolute joints could be replaced by a ball-and-socket joint and another by an universal or a ball-and-socket joint in order to prevent static over-determination.

5.2.4 Conclusions

In this section we have investigated spherical remote-center-of-motion manipulators and evaluated them with respect to their suitability as haptic interface for laparoscopic surgery simulation. This research lead to the development of the *PantoScope* mechanism which has two rotational degrees of freedom, and thus allows to provide force feedback on the pivoting movement of the trocar about the entrance point into the artificial body. In order to extend the *PantoScope* concept to exert forces and torques also on the instrument's translational and rotational movements, a translational sliding joint and a revolute joint need to be added as depicted in figure 5.2. This leads to a two-stage *hybrid parallel-serial drive chain*, which allows to provide force reflection on all four degrees of freedom of motion of the surgical instrument. In the following, we will make use of this conceptual decomposition by referring to *trocar degrees of freedom* and *instrument degrees of freedom.*

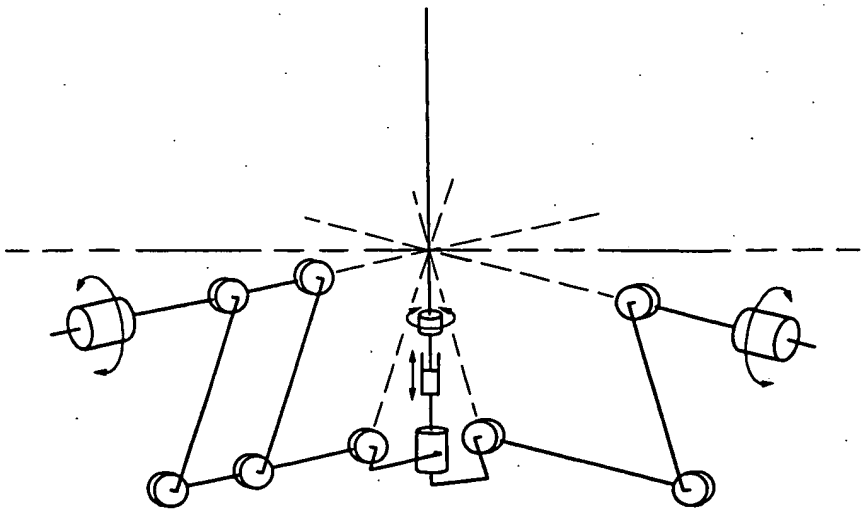

Figure 5.2: Extended PantoScope structure with four degrees of freedom.

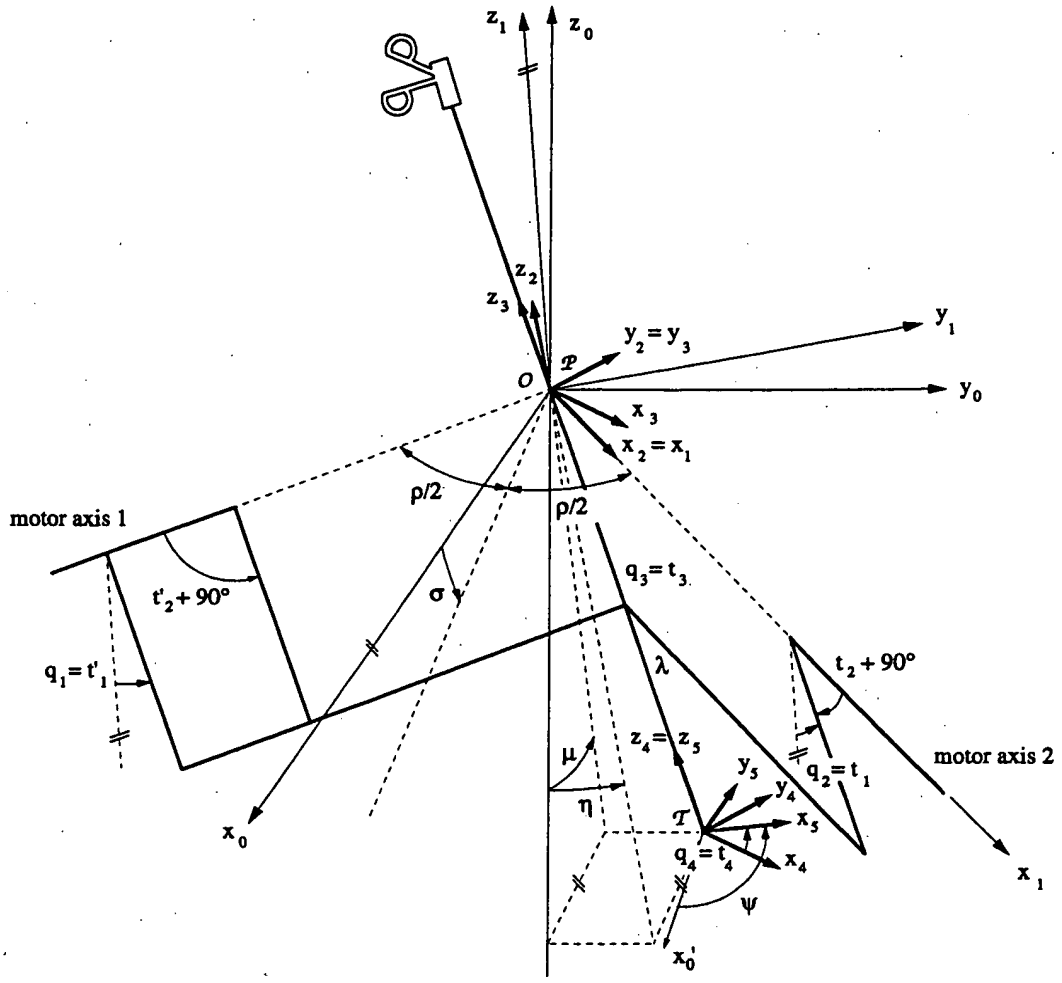

Figure 5.3: Coordinate frames and parameterizations.

While the joint space variables, q_1, q_2, q_3, q_4, are given by the manipulator's structural design, the parameterization of the operational space can be more or less freely defined. Cartesian coordinates are generally used in practice to specify the end-effector's position. Orientations are most often described by Euler angles, direction cosines, or roll, pitch, and yaw angles. However, these representations require the mapping of the four joint coordinates into six generalized coordinates of the world space. In order to avoid a redundant description, a four variable representation[8] of the operational space has been defined in accordance with the four-degree-of-freedom spherical movement of the end-effector.

---

[8] A six parameter representation based on Cartesian coordinates and yaw, pitch, and roll angles is used by the graphical programming environment Perfomer™. Details are provided in appendix A.1.

$$t_2 = \text{atan}\,2\big(\cos(\rho)\sin(q_2) - \cos(q_2)\tan(q_1), \sin(\rho)\big), \tag{5.6}$$

and from figure 5.3:

$$t_3 = q_3, \tag{5.7}$$

$$t_4 = q_4. \tag{5.8}$$

Note that equation (5.6) has a second physically meaningful solution at $t_2 + 180°$.

Direct Geometric Model

The geometric transformation from the world frame $O(\mathbf{x}_0, \mathbf{y}_0, \mathbf{z}_0)$ to the end-effector frame $\mathcal{T}(\mathbf{x}_5, \mathbf{y}_5, \mathbf{z}_5)$ is defined by the homogeneous transformation matrix ${}^0\mathbf{T}_5$:

$${}^0\mathbf{T}_5 = \text{Rot}(\mathbf{y}, \sigma)\,\text{Rot}(\mathbf{z}, \frac{\rho}{2})\,\text{Rot}(\mathbf{x}, t_1)\,\text{Rot}(\mathbf{y}, t_2)\,\text{Trans}(0,0,t_3)\,\text{Rot}(\mathbf{z}, t_4). \tag{5.9}$$

Thus, ${}^0\mathbf{T}_5$ is completely defined and has the form

$${}^0\mathbf{T}_5 = \begin{bmatrix} n_x & o_x & a_x & p_x \\ n_y & o_y & a_y & p_y \\ n_z & o_z & a_z & p_z \\ 0 & 0 & 0 & 1 \end{bmatrix} = \begin{bmatrix} {}^0\mathbf{R}_5 & {}^0\mathbf{p}_{5org} \\ \mathbf{0} & 1 \end{bmatrix}, \tag{5.10}$$

where ${}^0\mathbf{p}_{5org}$ is the position of the end-effector frame's origin, and ${}^0\mathbf{R}_5$ the 3×3 matrix of the direction cosines of its base vectors with respect to the world frame O. The unit vectors $\mathbf{n}$, $\mathbf{o}$, and $\mathbf{a}$ are commonly known as the normal, orientation, and approach vectors, lying in the $\mathbf{x}_5$, $\mathbf{y}_5$, and $\mathbf{z}_5$ directions of the end-effector frame $\mathcal{T}$.

From the ${}^0\mathbf{T}_5$ transformation matrix, we can now compute the previously defined world space representation of the end-effector's position and orientation. From figure 5.3, we obtain:

$$\eta = \text{atan}\,2(-a_y, a_z), \tag{5.11}$$

$$\mu = \text{atan}\,2(a_x, a_z), \tag{5.12}$$

$$\lambda = \sqrt{p_x^2 + p_y^2 + p_z^2}, \tag{5.13}$$

$$\psi = \text{atan}\,2(-o_x, n_x). \tag{5.14}$$

From the closure equations (5.4), we can finally determine q_1 and q_2 by eliminating t_1' and t_2' :

$$q_1 = \operatorname{atan2}\left(\cos(\rho)\sin(t_1) - \sin(\rho)\tan(t_2), \cos(t_1)\right), \tag{5.22}$$

$$q_2 = t_1, \tag{5.23}$$

and from figure 5.3, we know:

$$q_3 = t_3, \tag{5.24}$$

$$q_4 = t_4. \tag{5.25}$$

The inverse problem has a total of four physically meaningful solutions, corresponding to the two solutions for each t_1 and t_2 from equations (5.16) and (5.17).

5.3.3 Instantaneous Kinematics and Statics

Velocities and static forces at the end-effector relate to joint velocities and joint torques by the manipulator Jacobian. The Jacobian, $\mathbf{J}$, is a multi-dimensional form of the derivative and describes differential relationships between coordinate frames. Thus, differential changes in the manipulators position and orientation expressed in world frame coordinates, $\dot{\mathbf{x}}$, relate to differential changes in the joint space variables, $\dot{\mathbf{q}}$, by

$$\dot{\mathbf{x}} = \mathbf{J} \cdot \dot{\mathbf{q}}, \tag{5.26}$$

$$\dot{\mathbf{q}} = \mathbf{J}^{-1} \cdot \dot{\mathbf{x}}. \tag{5.27}$$

Following the principle of virtual work [Craig, 1989], static forces and moments applied at the end-effector, $\mathbf{f}$, and the torques acting on the actuator axes in joint space, τ, are related by the transpose of the Jacobian:

$$\tau = \mathbf{J}^{\mathrm{T}} \cdot \mathbf{f}, \tag{5.28}$$

$$\mathbf{f} = \mathbf{J}^{-\mathrm{T}} \cdot \tau. \tag{5.29}$$

Following the previously applied two step approach from actuator joint space to an intermediate serial chain joint space, and from this intermediate space to world space, we can write the Jacobian $\mathbf{J}$ as the product of two other Jacobians, $\mathbf{J}_1$ and $\mathbf{J}_2$:

$$\mathbf{J} = \mathbf{J}_2 \cdot \mathbf{J}_1, \tag{5.30}$$

effector cannot resist. This is an amazing property of manipulators with closed kinematic chains. In these configurations, the robot becomes uncontrollable since some displacements of the end-effector are possible without any action on the actuators. Thus, we speak of *static* [Ouerfelli and Kumar, 1994] or *inverse* [Guglielmetti, 1994] singularities. From the determinant of the Jacobian $\mathbf{J}_1$, we see that this occurs for $q_2 = \pm 90°$, i.e. when the end-effector falls into the $\mathbf{x}_1$-$\mathbf{y}_1$ plane:

$$\det(\mathbf{J}_1) = \frac{\sin(\rho)\sec^2(q_1)\cos(q_2)}{\sin^2(\rho)+\cos^2(\rho)\sin^2(q_2)-\cos(\rho)\tan(q_1)\sin(2q_2)+\tan^2(q_1)\cos^2(q_2)}. \tag{5.33}$$

For $\rho = 0°$ or $\rho = 180°$, the entire workspace is singular. For all other cases, it is possible to delineate two sections of the workspace that are free of singularities. These are the two hemispheres separated by the $\mathbf{x}_1$-$\mathbf{y}_1$ plane. Thus, the theoretically usable workspace is restricted to a hemisphere. Practical considerations, however, limit the usable range to a spherical sector with considerably less than 180° central angle, since the static singularities of a parallel manipulator imply the complete loss of the structural stiffness.

5.3.5 Conclusions

In this section the direct and inverse geometric models of the *PantoScope* structure have been derived. The relationships between end-effector motions and joint velocities, and between applied actuator torques and exerted forces and moments have been determined. Furthermore, the singular configurations and usable workspace of the mechanism have been investigated.

Based on the output force and torque requirements stated in table 3.1, we can now compute a first approximation of the required actuator torques. In order to determine the specifications for the base actuators, we investigate τ_1 and τ_2 over the entire workspace for the exertion of a continuous torque of 2 Nm about the virtual pivot in any direction perpendicular to the instrument. It can be shown that the most disadvantageous conditions arise at the workspace boundary. This is not surprising as we are then in closest proximity to the manipulator's singular configurations. Figure 5.4 shows the torques τ_1 and τ_2 for the instrument inclined by 50° with respect to the vertical, plotted against the angle φ between the $\mathbf{x}_0$ axis and the projection of the instrument axis onto the $\mathbf{x}_0$-$\mathbf{y}_0$ plane, and the angle ξ, defining the direction of the torque vector acting perpendicular to the instrument with respect to the $\mathbf{x}_0$-$\mathbf{z}_3$ plane.

5.4.1 Actuators

Many mechanism properties such as compliance, friction, inertia, backlash, and torque ripple affect and often degrade manipulator performance in force reflecting man-machine interfaces. The quality of a haptic device is often characterized by its degree of *transparency*. Transparency implies that no forces are exerted on the operator's hand when no physical interactions occur in the virtual world. The actuators should therefore present minimal inertia and resistance to human hand motion, a quality called back-driveability. Transparency also implies the absence of any noticeable force and torque non-linearities such as position dependent torque ripple and cogging.

Application specific requirements pose further constraints on the size and weight of the employed actuators. Besides torque capacity, the torque-to-weight ratio is an important selection criterion for mobile motors. Another significant measure for overall simulation fidelity is the mechanical bandwidth which should match the human sensori-motor capabilities discussed in chapter 4. In the following, we will evaluate today's most important actuator technologies in terms of torque capacity, torque-to-weight ratio, backdriveability, and bandwidth.

Electromagnetic actuators

Electromagnetic servo actuators comprise a wide variety of dc and ac induction motors. Although different in their mechanical and electrical structure, they are all based on the common principle of two interacting, time-varying magnetic fields. In the following we will concentrate our discussion on dc motors. Ac induction motors are more demanding in terms of control and have not been considered.

In a **conventional dc motor**, the magnetic field of the stator is produced by permanent magnets or by current through field winding coils. The second magnetic field is generated by currents through the rotor's armature winding which is connected to a commutator assuring electrical contact with the dc power supply through sliding contacts called brushes. Permanent magnet dc motors are used in many of today's haptic interface devices. They are comparatively clean, quiet, and efficient, they generally provide for high linearity and high bandwidth (typically on the order of 100Hz), and are easy to control and maintain. Their main disadvantage is the mechanical commutation provoking friction and wear, but also their low torque-to-weight ratio imposed by the maximum current that can be sustained for a given period of time. Torque ripple is another frequently encountered problem.

Hydraulic actuators

In terms of torque-to-weight ratio hydraulic actuators are ideal. Hydraulic actuators convert energy supplied by pressurized hydraulic fluid into rotary or linear motion. The hydraulic fluid flowing through the hydraulic actuator is controlled either by servo valves which are usually electromagnetically actuated, or directly by variable displacement pumps. The exceptional torque-to-weight ratio explains the popularity of hydraulic actuation for large robots and machinery. The presence of fluids, however, poses a number of problems in terms of mechanical design. Increased friction and leakage are among the most often cited disadvantages. Despite their very high torque-to-weight ratio, hydraulic actuators also tend to be heavier and larger than electrical actuators. Moreover, electrohydraulic servo valves typically exhibit complex non-linear dynamics, and are therefore more demanding in terms of control [Hollerbach et al., 1992]. The main drawback of hydraulic actuation for force reflection, however, is the lack of backdriveability.

Pneumatic actuators

Commonly, pneumatic actuators involve a piston driven by pressurized gas, much in the same way as hydraulic actuators. Since the pressures used in pneumatic actuators are generally smaller than in hydraulic actuators, pneumatic actuators typically have a lighter structure than hydraulic ones, resulting in similarly high force-to-weight ratios [Hollerbach et al., 1992]. Important advantages of pneumatic over hydraulic actuators are their cleanliness and simplicity. The main drawback of pneumatic actuators is gas compressibility which makes them inherently compliant. To overcome limitations of compressibility on bandwidth, pressure control may be used. However, the speed of the servo valve employed to regulate pressure and air flow into the pneumatic piston will ultimately limit the actuator's dynamic performance.

Shape memory alloy actuators

The shape memory effect of certain alloys involves, after a mechanical deformation, a return to an undeformed state when heated. The main advantages of shape memory alloys (SMA) are their high force-to-weight ratio, their compactness and lightness. Main disadvantage of SMA actuators is their very low bandwidth of typically less than 1 Hz due to the relatively long time required to cool back after heating. Another drawback is the low energy efficiency of about 2-5% [Burdea, 1996].

Direct drive

With the use of direct drive actuators, transmission stages can be avoided altogether. Transmission free drives have the advantage of avoiding backlash while minimizing friction. They also provide high stiffness and good backdriveability. All these features are important for transparent force feedback systems. The use of true direct drive, however, imposes two important restrictions. First, there is no speed reducer between the motor and the actuated joint, so the joint torques are limited to the output torque of the motor. In general, larger and heavier actuators are therefore required. Second, the weight and bulk of direct-drive motors must be placed directly at the joints they drive, leading quite often to considerable inertial and gravitational effects.

Mechanical transmission

Mechanical transmission elements include a wide range of gear trains, friction drives, tension-element drives, tendon drives, and rigid link drives [Clavel, 1992]. The various transmission principles are not equally well suited for the application in force reflecting haptic interfaces:

Toothed transmission elements such as gears, lead screws, synchronous belts, etc. should be avoided as they introduce torque ripples, severely compromising the fidelity of force simulations. Gears, and in particular lead screws and harmonic drives, additionally contribute excessive friction and backlash, limiting backdriveability and making accurate control difficult. Better suited in terms of transmission smoothness are **friction drives**. However, also friction drives may compromise backdriveability and in addition suffer from the limitations on the maximal torques they can transmit without slippage. The criterion on backdriveability further restricts the use of **tendon transmissions**. The transmission sheaths generally introduce a high amount of static and dry friction leading to undesirable stick-slip effects [Steinmetz, 1994]. **Tension-element drives** such as steel cables or strips are well suited to high-performance transmissions. When properly designed, these drives feature high material strength, low weight, very low torque ripple, no backlash, and low friction. Tension-element transmissions also provide for high bandwidth and low inertia compared to other transmission principles. The need for idler pulleys, however, may lead to more complex mechanical design. **Rigid link drives**, finally, have similarly good transmission characteristics as tension-element drives, and provide for even improved bandwidth. Mechanical interferences and the relatively low achievable transmission ratio, however, often restrict their use, particularly in cases where a large working range is required.

5.4.3 Actuation of Trocar Degrees of Freedom

The hybrid parallel-serial structure of the *PantoScope* mechanism allows to install the two base actuators, providing force feedback on the pivoting degrees of freedom of the trocar, fixed to the ground. Direct drive actuation using torque motors seems therefore a conceivable solution as no disadvantageous gravitational and inertial effects have to be faced. However, the size of dc torque motors providing continuous output torques in excess of 2Nm is prohibitive in our application. The available space is very limited as a total of three force feedback devices, corresponding to three laparoscopic instruments, have to be integrated into one simulator mannequin.

A combination of electromagnetic actuation with low reduction transmission is therefore proposed. Pre-tensioned cable reduction stages are employed to multiply and transmit the actuator output torques to the *PantoScope*'s base axes, allowing for smooth and backlash-free transmission (figure 5.5).

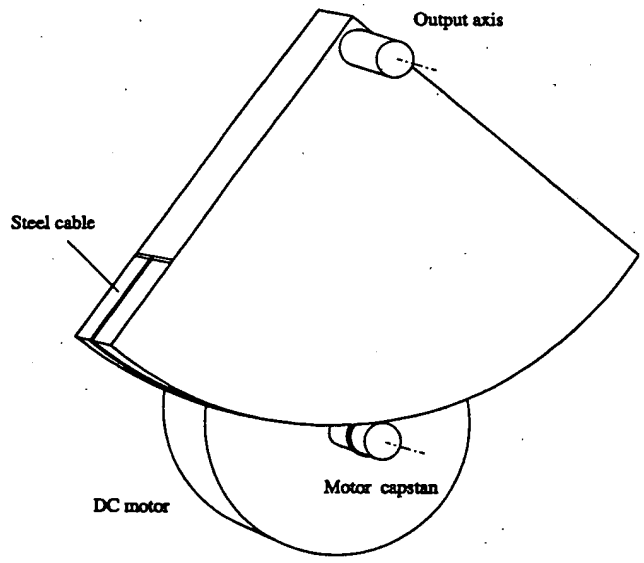

Figure 5.5: Pre-tensioned cable drive.

For actuation, a variety of different dc motors have been investigated, and the performance of two particularly promising actuators has been evaluated in detail on our prototype system. One of these motors is a conventional dc actuator with ironfree rotor, characterized by a particularly high electrical and mechanical bandwidth and low friction (escap® HPR 3N63 from Portescap, Inc.). The HPR 3N63, however, suffers from significant torque ripple with an amplitude on the order of 10% of the exerted torque.

agrees particularly well with the demanded large range of motion and the restricted available space. However, excessive friction and related stick-slip effects often prevent its successful application. In order to avoid stick-slip due to static friction of the piston rings and gaskets, a dynamic friction scheme is proposed [Bubendorf, 1997]. The piston rods are continuously rotated about their longitudinal axes which makes the system behave as under pure viscous friction conditions [Spinnler, 1997].

Figure 5.6 shows the proposed actuation of the instrument degrees of freedom. The two motors (1) and (2) are permanently rotating, in this way putting the pistons (3) and (4) of the hydraulic transmission stage under condition of permanent viscous friction. Since the motors (1) and (2) have to overcome only gasket friction and do not need to carry any additional load, they can be dimensioned very small. In order to provide force feedback to the operator manipulating the instrument (9), the dc motor (5) drives the cylinder (7) via the pre-tensioned steel cable (6). The translational displacement of the cylinder (7) provokes a fluid transfer to the cylinder (8), which itself causes the

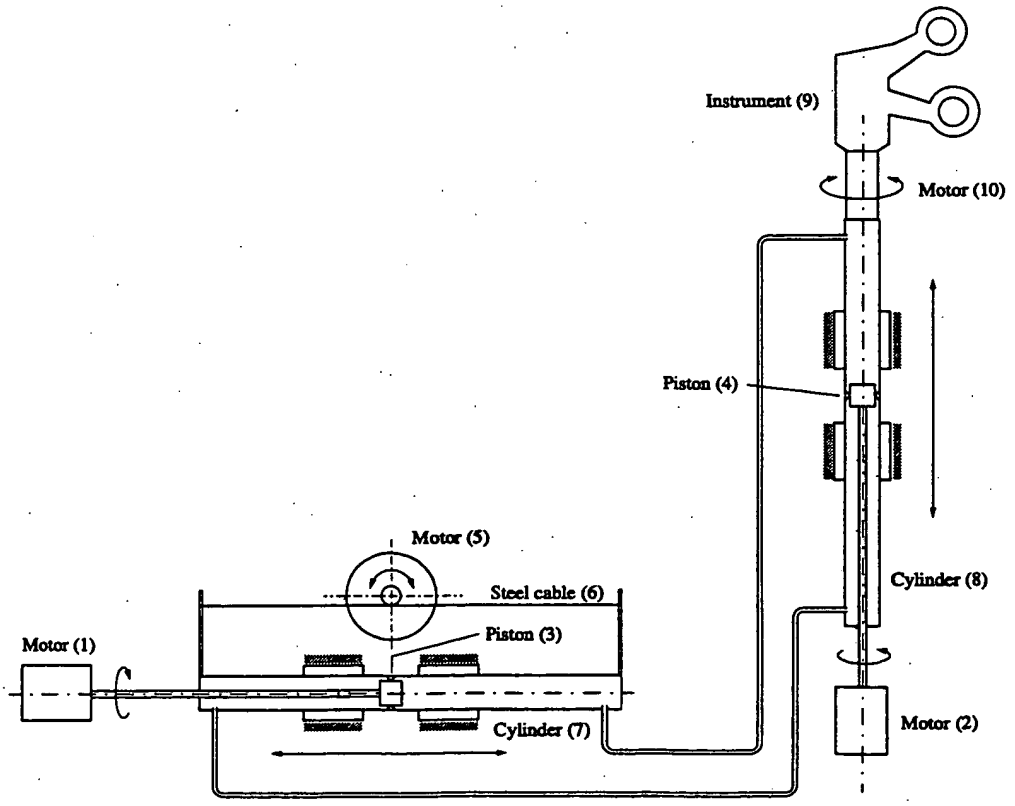

Figure 5.6: Actuation of translational and rotational degrees of freedom of the instrument (adapted from [Bubendorf, 1997]).

For the actuation of the pivoting degrees of freedom of the *PantoScope* mechanism, special attention has been devoted to the prevention of torque variations. Parasitic torque ripples provoking unnatural force sensations immediately destroy the operator's sense of presence in the virtual world and are a key issue to realistic and immersive force simulation. Printed armature dc motors in combination with high-tension cable transmissions have therefore been selected.

In order to provide force feedback on the translational movement of the instrument with respect to the trocar, the power of a base mounted conventional dc actuator is transmitted to the *PantoScope*'s end-effector via a hydraulic transmission. The proposed approach allows for high mechanical compactness and kinematics decoupling. Stick-slip problems are avoided by continuously rotating the piston rods about their longitudinal axes, thus making them permanently subject to dynamic friction conditions. For force reflection on the rotational movement of the instrument about its longitudinal axis, finally, a small conventional dc motor combined with a reducing gear has been selected for integration into the instrument's hand-grip.

5.5 Implementation

In this section the practical implementation of the *PantoScope* force feedback manipulator will be described. The required large workspace and potential interferences among adjacent force feedback devices when installed in one simulator mannequin represent severe constraints on the constructional design. Compactness has therefore been among the most important design issues, besides structural rigidity and backdriveability.

Figure 5.7 shows a general view of the *PantoScope* prototype. The manipulator fits into a cylindrical segment of 60° opening angle, 300 mm radius, and 200 mm height. In order to avoid any interference among neighboring force feedback manipulators, the angle between the base axes, ρ, has been set to 60°. The base axes are slightly inclined with respect to the horizontal plane by $\varepsilon = 10°$, thus allowing to completely hide the manipulator below the skin of the simulator mannequin. The practically usable workspace is a spherical segment with 100° central angle. The surgical instrument can thus be inclined as much as 50° in any direction with respect to the vertical. Linear stroke is 100 mm, and the rotational range of motion is only restricted by the cable departing from the instrument handle.

Figure 5.9 shows the actuation of the trocar degrees of freedom. The employed dc servo disk motors, together with the high-tension cable transmission stages, allow for smooth, backlash-free, high torque actuation. The sustained output torque is approximately 2Nm. Optical laser encoders (Canon TR-36) with 3600 physical increments per revolution are used for position sensing. Quadrature decoding and the reduction factor of 10.5 of the cable transmission stages provide a maximum angular resolution of 0.0024°. Velocity and acceleration sensors are not employed.

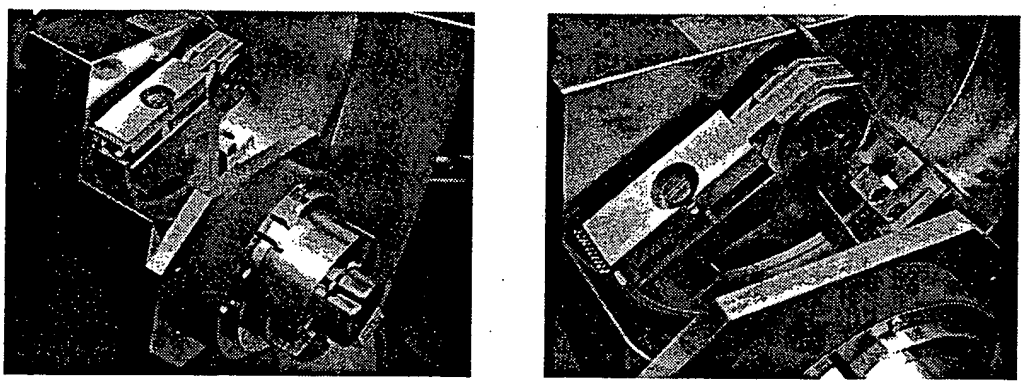

(a) (b)

Figure 5.9: Actuation of trocar degrees of freedom: (a) general view of actuator-transmission stage, (b) detail view of high-tension steel cable drive.

5.5.2 Instrument Degrees of Freedom

Figure 5.10 shows a design worksheet and the practical realization of the *PantoScope*'s instrument degrees of freedom. The core of the *PantoScope*'s distal end's mechanical structure are two concentric steel tubes (1, 2) serving as hydraulic cylinder and conduit. Linear motion ball bushings (3) allow to translate the tubes and the attached instrument handle[11] with respect to the *PantoScope* drive chains (4) and the hydraulic piston (5).

---

[11]The instrument handle is rigidly attached to the force feedback structure which prohibits the simulation of instrument exchanges as originally demanded in the specifications stated in chapter 3. This compromise was made in order to prevent the constructional re-design of the *PantoScope*'s drive arms realized in the first phase of the project. The use of standard, traversing instruments would require a larger diameter of the trocar structure which is not possible with the actual implementation of the base drive arms.

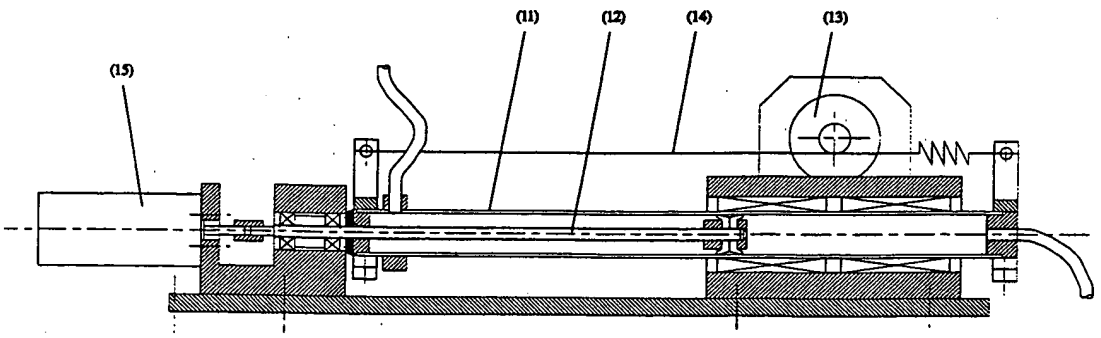

(a)

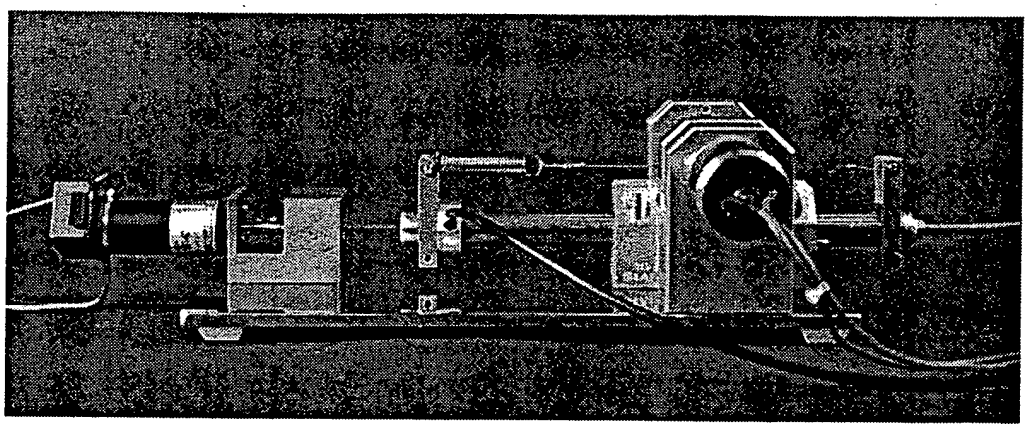

(b)

Figure 5.11: Actuator unit for force feedback on linear stroke: (a) design worksheet [Bubendorf, 1997], (b) practical implementation.

The escap® dc actuator employed for driving the translational degree of freedom provides a continuous output torque of 110mNm, which, considering the losses in the cable drive and hydraulic transmission, results in a sustained output force at the instrument of approximately 12 N. The driving motor is equipped with a rotary optical encoder (Canon TR-36) providing a position resolution at the instrument of 0.0035mm under the assumption of fluid incompressibility.

Figure 5.12 shows a detail view of the instrument handle which hosts a small dc actuator with planetary gear reducer for driving the instrument's rotational degree of freedom. The employed actuator from Minimotor, Inc., together with the gear reduction of 43, provides the required 50mNm continuous output torque. An optical encoder (MINIMOTOR 03B22) allows for a position resolution at the output shaft of 0.14°. The handle's upper part diameter of 26mm is slightly larger than the one of conventional laparoscopic instruments, does, however, not obstruct instrument handling.

the actual implementation are the slightly modified shape of the instrument handle and the lack of instrument exchangeability, as well as non-negligible inter-chamber leakage in the hydraulic transmission stage.

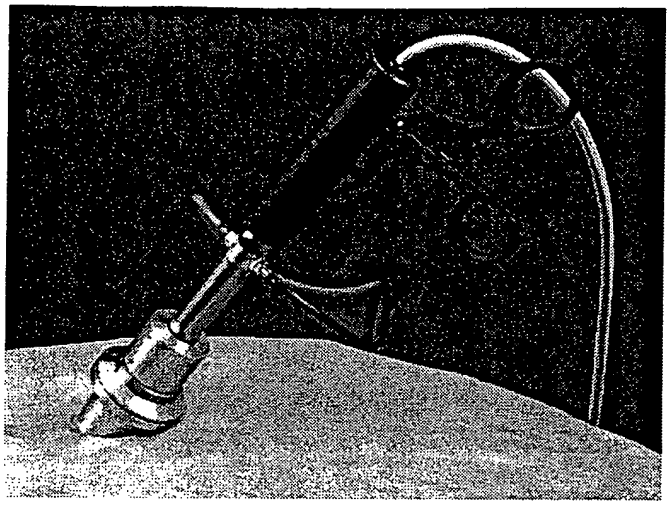

Figure 5.13: Mannequin hosting PantoScope force feedback manipulator.

5.6 Open Loop Characteristics

In the preceding sections, mechanical design issues for force reflecting man-machine interfaces and the implementation of the *PantoScope* prototype system have been discussed. Actuators and transmission elements have been selected based on an evaluation of their suitability for haptic devices. So far, no quantitative data has been provided on overall system performance. This section will summarize the open-loop characteristics of the *PantoScope* force feedback prototype.

5.6.1 Trocar Degrees of Freedom

Evaluation measurements on the employed printed armature dc motors (without transmissions) have confirmed the expected smooth torque exertion. Peak-to-peak actuator torque ripples are over the entire output torque range within the resolution of 2.5 mNm of the torque sensor employed for the measurements. Actuator static friction is on the order of 15 mNm, dry friction is below 10 mNm. The measured actuator torque for a commanded constant output of 150 mNm, where the motor axis was slowly moved by hand in and against the direction of the applied torque, is shown in figure 5.14.

Friction and torque variations introduced by the steel cable transmission are on the order of 10-20mNm (figure 5.16). The slow torque variations are due to misalignment of the drive input and output axes, whereas the superimposed fast torque ripples result from the ragged surface of the employed steel cable. The latter could be avoided by using steel strips or coated cables. However, steel strips require a larger mechanical construction and tend to introduce more internal friction, and coated cables have a more limited working life.

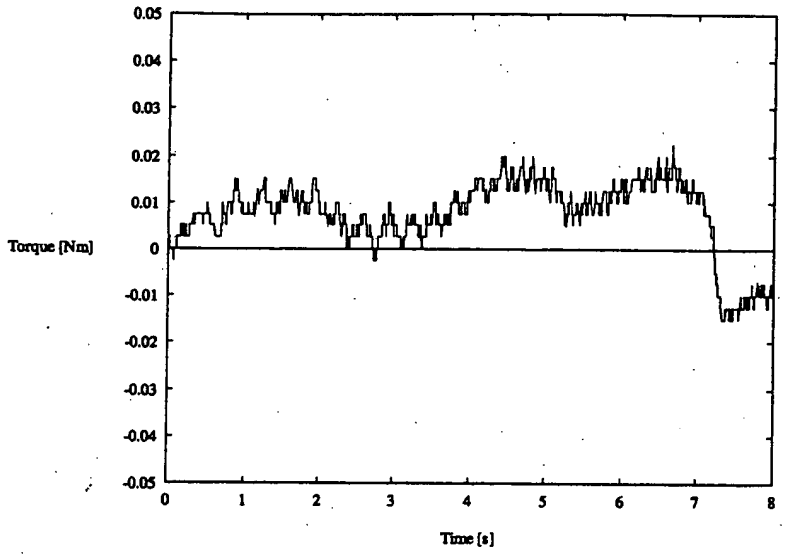

Figure 5.16: Friction and torque ripples due to tensioned cable transmission stage.

Figure 5.17, finally, shows the overall friction and torque ripples of the complete actuator-transmission stage for commanded zero output torque and alternate movements in both directions. Overall friction seen at the *PantoScope* axes amounts to about 150mNm, corresponding to 7.5% of the maximum sustained output torque of 2 Nm. Torque variation amplitudes vary considerably with the quality of the alignment of motor shafts and cable drive output axes, and are on the order of 25-50mNm peak-to-peak.

Measurements on the *PantoScope*'s mechanical linkage have confirmed the expected stiffness and backdriveability of the parallel, lightweight aluminum structure. The realization of all joints with ball bearings limits the maximum dry friction within the mechanism without actuation to less than 10mNm. This value is well below the aforementioned 150 mNm friction torque in the actuator-transmission stages. The measured characteristics for the trocar degrees of freedom actuators, transmissions, and mechanical linkage are summarized in table 5.4.

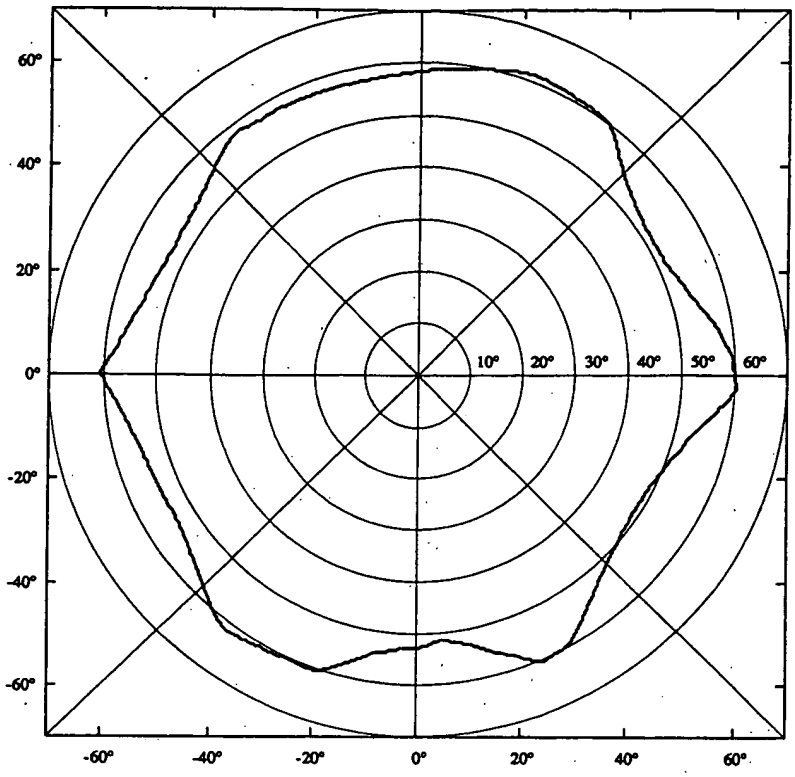

Figure 5.18: Working volume of the PantoScope's trocar degrees of freedom.

5.6.2 Instrument Degrees of Freedom

Force measurements on the translational degree of freedom of the instrument confirmed the efficiency of the dynamic friction scheme proposed for the hydraulic transmission. The continuous rotation of the cylinder pistons allows to drastically enhance manipulator backdriveability. Static friction of the piston gaskets is approximately 6 N, which would largely impair backdriveability and lead to highly undesirable stick-slip effects. With the permanent rotation of the pistons this problem is avoided; the remaining friction for both pistons installed on the *PantoScope* structure and in the driving unit is on the order of 1 N each. Mechanical bearing friction is below 0.25 N, while the driving actuator's static and dry friction is approximately 3 mNm.

Although a very low viscous oil[13] is used for hydraulic transmission, fluid viscosity is clearly felt during instrument motion. This is mainly due to the small section

[13]Shell ASEOL Plus 16/100, with a viscosity of $2.2 \cdot 10^{-3}$ Ns/m^2 at 40°C. Lower viscosity fluids, such as water or alcohol, have not been considered for reasons of corrosion and inflammability.

Maximum sustained actuator torque	0.11 Nm
Maximum sustained output force	12N
Transmission ratio (hydraulic)	0.617
Transmission ratio (mechanical)	200rad/m
Dry friction, actuator only	3mNm
Overall friction (slow movements)	3.5N
Overall torque variations	0.5N (peak-to-peak)

Table 5.5: Measured actuator and transmission characteristics of the PantoScope's translational degree of freedom.

Friction and torque variation measurements on the instrument's rotational degree of freedom are summarized in table 5.6. As expected, the high reduction planetary gear introduces a considerable amount of backdrive friction on the order of 5-7.5mNm, corresponding to approximately 10% of the 60mNm maximum sustained output torque. This amount of friction is considered acceptable since in real instrument-trocar movements friction arising from the trocar valve amounts to approximately 5mNm (Ethicon Endopath™ 5mm trocar) and is therefore equally felt. Torque ripples are within the resolution of 2.5mNm of the sensor employed for the torque measurements. Experimental evaluations performed by surgeons revealed that these torque ripples do not excessively disturb force sensations [Cuttat, 1997].

Maximum sustained actuator torque	2mNm
Maximum sustained output torque	60mNm
Transmission ratio	43
Transmission efficiency	70%
Backlash	<2°
Overall dry friction	5 - 7.5mNm
Overall torque variations	<2.5mNm (peak-to-peak)

Table 5.6: Measured actuator and transmission characteristics of the PantoScope's rotational degree of freedom.

5.6.3 Conclusions

The above discussed evaluation measurements allow to compare the characteristics of the mechanical force feedback system with the specifications set out in chapter 4. The open-loop characteristics of the realized prototype system are summarized in table 5.7.

Continuous force capacity[15]	2Nm / 12N / 0.06Nm
Peak force capacity (hardware limited)[15]	4Nm / 20N / 0.10Nm
Force accuracy	-
Force update rate	-
Force ripple amplitude	1-2% of continuous force capacity
Backdrive friction[15]	7.5% / 30% / 10% of cont. force cap.
Dynamic range[15]	1:13 / 1:3.4 / 1:10
Gravitational balancing	no
Backlash	<2° on rotational dof, otherwise zero
Position resolution[15]	0.0024° / 3.5μm[16] / 0.14°
Position update rate	-
Range of motion[15]	cone 100° / 100mm / unlimited
Maximum object stiffness	-

Table 5.7: Open-loop characteristics of the PantoScope system.

By comparing tables 5.7 and 4.1, we see that the workspace and output force requirements are fulfilled. Even though the maximum measured torque ripples are slightly exceeding the specified limits, they are not haptically perceivable and are therefore considered acceptable. The overall friction, however, is clearly too high in both the trocar degrees of freedom and the instrument's translational degree of freedom. In addition, the weight of the mechanical force feedback structure is clearly felt when the handle is moved. The compensation of frictional and gravitational effects is therefore an important issue in terms of manipulator control and will be treated accordingly in the following chapter.

5.7 Conclusions

In this chapter, we have presented the mechanical design and implementation of the four-degree-of-freedom force reflecting manipulator. Starting with a discussion of remote-center-of-motion spherical mechanisms, we have developed a novel mechanical structure, named *PantoScope*, which combines a number of important advantages. The hybrid parallel-serial mechanism allows to install the two base actuators for force re-

---

[15]Values refer to the pivoting degrees of freedom, the translational degree of freedom, and the rotational degree of freedom of the force feedback manipulator.

[16]Without consideration of fluid compressibility and conduit deformations in the hydraulic system. The actual resolution is on the order of 1mm.

6 System Supervision and Control

The screen is a window through which one sees a virtual world. The challenge is to make that world look real, act real, sound real, feel real.

Ivan E. Sutherland - *The Ultimate Display*

6.1 Introduction

The ultimate objective of a truly versatile force reflecting man-machine interface is to provide the ability to produce any arbitrary mechanical load to the human operator. Such mechanical loads could be as small as a feather moving in free space and as large as a rigid concrete wall; they may range from constant linear impedances like linear springs and dampers to complicated non-linear time varying environments. The quality of a force reflecting interface is thus determined by the range of mechanical loads it is able to simulate. This range is inherently restricted by the limited actuator output forces and the simulator's mechanical and computational bandwidth.

This chapter will detail the control strategy for the *PantoScope* force reflecting manipulator system with the objective to provide the widest possible dynamic range. In the following section, we will present the adopted implicit force control scheme, the compensation of disturbing gravitational and frictional effects, and the connection of the force controller to the object impedance models implemented on a remote graphic workstation. The remaining sections will treat human-machine coupled stability and security aspects. We will briefly discuss the practical implementation of the proposed control concepts, and evaluate the realized system with respect to its closed-loop performance. This will allow to compare the controlled prototype force feedback interface with the performance goals stated in chapter 4.

ator and control the force being applied to the operator, and *admittance controlled* systems that detect the force commanded by the operator and control the velocity or displacement of the force reflecting manipulator. The two elementary control concepts, impedance control and admittance control, are schematically depicted in figure 6.1.

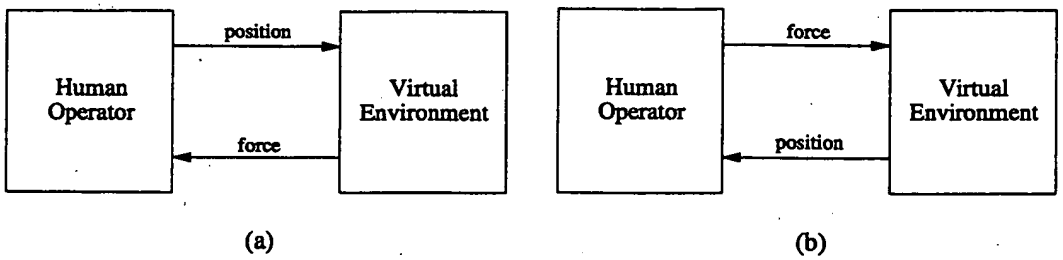

Figure 6.1: Two types of kinesthetic feedback control: (a) impedance control, (b) admittance control.

It is important to recognize that the two control concepts are *not* generally equivalent and thus cannot generally be used interchangeably. Depending on the control scheme adopted, we can either simulate a virtual environment that can be fully described in terms of impedances, or which can be fully represented in terms of admittances. Yet, real physical environments exist which comprise both systems with pure impedance characteristics and systems with pure admittance characteristics [Hogan, 1985]. While a constrained inertial object can always be pushed on, it cannot always be moved. On the opposite, a completely unconstrained and massless object can be freely moved, but cannot resist any forces. Hence, the simulation of ideally rigid walls and the simulation of movement in ideally free space within the same virtual environment are mutually exclusive!

For surgery simulation we need to simulate environments with predominant impedance characteristics, such as weight or motion in free space. Objects with predominant admittance characteristics, such as rigid virtual walls, are less frequently encountered. For the control of the *PantoScope* force feedback system, we have therefore adopted the impedance control concept[18].

---

[18]Note that the actuator and transmission performance requirements in chapters 4 and 5 have been stated in view of the employed impedance control concept. The requirements are somewhat different for admittance control, where the actuators must be good generators of displacement, independent of applied forces.

$\mathbf{f}_{act}$ $n \times 1$ vector of commanded actuator forces[20] expressed in world space,
$\mathbf{x}_r$ $n \times 1$ vector describing manipulator reference position in world space,
$\mathbf{x}$ $n \times 1$ vector describing manipulator actual position in world space,
$\mathbf{K}$ $n \times n$ gain matrix of stiffness coefficients in world space,
$\mathbf{B}$ $n \times n$ gain matrix of damping coefficients in world space,
$\mathbf{f}_b$ $n \times 1$ vector of bias forces expressed in world space.

The linear control law restricts the target behavior to the one of a piecewise linear system[21]. Its implementation requires the specification of $\mathbf{x}_r$, $\mathbf{K}$, $\mathbf{B}$, and $\mathbf{f}_b$. The manipulator's reference position $\mathbf{x}_r$ is the nominal equilibrium position at steady state in the absence of any external and bias forces. The controller gain matrices $\mathbf{K}$ and $\mathbf{B}$ determine the dynamic (elastic and viscous) behavior of the simulated virtual objects. The diagonal elements of each gain matrix define feedback gains about a particular world space axis, off-diagonal elements represent cross-coupled terms. In general, $\mathbf{K}$ and $\mathbf{B}$ are diagonal. $\mathbf{f}_b$ is a position dependent bias force vector which allows to simulate static forces such as gravity.

In the case of the four-degree-of-freedom *PantoScope* force reflecting manipulator, n equals 4. The actual and reference positions of the end-effector defined in world space, $\mathbf{x}$ and $\mathbf{x}_r$, are thus $\mathbf{x} = [\eta \ \mu \ \lambda \ \psi]^T$ and $\mathbf{x}_r = [\eta_r \ \mu_r \ \lambda_r \ \psi_r]^T$. The output force vector $\mathbf{f}_{act}$ describes the forces and moments exerted by the simulated object about the world $\mathbf{x}_0$ and $\mathbf{y}_0$ axes, and along and about the tool $\mathbf{z}_5$ axis: $\mathbf{f}_{act} = \left[\tau_{x_0} \ \tau_{y_0} \ f_{z_5} \ \tau_{z_5}\right]^T$.

The world space control law (6.1) is transformed into actuator and sensor coordinates by means of the forward kinematic equations relating handle position to motor shaft angles, and the forward differential kinematic equations relating handle velocity to shaft angular velocities:

$$\mathbf{x} = \mathbf{a}(\mathbf{q}), \tag{6.2}$$

$$\dot{\mathbf{x}} = \mathbf{J}(\mathbf{q})\,\dot{\mathbf{q}}. \tag{6.3}$$

Thus, using the virtual work principle,

$$\tau_{act} = \mathbf{J}^T(\mathbf{q})\,\mathbf{f}_{act}, \tag{6.4}$$

---

[20] In the following discussion, force refers to force *and* torque, position refers to position *and* orientation.

[21] The parameters $\mathbf{x}_r$, $\mathbf{K}$, $\mathbf{B}$, and $\mathbf{f}_b$ can be dynamically changed, thus the behavior is *piecewise* linear.

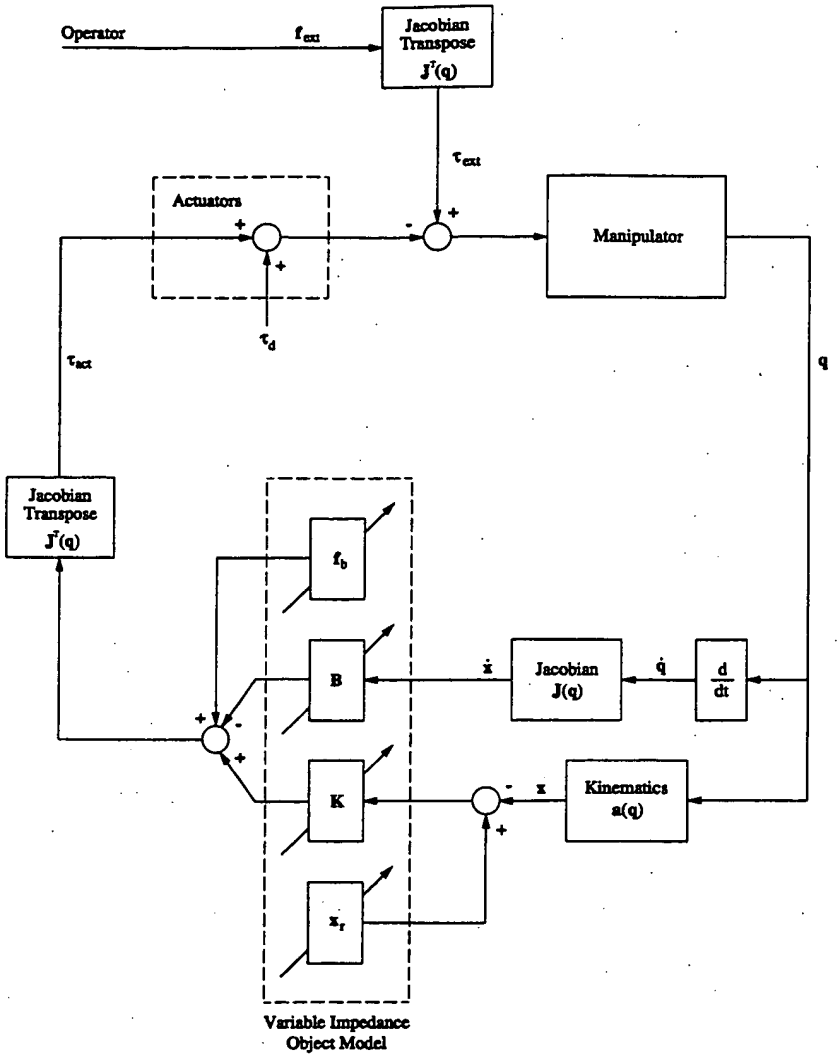

Figure 6.2: Implicit force control scheme.

and from equation (6.6), (6.1), and (6.4) we obtain

$$\begin{aligned}\mathbf{f}_{ext} = \mathbf{K}(\mathbf{x}_r - \mathbf{x}) - \mathbf{B}\dot{\mathbf{x}} + \mathbf{f}_b + \\ + \mathbf{J}^{-T}(\mathbf{q})\left(\mathbf{M}(\mathbf{q})\ddot{\mathbf{q}} + \mathbf{h}(\mathbf{q},\dot{\mathbf{q}}) + \mathbf{b}(\mathbf{q},\dot{\mathbf{q}}) + \mathbf{c}(\mathbf{q})\right) + \mathbf{J}^{-T}(\mathbf{q})\,\tau_d\,.\end{aligned} \tag{6.8}$$

Thus, the forces seen at the manipulator handle comprise not only the desired object force characteristics but also terms accounting for the friction and inertia of the display mechanism. Minimization of manipulator mass and friction is therefore an important issue. Unless the device is of a dynamically decoupled design, Coriolis and centrifugal terms dependent on velocity will further add disturbance forces when velocity is significantly different from zero.

The accompanying control block diagram is depicted in figure 6.3. Note that $\mathbf{c^*(q)}$ can in general be computed at a rate well below the sampling frequency without excessively impeding performance.

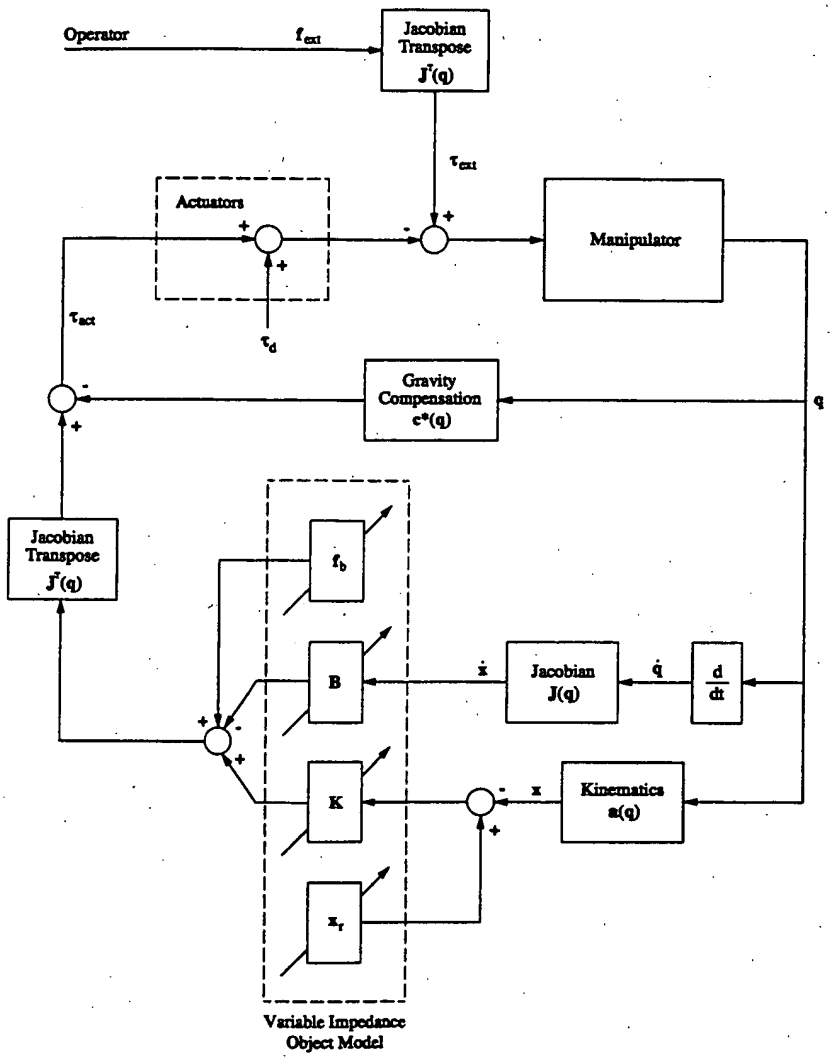

Figure 6.3: Implicit force control scheme including gravity compensation.

Obviously, the feedforward compensation of gravitational effects requires an accurate mathematical model of the considered manipulator. The derivation of the static model of the *PantoScope* force feedback mechanism for the computation of $\mathbf{c^*(q)}$ is presented in appendix C, together with a listing of the various link masses and centers of gravity.

Figure 6.4 shows the required base actuator compensation torques τ_1 and τ_2 for the worst case configuration when the instrument is fully retracted. The maximum nec-

Friction is typically regarded as the sum of three components: static friction or stiction, which is the break-away force required to allow two objects in mutual contact to begin relative motion, Coulomb friction (or dry friction), which is a constant force resisting motion, independent of the magnitude of velocity, and viscous friction, which is a force proportional to the relative velocity of the mutual contact surfaces [Townsend and Salisbury, 1987]. A variety of more elaborated friction models have been discussed by Armstrong [1991]. He demonstrated that some of these effects can be accurately modeled, identified, and compensated for in the control algorithm by means of feedforward compensation torques. We call this type of force control, where explicit force measurement is absent, *open-loop force control*, although the motor current itself may be controlled in a closed loop, and the controller may use motor-position or motor-velocity feedback. The feedforward compensation of friction may lead to excellent results under dynamic conditions, however, Coulomb friction and stiction both are discontinuous functions of velocity with a stepwise variation at zero velocity and can therefore not be compensated for at standstill or during the inversion of speed.

Force control by its nature is often applied in the low or zero velocity range, where the discontinuous characteristics of static and Coulomb friction are most apparent. Many force control implementations rely therefore on force sensor feedback to defeat the transmission and actuator shortcomings of open-loop force control. We call this type of control *closed-loop force control*. The drawback of closed-loop force control is that instabilities and limit-cycles may occur in the presence of firm constraints [Townsend and Salisbury, 1987]. This phenomenon is generally attributed to the fact that the actuators and sensors are typically not attached to the same point on the manipulator and has been termed the *non-collocation problem*. Eppinger and Seering [1987] have shown that any unmodeled dynamics between the actuators and the sensors may lead to instabilities as the loop is closed by the force control law. Stability can be maintained if the net stiffness of the sensor and environment is lower than the stiffness of the manipulator itself, but still only for highly limited bandwidth. High stiffness between actuators and sensors is therefore essential for avoiding limit cycles and instabilities [Armstrong, 1991].

Closed-loop *endpoint force control* involves joint actuator force commands and sensed endpoint force feedback. Since the force feedback is at the endpoint rather than at the actuator, the unmodeled dynamics in the transmission system and links become vitally important. Therefore, often only a low gain, slow closed-loop system can be implemented stably using an endpoint force sensor.

Vischer and Khatib [1990a, 1990b] have shown that a lag controller combined with a feedforward term is most suitable for such zero-order systems. The block diagram for a simple proportional-integral controller with feedforward is shown in figure 6.5.

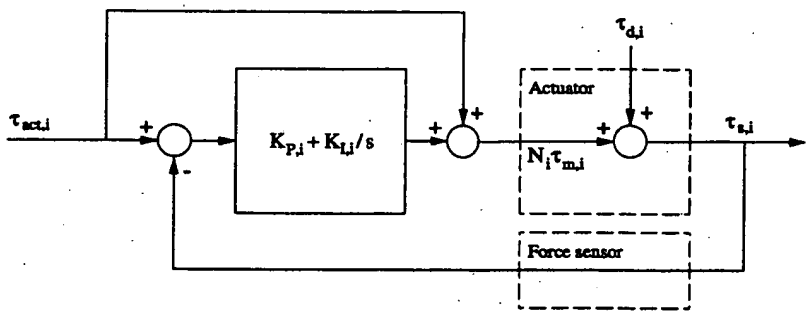

Figure 6.5: Proportional-integral joint torque controller with feed-forward term.

The corresponding control law is

$$N_i \tau_{m,i} = \tau_{act,i} + \left(K_{P,i} + \frac{K_{I,i}}{s} \right) \left(\tau_{act,i} - \tau_{s,i} \right), \tag{6.13}$$

where $K_{P,i}$ and $K_{I,i}$ denote the proportional and integral feedback gains of the torque servo loop around actuator i, and $\tau_{act,i}$ is the commanded actuator torque of actuator i. Thus, the closed-loop transfer function for each joint torque controlled actuator follows from equations (6.12) and (6.13) to

$$\tau_{s,i} \approx \tau_{act,i} + \frac{s}{s\left(1 + K_{P,i}\right) + K_{I,i}} \tau_{d,i} \,. \tag{6.14}$$

The resulting implicit force controller including actuator friction compensation by means of inner joint torque control loops is depicted in figure 6.6.

The manipulator's dynamic behavior follows now to

$$\mathbf{M}(\mathbf{q})\ddot{\mathbf{q}} + \mathbf{h}(\mathbf{q}, \dot{\mathbf{q}}) + \mathbf{b}(\mathbf{q}, \dot{\mathbf{q}}) + \mathbf{c}(\mathbf{q}) = \boldsymbol{\tau}_{ext} - \boldsymbol{\tau}_s \,, \tag{6.15}$$

where $\boldsymbol{\tau}_s$ is the 4×1 vector of sensed actuator output torques and forces. Using equations (6.14) and (6.10), and proceeding analogous to sections 6.2.2 and 6.2.3, the force perceived at the manipulator handle can be computed to

the translational degree of freedom, a simple proportional controller is used with $K_{P,3} = 2.8$ ($K_{I,3} = 0$). No torque servo loop has been closed around the actuator for the instrument's rotational degree of freedom, thus $K_{P,4} = K_{I,4} = 0$. Pre-filtering the inputs and the feedback torques and forces to frequencies below the lowest structural resonance is used to closely approximate the zero-order transfer function assumed in equation (6.12) and removes high frequency noise in the sensor signals.

Clearly, there exists no perfect compensation of frictional effects, the disturbance rejection bandwidth, and thus the feedback gains, would need to be infinity in the case of sudden friction changes such as stiction. It is therefore important to recognize that, although joint friction can be substantially reduced by closed-loop torque control, a wide dynamic range is difficult to achieve without actually reducing the inherent friction and non-linearities in the actuator-transmission stages [Khatib and Roth, 1991].

For the purpose of joint torque control, strain gauge torque sensors have been installed on the transmission output shafts of the two base actuators. The achieved torque sensing resolution exceeds 15mNm over a measurement range of ±4Nm. For the compensation of friction in the hydraulic cylinders and conduits employed for the translational degree of freedom, a commercial six-axes strain gauge force-torque sensor[25] has been installed just below the instrument handle, as shown in figure 6.7. Tension-compression forces at the instrument shaft are measured over a range of ±20N with a force resolution of approximately 0.2N. The characteristics of the employed torque and force sensors are shown in appendix B.5.

6.2.5 Supervisory Control

So far we have been dealing with the issue of how to apply forces as faithfully as possible to the human operator. An implicit force control scheme has been proposed which defines *how* to compute the exerted forces based on the impedance model parameters $\mathbf{K}$, $\mathbf{B}$, $\mathbf{x}_r$, and $\mathbf{f}_b$. Nothing has been said about *where* and *when* these forces are computed, and how the controller parameters are determined.

---

[25] A six-axes force-torque sensor has been employed for reasons of availability. Only one of the six axes is actually used for the compensation of frictional effects in the translational degree of freedom.

Another important issue is the maximum allowable time delay. A fundamental requirement for the feel of presence in a virtual environment is a strong correlation between the operator's hand movements, as perceived kinesthetically, and the corresponding manipulations in the virtual world, as perceived visually and haptically. Rosenberg [1994] has found that time delays as small as 100ms between visual and force feedback already lead to a deteriorated sense of presence.

Finally, issues related to stability and variable computational latency have to be considered. Today's high performance graphic workstations typically are UNIX based systems and lend themselves not particularly well to real-time applications. Since an assured constant force update frequency is difficult to achieve, closing the implicit force control loop via the external graphic workstation leads to reduced reliability and performance, and may cause instability if the update frequency drops below a minimum acceptable level.

The required 300Hz force update rate is clearly out of the range of even state-of-the-art high performance graphic workstations if complex virtual environments implying a large number of object intersections have to be computed[27]. In order to make up for the low force update rate, force interpolation and position prediction techniques for smoothing and anticipating the commanded forces from the graphic workstation have been investigated [Da Lan, 1997]. Although these techniques may lead to considerably enhanced force sensations with smooth force transitions, they cannot improve stability. In fact, they even lower the stability limits due to additional delays.

We therefore propose the *supervisory control scheme* depicted in figure 6.8. In this approach the force control algorithm is split into two loops: a fast internal loop that computes the simulation forces based on the implicit control law of equation (6.1) entirely on the force feedback controller at an update frequency of 500Hz, and a slow external supervisory loop that determines the control parameters $\mathbf{K}$, $\mathbf{B}$, $\mathbf{x}_r$, and $\mathbf{f}_b$ based on the instrument position in world coordinates. The collision detection and organ deformation computations are thus completely separated from the low level implicit force control loop. The graphic workstation is merely acting as system supervisor which sets and constantly updates the implicit force control parameters and transfers data on the operator's manual activity to the video display.

---

[27]On the employed Indigo 2 Extreme™ (100MHz, 32MB RAM) from Silicon Graphics, Inc., the force update rate did not exceed 14-20Hz even for extremely simple scenes.

The flow of information thus forms a closed loop: position sensors track the user's physical motions and relay this information to the controller. The force feedback controller then computes the forces and torques that the user should feel as a result of the physical motion as well as the defined contents and structure of the simulated virtual environment. Haptic sensations are produced by driving the actuators of the force reflecting interface.

The compensation of gravitational effects introduced by the weight of the force feedback manipulator's mechanical structure is achieved by adding feedforward compensation torques to the commanded actuator torques. Actuator friction is compensated for by means of explicit joint torque control loops that are closed around the motors and transmissions. Since the force sensors are not located at the manipulator's handle, friction in the mechanism itself cannot be suppressed. However, this represents no limitation, since, as we have shown in chapter 5.6, friction within the mechanism linkage is very small and thus practically negligible.

Finally, we have considered the connection of the force feedback system with the corresponding graphical simulation environment and the governing organ impedance models. A supervisory control scheme has been proposed that allows to maintain stability even for extremely limited-bandwidth communication to the organ models. Although conceptually simple, the proposed supervisory control scheme represents an important step towards the connection of force and visual feedback with highly differing bandwidth requirements.

6.3 Stability Issues

The quality of a haptic interface is generally reported in terms of the range of sensations or impedances it can produce. Ideally, a haptic display should be able to represent both complete freedom of motion and complete constraint in any direction and at any time. At the low end, the range of achievable impedances is limited by the inherent inertia and friction of the interface. At the high end, the impedance range is typically confined by stability limitations.

Researchers have identified a variety of factors affecting stability in force controlled systems, including sampling rate, sensor resolution, actuator bandwidth and saturation, inherent damping, noise and delay from numerical derivation, backlash, friction, and the non-collocation of actuators and sensors [Eppinger and Seering, 1987] [Minsky et al., 1990][Brooks et al., 1990][Colgate et al., 1993a]. In the following we

Colgate and his colleagues investigated the effects of sampling and interface dynamics on the passivity of a simple one-degree-of-freedom haptic interface, where the position signal is sampled at a rate $1/T$ and the control signal is passed through a zero-order hold. The virtual environment is modeled as a linear combination of virtual stiffness $K \geq 0$ and virtual damping B. Assuming that the manipulator behaves as a rigid body with mass m and viscous friction b, and neglecting amplifier and sensor dynamics and non-linearities, it can be proven that the necessary and sufficient condition[29] for passivity is given by [Colgate and Brown, 1994][Colgate and Schenkel, 1994]:

$$b > \frac{KT}{2} + |B| \,. \tag{6.18}$$

Obviously, the above passivity condition is based on a very simplistic model and is therefore not directly applicable to real multi-degree-of-freedom systems. Effects such as unmodeled dynamics, actuator/sensor non-collocation, and non-linearities as well as couplings in the degrees of freedom may cause non-passive behavior even when equation (6.18) is fulfilled. Conversely, the criterion of passivity is a potentially too conservative property: even if a haptic display is not passive, a human operator may not necessarily be able to destabilize it [Colgate et al., 1993b]. Despite these limitations, the above relationship still provides useful insight in how sampling rate, inherent damping, and stiffness may influence the stability of the operator-coupled system:

- To achieve passivity (and thus assure stability) of a sampled-data system, some inherent viscous damping is important. The greater the interface's internal damping b, the greater is the range of virtual stiffness K and damping B it can produce.
- Given fixed physical damping b and virtual damping B, the maximum achievable virtual stiffness K increases with increasing sampling rate $1/T$.
- For given inherent damping b and sampling time T, higher virtual stiffness K can be achieved at lower values of virtual damping B.

---

[29] It may be argued that a haptic interface implementing a virtual environment whose physical counterpart is passive automatically fulfills the passivity criterion. Yet, this is not true for a sampled-data system! Consider a haptic interface contacting a virtual wall. Due to discrete time control, the wall does not 'turn on' and 'turn off' at precisely the same location. Thus, the act of making and breaking contact can be a source of energy resulting in potential instability.

Figure 6.9 shows the topology of the force feedback controller as actually implemented. The transputer network consists of seven T805 transputers [Inmos, 1989], one of which is connected via a transputer link to a PC serving as console for the transputer developing system. Another two transputers are available for the interface to the virtual reality environment and object force model database implemented on a Silicon Graphics workstation, and an auxiliary force/torque sensor employed for evaluation measurements. Three transputers allow to control up to three force feedback manipulators in parallel and host three copies of the force feedback control routines implementing the algorithms described in section 6.2. The connection to the actuators and sensors is based on a VME bus which interfaces to three axes motion controller boards controlling each up to four actuators and two analog-digital converter boards for reading the strain gauge force and torque sensors. The I/O handling to the VME bus is mapped on a single transputer serving as bus master.

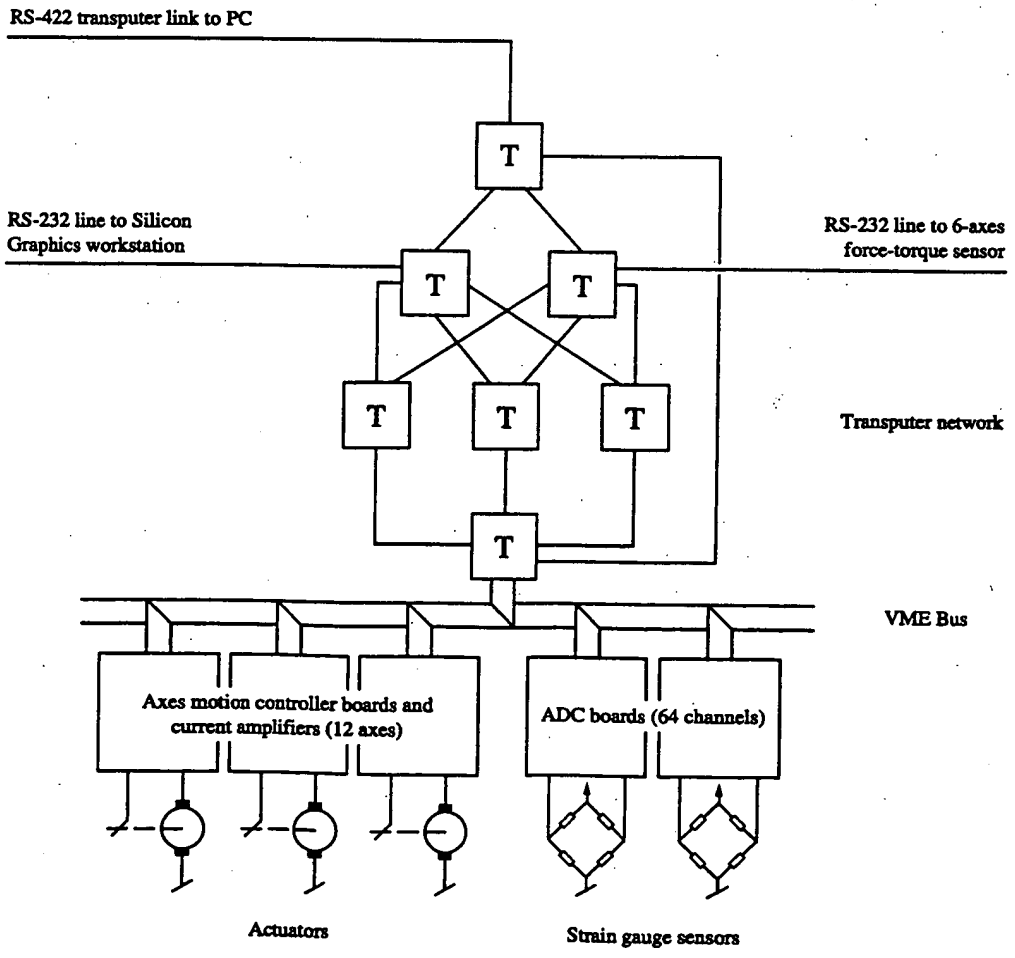

Figure 6.9: Controller hardware architecture.

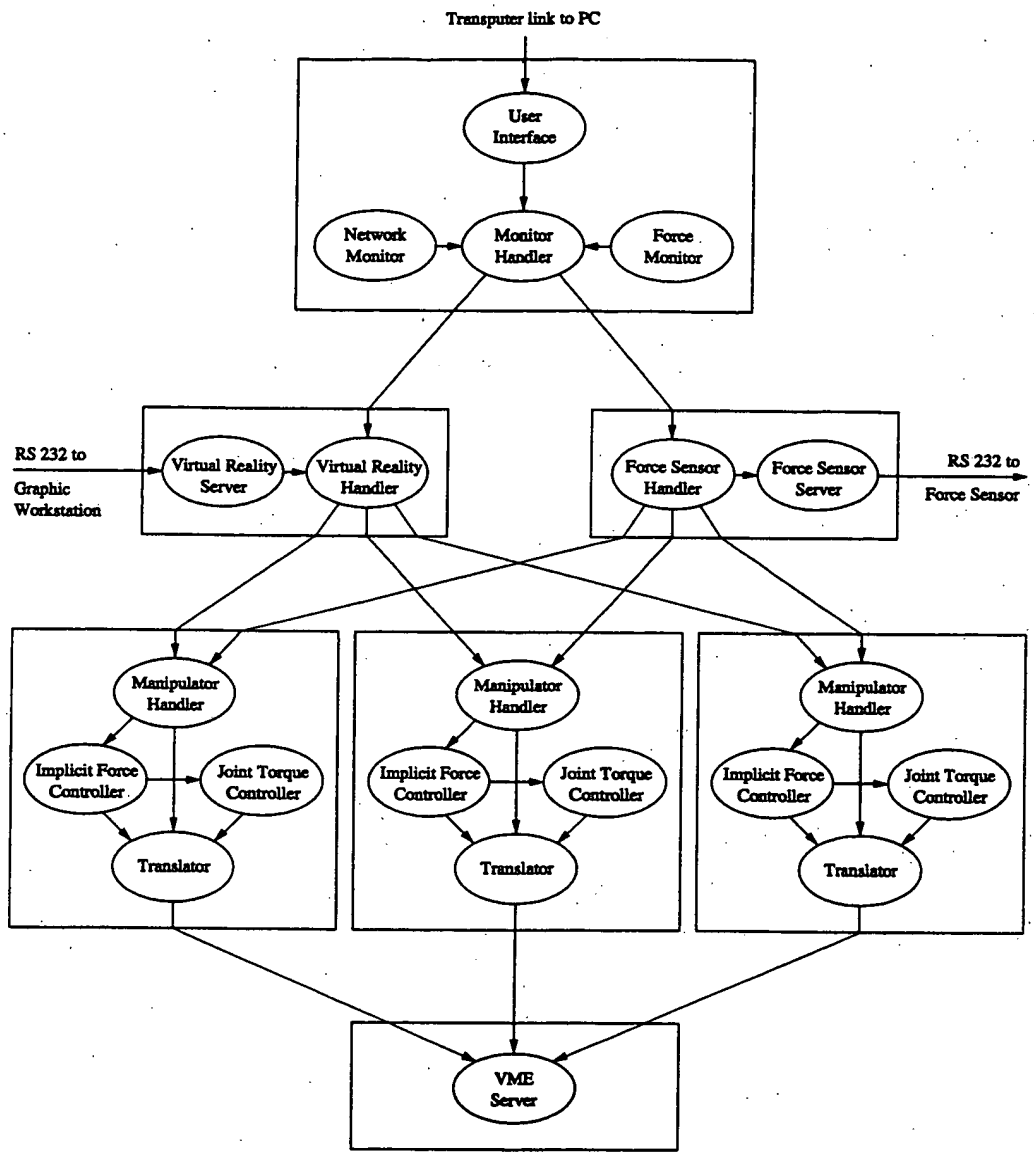

Figure 6.10: Software architecture. Transputers are represented by rectangles, software processes are shown as ellipses. The direction of the arrows indicates the hierarchy of communication.

Network Monitoring routine is constantly observing the transputer network for unexpected system failures by sending test messages to all running processes on the controller. The *Force Monitor* allows to continuously monitor all activities in the controller and to memorize the temporal evolution of the various control variables such as the commanded and actual force at the instrument and the actuators, the instrument's actual position in world and joint coordinates, strain gauge force and torque sensor readings, the controller parameters etc. The user interface allows to subsequently store these data on the disk of the PC for further processing and display.

Forces, accelerations, and velocities should therefore be restricted. During sudden interface fault conditions, there must be faithful detection of errant behavior and effective, reliable reaction to the problem. Although safety issues were not among the most considered concerns during the development of the prototype system, a few basic measures have been implemented to limit potential hazard to the user and damage to the system:

- A very effective passive safety feature is the inherently limited range of motion of the force feedback device. As shown in figure 5.18, the instrument cannot be inclined more than 60° from the vertical due to mechanical limits.

- The maximum peak torque of the actuators has been limited to 4Nm for the trocar degrees of freedom, 20N for the translational degree of freedom, and 100mNm for the rotational degree of freedom by electronically limiting the peak current outputs from the amplifiers.

- Hardwired electronic circuitry opens relays located in the power units if the axes motion controller boards are not accessed at regular time intervals. Thus, on start up of the system, the power units remain switched off until the force control loop is entered. If the registers on the motion controller boards are not updated for more than 500ms during the execution of the force control routines, the power units are shut down.

- Software safety measures include the continuous monitoring of the entire transputer network by means of the network monitoring routine. Dummy messages requiring a response are continuously sent to all processes running. If not all return messages are received within a 100ms time interval the system is shut down.

- The system is equipped with an external panic button that allows to immediately shut down the system by resetting the power relays.

The implemented safety measures proved well adapted to the prototype system under development. Hardware and software fault conditions are reliably detected and the system shut down within at most 500ms. This relatively long response time, however, may be an issue of concern for use of the system in a clinical environment. To ensure safety for human use beyond the development phase, safety issues are worth to be reconsidered.

Figure 6.11a shows typical data collected from the zero force tests with the joint torque controller gains set to zero (friction compensation not activated). The average friction level is approximately 250mNm, with peaks as high as 400mNm. The high torque variations are due to the fact that for certain movements only one of the base motor axes is in motion, while for others both motors are rotating. The trajectory of the handle is shown in figure 6.11b.

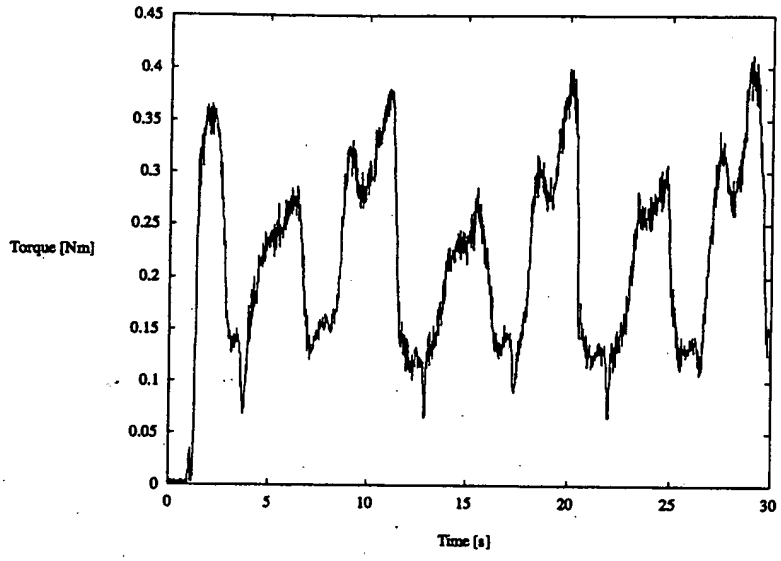

(a)

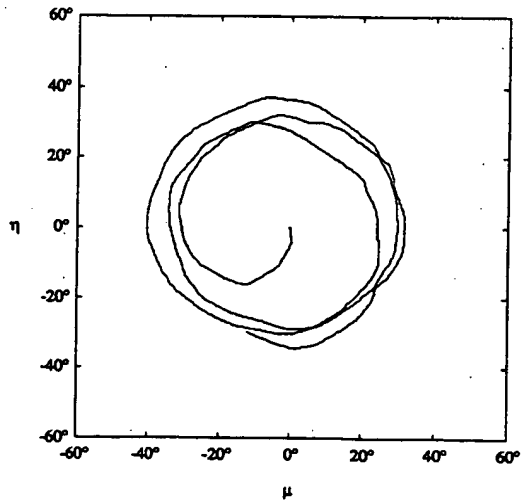

(b)

Figure 6.11: (a) Sensed parasitic torque at instrument handle without friction compensation, (b) handle trajectory represented as a function of η and μ.

The small high-frequency torque ripples of figure 6.12a are not haptically perceptible and do not impede natural and realistic force sensations. Yet, the larger torque peaks may be identified as small, but perceptible jerks. These torque peaks are attributed to the relatively high mechanical time constant of the AXEM™ F9M4R motors introducing delays in the joint torque control loops[32].

6.5.2 Instrument Degrees of Freedom

Force measurements on the instrument's translational degree of freedom confirmed the effectiveness of the joint force control loop around the actuator and hydraulic transmission stage. Figure 6.13 shows the apparent forces at the instrument handle for slow translational up and down movements along the instrument axis with the joint force controller gains set to zero. The weight of the instrument has been compensated for by means of feedforward compensation forces. As expected, we find an average friction level on the order of 3.5N.

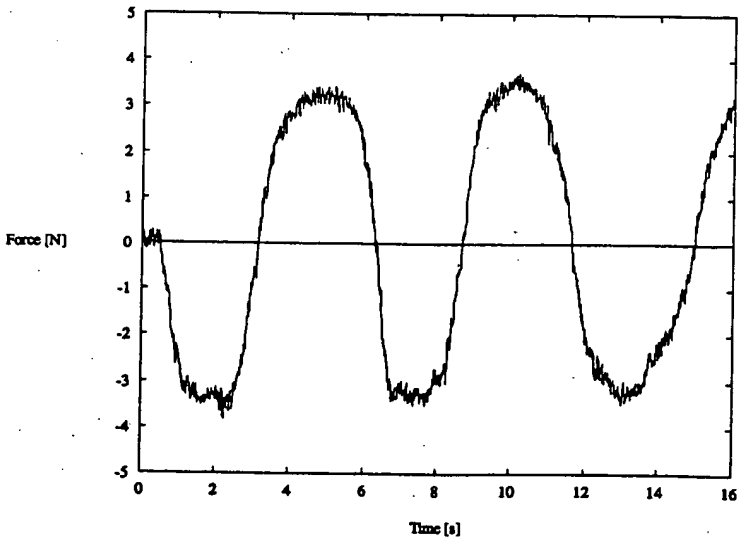

Figure 6.13: Opposing forces at instrument handle for slow translational up and down movements without friction compensation.

---

[32]Our evaluations revealed that such torque peaks are highly attenuated with the use of motors with a sufficiently small mechanical time constant. The alternatively considered escap® HPR3N63 conventional dc motors (see appendix B.2) with a mechanical time constant of 1.6ms, however, suffer from highly disturbing torque ripples due to the small number of commutator bars. Note that a high mechanical time constant does not represent a *general* limitation of printed armature dc actuators.

Continuous force capacity[33]	2Nm / 12N / 0.06Nm
Peak force capacity[33]	4Nm / 20N / 0.10Nm
Force accuracy	<5% (see chapter 7)
Force update rate	500Hz
Force ripple amplitude	1-2% of continuous force capacity
Backdrive friction[33]	1% / 7% / 10% of cont. force capacity
Dynamic range[33]	1:100 / 1:15 / 1:10
Gravitational balancing	yes
Backlash	<2° on rotational dof, otherwise zero
Position resolution[33]	0.0024° / 3.5μm[34] / 0.14°
Position update rate	≈18Hz
Range of motion[33]	cone 100° / 100mm / unlimited
Maximum object stiffness	20-50Nm/rad (see chapter 7)

Table 6.1: Closed-loop characteristics of the PantoScope system.

Universitaire Vaudois, Lausanne), indicate that these shortcomings are not overly disturbing since instrument-trocar movements imply a significant amount of friction also in reality.

6.6 Conclusions

In this chapter we have presented the employed control concept for the four-degree-of-freedom *PantoScope* force reflecting manipulator. Starting with a discussion of the two fundamental kinesthetic feedback control strategies, impedance and admittance control, we have developed a simple and robust implicit force control scheme for virtual object simulations. The time-varying linear control law allows to simulate elastic and viscous dynamic behavior as well as static forces. Underlying joint torque control loops are used to reduce the apparent friction in the actuator-transmission stages, thus providing a wide dynamic range. The weight of the *PantoScope*'s mechanical structure has been compensated for by means of a feedforward gravity compensation scheme. For the connection of the haptic interface to the organ impedance models computed on a remote graphic workstation, a supervisory control scheme has been proposed, which allows to

---

[33]Values refer to the pivoting degrees of freedom, the translational degree of freedom, and the rotational degree of freedom of the force feedback manipulator.

[34]Without consideration of fluid compressibility and conduit deformations in the hydraulic system. The actual resolution is on the order of 1 mm.

7 Experimental Results and Evaluation

The human mind is exquisitely tailored to make sense out of the world. Give it the slightest cue and off it goes, providing explanation, rationalization, understanding.

Donald Norman - *The Design of Everyday Things*

7.1 Introduction

So far, we have characterized our force reflecting interface in terms of quantitatively measurable parameters such as maximum output force, backdrive friction, force and torque ripple, bandwidth, etc. We will now turn to the evaluation of more subjective criteria such as the user's satisfaction with the device in terms of the quality and realism of force sensations. For this purpose, the force feedback system is considered in connection with the graphical simulation environment. In this framework, the ability of the force feedback system to reproduce the behavior of different virtual objects will be investigated. Our own qualitative assessment will be complemented with a more quantitative analysis of the simulated impedances by means of force and torque measurements.

The following section will deal with the simulation of the two fundamental object impedance building blocks, elasticity and viscosity. The ability of the system to convincingly represent virtual springs and dampers will be evaluated, and the influence of important system parameters such as force update rate, computational latency, and position resolution will be discussed. Finally, we will demonstrate the implementation of more sophisticated virtual objects such as virtual walls and discuss first efforts towards the simulation of virtual organic tissue. The chapter concludes with a discussion of the achieved results.

The graphical simulation captures only the salient features of the task that the operator is supposed to carry out in the virtual environment such as moving in a virtual viscous fluid or bumping against a virtual wall[36]. For details on the implementation of the graphical interfaces based on Silicon Graphics' graphics library Perfomer™ [Silicon Graphics, 1994a, 1994b] and the graphics extension library libPTK developed at the Institut de Microtechnique [Nguyen, 1995a, 1995b][Mattei, 1996], the reader is referred to [Da Lan, 1997].

7.2.1 Virtual Springs

For the qualitative analysis of elasticity simulations, the virtual environment depicted in figure 7.2 has been implemented, which allows to probe the behavior of a virtual linear spring represented by a push-button. The spring compliance can be changed dynamically during the simulation allowing for simplified testing and evaluation. Besides haptic feedback on the hand-grip of the *PantoScope*, the user receives visual feedback through the graduation on the 'tower' indicating the magnitude of the actually applied reaction force.

Subjective evaluations of several visitors and students in our lab indicate that different spring elasticities can be simulated in a very convincing way. Smooth, ripple-free behavior without any stepping effects due to sampling has been achieved over a wide range of simulated compliance. Some users, however, complained about the 'slippery feeling' of the push-button due to the lack of simulated surface friction. The low update rate of the stiffness parameters on the order of 14 to 20 Hz does not degrade the stability of the haptic interface. The related delay, however, causes the push-button to feel 'sticky' when releasing it. This is because the stiffness parameter K is only set back to zero at the beginning of the next supervisory sampling period after the instrument tip has been retracted from the spring. Consequently, a small negative spring force is produced, attracting the cursor back to the push-button.

---

[36]For surgery training, an effective visual representation of the virtual environment by means of elaborately detailed and realistic images is clearly indispensable. For testing purposes, however, already a simplistic graphical simulation may entail a sufficiently convincing immersive sense of presence in the virtual world.

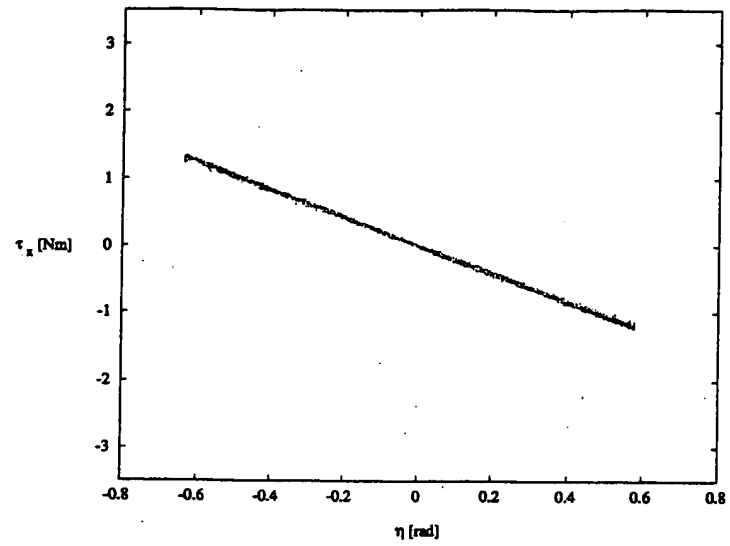

(a)

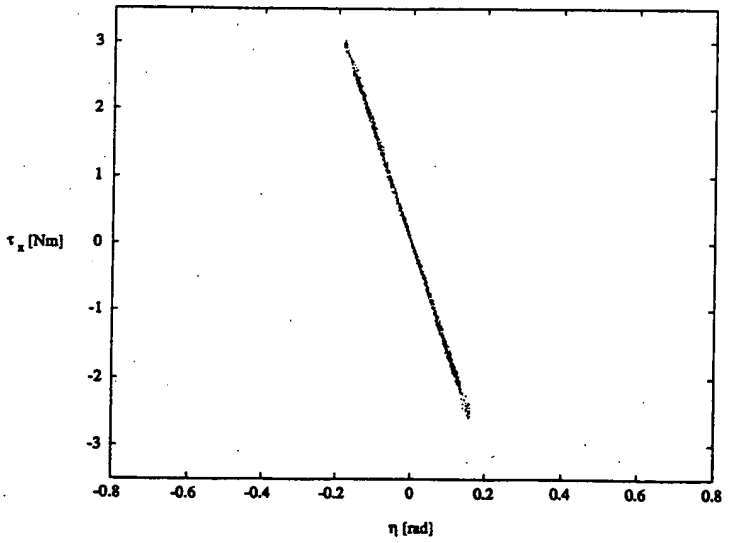

(b)

Figure 7.3: Torque versus angular displacement for (a) low stiffness, $K_\eta = 2\,Nm/rad$, and (b) high stiffness, $K_\eta = 16\,Nm/rad$, spring simulations about the world $\mathbf{x}_0$ axis.

The average stiffness error amounts to 3.3% with a maximum error of 12% at very low impedance settings. Above a stiffness of approximately 36 Nm/rad about the $\mathbf{x}_0$ axis, and 14 Nm/rad about the $\mathbf{y}_0$ axis, the sensations are obstructed by slight vibrations. The system goes unstable for stiffnesses higher than about 50 Nm/rad and 20 Nm/rad, respectively. The highly differing performance about the world $\mathbf{x}_0$ and $\mathbf{y}_0$ axes is attributed to the varying rigidity of the *PantoScope* manipulator with respect to

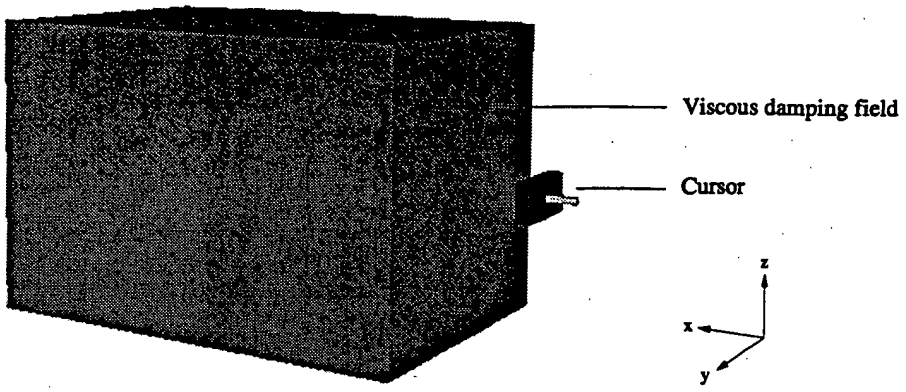

Figure 7.4: Virtual basin of uniform viscous damping.

avoid perceptible vibrations arising from the relatively low velocity resolution[38] of approximately 0.083 rad/s.

Analogous to the stiffness investigations discussed in the preceding section, the capability of the manipulator to simulate viscous damping has been evaluated quantitatively. For this purpose, the damping parameter B of the axis under consideration was set to a constant value, while the damping factors of the other axes and the elements of the stiffness matrix were all kept at zero. Again, the handle was moved back and forth manually. In these tests, however, handle motion was intentionally executed at variable speed in order to achieve a wider range of velocity. Typical data from the viscous damping tests are shown in figure 7.5 for damping factors $B_\eta = 0.1\,\mathrm{Nm/rads^{-1}}$ and $B_\eta = 0.5\,\mathrm{Nm/rads^{-1}}$ about the $\mathbf{x}_0$ axis. In contrast to the elasticity measurements, the damping data contain a significant amount of noise. This is particularly striking near zero velocity, and is mainly attributed to inertial effects at the inversion of speed during the measurement process. Other noise sources are the numerical derivation of the position signal for velocity estimations, and the manual operation of the device during all measurements.

The damping constants for each of the repetitive motion tests were determined from linear regressions of torque against velocity. The results of these regression analyses, averaged from three individual tests at each controller setting, are presented in table

---

[38] The minimal detectable speed v_{min} is related to the position sampling frequency f_s, the resolution of the optical encoders $2\pi/n_{incr}$, and the transmission ratio r_v by $v_{min} = 2\pi f_s/(r_v \cdot n_{incr})$.

Commanded damping [Nm/rads^{-1}]	Measured damping about x_0 axis [Nm/rads^{-1}]	Measured damping about y_0 axis [Nm/rads^{-1}]
0.1	0.094 ± 0.009	0.101 ± 0.002
0.2	0.194 ± 0.003	0.207 ± 0.003
0.3	0.298 ± 0.004	0.307 ± 0.004
0.4	0.381 ± 0.006	0.374 ± 0.036
0.5	0.470 ± 0.011	-

Table 7.2: Commanded and experimentally measured damping about the world x_0 and y_0 axes. Each measurement value is reported as the mean ± standard deviation of the regression slope of measured torque versus angular velocity.

7.2.3 Virtual Walls

The haptic simulation of rigid walls has been demonstrated in a variety of experimental studies [Colgate et al., 1993a][Rosenberg, 1994][Adachi et al., 1994] and has become almost a standard for assessing the achievable impedance range of a force reflecting device. Although the emulation of virtual walls does not immediately relate to the simulation of laparoscopic interventions (except maybe for the simulation of instrument interference), it was taken as a challenge to accomplish the generation of perceptual stimuli such as crispness and hardness.

Inherent hardware limitations such as confined computing power and actuator bandwidth prevent force reflecting interfaces from accurately modeling stiffness values on the order of magnitude of a real rigid surface. Nonetheless, hard walls can be simulated quite effectively when combining stiffness and damping simulations at sufficiently high force update rates. Interestingly enough, virtual wall implementations which strive for closest possible physical modeling of hard contact as hardware constraints allow are not necessarily *perceived* as hardest or most realistic. As has been demonstrated by Rosenberg [1994], the construction of virtual force simulations from a perceptual rather than physical perspective may result in the generation of more convincing wall representations within the hardware limitations of force reflecting systems.

Figure 7.6 shows a schematic image of a wall being contacted by the cursor. The wall is modeled as a massless plate backed by a stiff linear spring, K_w, in parallel with a viscous linear damper, B_w. When the position of the cursor passes the wall boundary

crossing into the wall, in the ideal case bringing the movement to zero. Thus, the new control law is given by

$$f = \begin{cases} K_w(p_r - p_c) - (B_w + m/T)\dot{p}_c & \text{for} \quad p_{c,t} \geq p_r \wedge p_{c,t-T} < p_r, \\ K_w(p_r - p_c) - B_w \dot{p}_c & \text{for} \quad p_c \geq p_r \wedge \dot{p}_c > 0, \\ K_w(p_r - p_c) & \text{for} \quad p_c \geq p_r \wedge \dot{p}_c \leq 0, \\ 0 & \text{otherwise}, \end{cases} \tag{7.3}$$

where T is the sampling period of the implicit force control loop and m the equivalent mass of the moving manipulator including the operator's hand. The latter varies considerably depending on the way the manipulator handle is held; the value of m should therefore be chosen with care in order to prevent the manipulator violently bouncing back from the virtual hard surface in case of unconstrained motion.

The behavior of various virtual wall implementations in accordance with equation (7.3) has been evaluated on the *PantoScope* force feedback device in terms of perceptual naturalness. A record of the exerted torque about the world $\mathbf{x}_0$ axis against instrument tip displacement η is depicted in figure 7.7 for a virtual wall along $\eta = 0$. The particular wall model that has been used here was a parallel combination of a linear spring element with $K_{\eta,w} = 30\,\text{Nm/rad}$ and a directional damper element with $B_{\eta,w} = 0.3\,\text{Nm/rads}^{-1}$; the braking pulse term m/T was set to zero.

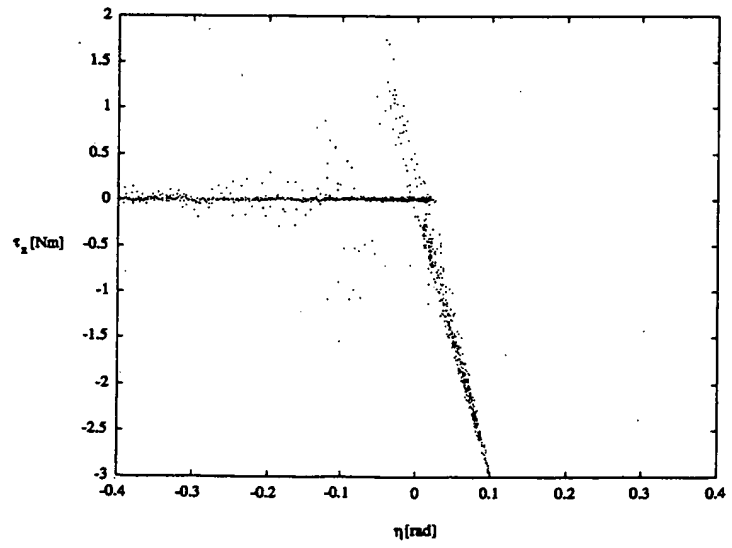

Figure 7.7: Virtual wall along $\eta = 0$: torque measured by the force-torque sensor as the instrument approached, contacted, and rapidly withdrew from the wall over repeated cycles.

thus modeling techniques have to be developed that allow to deal with elastically and plastically deformable objects. Moreover, in order to achieve a visually appealing simulation, textures need to be applied on the organ models.

A challenge by its own is the physical modeling of organ behavior. Figure 7.9 shows our force feedback system together with the graphical representation of a deformed virtual gallbladder. A force profile approach is employed for modeling the dynamic behavior of the organ interacting with the virtual representation of a surgical instrument. All points constituting the three-dimensional envelope of the object are linked together via elastic elements. When a force is applied to a given vertex, all its neighbors will experience a force directly depending on their position relative to the application point and the force profile considered [Marti, 1996].

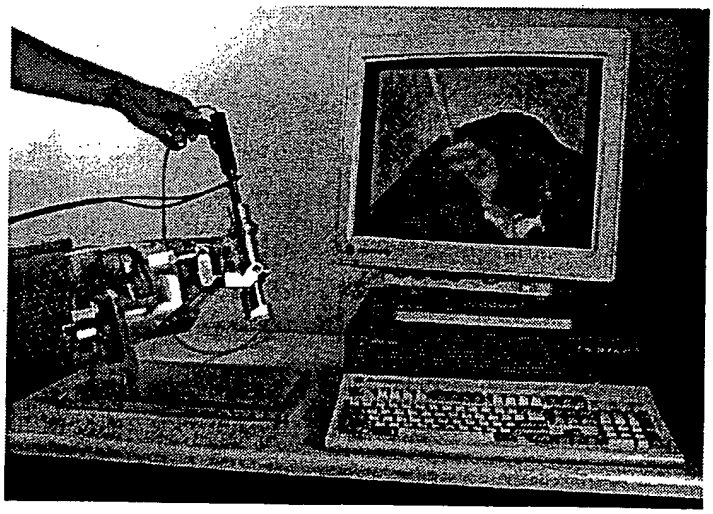

Figure 7.9: Surgery simulation environment representing a three-dimensional model of a deformed virtual gallbladder. The system as depicted is shown for illustration only, and is not actually operational at this level of graphical scene complexity. Due to hardware limitations of the employed graphic workstation, object models incorporating texturing and a large number of vertices cannot be simulated interactively[39].

[39]Interactive graphical simulation including surface texturing has been accomplished on a more powerful graphic workstation [Marti, 1996], but has not been combined yet with the *PantoScope* force feedback system.

The compensation of gravitational effects has proven to be a very effective method to increase the realism of virtual haptic perceptions. A remarkable experiment is to have users moving the manipulator in free space for several minutes and switch off gravity compensation without notice. Several users misinterpreted the sudden perception of the manipulator weight as an odd feeling virtual spring!

The ability to mask actuator friction and other intrinsic mechanical properties by means of the joint torque control concept discussed in chapter 6.2.4 further enhances the fidelity of load simulations. Surfaces feel distinctly slippery, motion in free space is truly unconstrained. The price to be paid for this perceptively more attractive behavior is decreased stability and thus lower maximum allowable stiffness and damping levels. Considering the low accuracy of the human force sensing system, it might be interesting to adapt the joint torque controller gains to the actual simulation force, thus increasing stability without compromising perceptual realism.

A major difficulty in virtual organic tissue simulation is computing time. In order to achieve sufficient realism and accuracy, it is important that object deformations occur in real-time. This aspect is one of the key problems to be solved in order to provide surgeons with an efficient training environment. The employed force profile approach for the generation of deformations in the graphical simulation system may represent a viable solution, realistic physical organ impedance modeling, however, remains an open issue.

7.5 Conclusions

In this chapter, we have investigated the performance of the *PantoScope* force feedback system in terms of its ability to realistically produce various load simulations, such as virtual springs and dampers, virtual hard surfaces, and organic tissue behavior. Although no formal human factor studies have been carried out, our subjective assessment indicates that a wide range of object impedances can be simulated in a highly realistic way.

These qualitative findings have been confirmed by quantitative impedance measurements using a force-torque sensor. It has been shown that the average impedance error is well below 5% of the commanded value for both stiffness and damping simulations; greater errors were measured only for very low impedance settings or towards stability limits. Smooth torque outputs can be achieved up to stiffness values of approximately 36Nm/rad and damping values of about 0.8Nm/rads^{-1} about the x_0 axis, and

8 Conclusions and Outlook

If you can dream it, you can do it.

Walt Disney

8.1 Conclusions

This thesis has detailed the conception, development, realization, and experimental evaluation of a novel force reflecting interface for laparoscopic surgery simulation. It has been demonstrated that a convincing illusion of feel can be created for a variety of virtual object behaviors using a compact, high-bandwidth, and highly backdriveable manipulator combined with a simple, but robust force control concept.

The realized force feedback system contrasts with comparable haptic interfaces primarily in

- its spherical, remote-center-of-motion, hybrid parallel-serial mechanical design, which allows to simulate forces and torques in four degrees of freedom within a particularly large workspace,
- its simple, yet effective implicit force control architecture including the compensation of gravitational effects and actuator and transmission friction by means of high gain joint torque control loops, and
- its connection to the graphical simulation environment by means of a remarkably robust supervisory control scheme that allows to deal with the highly differing bandwidth requirements of the human visual and haptic sensory channels.

and position resolution. Considered as closed-loop force controlled robot, we have investigated in particular the system's capacity to compensate for actuator friction and gravitational effects. Finally, we have examined the manipulator's ability to simulate a variety of impedance characteristics such as virtual springs, dampers, walls, and virtual organic tissue.

This thesis has demonstrated that realistic haptic feedback for minimally invasive surgery simulation is feasible. Yet, the creation of a virtual environment which is completely indistinguishable from the real world is extremely difficult to achieve - a resourceful user will nearly always be able to find some imperfections which distinguish the simulation from reality. The human's haptic senses are so finely developed that even smallest vibrations, torque ripples, and delays can be determined reliably. However, absolute fidelity of haptic sensory feedback to the operator may not be required. As has been shown by other researchers, the sense of presence in a virtual environment is greatly enhanced by combining haptic, visual, and auditory feedback, making the virtual world feel much more real than does each single one component.

8.2 Outlook

During the realization and evaluation of the prototype haptic feedback system described in this thesis, insight was developed on how the system could be improved and further advanced in the future. In the following are listed a few directions for future work:

- One troublesome component of the actual system is the hydraulic transmission used for force reflection on the translational movement of the instrument. The actual design suffers from inter-chamber leakage in the hydraulic cylinders and excessive static friction due to insufficiencies in the mechanical implementation. The dynamic friction scheme proposed in chapter 5 allows to significantly improve backdriveability, but the use of two additional motors is hardly practical and inefficient. Commercially available high-performance cylinder-piston devices may here lead to more serviceable implementations. Hydraulic transmission is however only one of a series of possible alternatives to be further investigated. The combined actuation of the translational and rotational instrument degrees of freedom using ball-screw spline transmissions [Bachofen, 1996] or similar arrangements such as the Doverential™ from Robomatix, Inc. [1988] may lead to very interesting solutions which would allow to avoid hydraulic conduits and to employ standard, traversing surgical instruments. Such an alternative approach is actually being investigated in the course of a continuing project (figure 8.1).

- The simple serial communication line between the force controller and the graphic workstation has proven to be sufficient in the actual system. For more powerful workstations that can compute images and object impedance parameters at a faster rate, however, it may be necessary to provide a higher bandwidth communication channel. As stated in chapter 1, it is planned to extend the surgery training system to a surgery tele-teaching environment based on ATM (asynchronous transfer mode) network technology. ATM may therefore be the method of choice to connect the next generation force feedback interface with the graphical simulation environment. Alternatively, high-end multi-processor graphic workstations may provide the possibility to integrate the force feedback control algorithms and the graphical environment on one and the same host computer, making external data exchange obsolete.

- While the force feedback controller has been conceived to handle up to three four-degree-of-freedom force reflecting devices, as yet only one such device has been built. In order to achieve a truly realistic simulation environment, however, force feedback on more than one surgical instrument is a must. Therefore several haptic interfaces should be realized and integrated into a realistically looking artificial patient. How such a future virtual training environment may look like is depicted in figure 8.2 [Bédat, 1996].

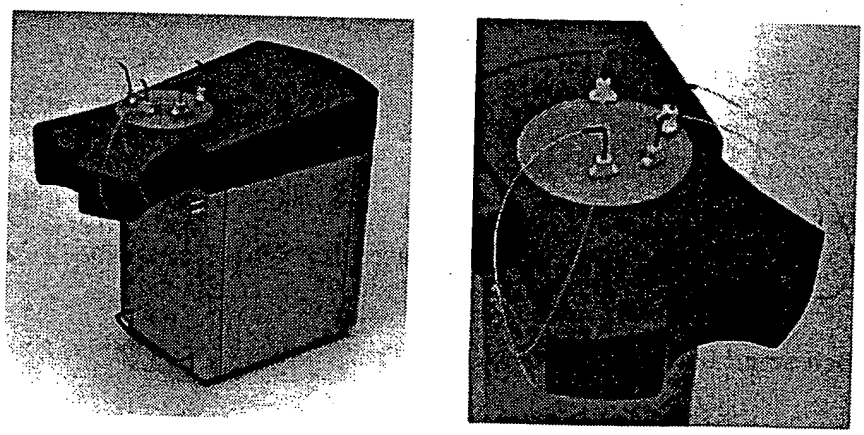

Figure 8.2: Possible design of a surgery simulator hosting several force feedback devices. (Courtesy of Ecole Cantonale d'Art, Bussigny, Switzerland.)

- Finally, the organ impedance representations should be extended to more complex models that allow for more realistic force feedback in four degrees of freedom of motion.

$$yaw = \operatorname{atan2}\left(-o_x, o_y\right), \tag{A.5}$$

$$pitch = \operatorname{atan2}\left(o_z, o_y \cos(yaw) - o_x \sin(yaw)\right), \tag{A.6}$$

$$roll = \operatorname{atan2}\left(a_x \cos(yaw) + a_y \sin(yaw), n_x \cos(yaw) + n_y \sin(yaw)\right). \tag{A.7}$$

The elements of the orientation and position vectors **n**, **o**, **a**, and **p** are computed from t_1, t_2, t_3, t_4 by means of equation (5.9), and these again from q_1, q_2, q_3, and q_4 using equations (5.5) - (5.8).

A.2 Jacobians of the *PantoScope* Manipulator

The Jacobian $\mathbf{J}_1$ relating differential variations in the joint space variables q_1, q_2, q_3, q_4 to differential changes in the intermediate space variables t_1, t_2, t_3, t_4 is

$$\mathbf{J}_1 = \begin{bmatrix} \frac{\partial t_1}{\partial q_1} & \frac{\partial t_1}{\partial q_2} & \frac{\partial t_1}{\partial q_3} & \frac{\partial t_1}{\partial q_4} \\ \frac{\partial t_2}{\partial q_1} & \frac{\partial t_2}{\partial q_2} & \frac{\partial t_2}{\partial q_3} & \frac{\partial t_2}{\partial q_4} \\ \frac{\partial t_3}{\partial q_1} & \frac{\partial t_3}{\partial q_2} & \frac{\partial t_3}{\partial q_3} & \frac{\partial t_3}{\partial q_4} \\ \frac{\partial t_4}{\partial q_1} & \frac{\partial t_4}{\partial q_2} & \frac{\partial t_4}{\partial q_3} & \frac{\partial t_4}{\partial q_4} \end{bmatrix} = \begin{bmatrix} 0 & 1 & 0 & 0 \\ U & V & 0 & 0 \\ 0 & 0 & 1 & 0 \\ 0 & 0 & 0 & 1 \end{bmatrix}, \tag{A.8}$$

where

$$U = \frac{-\cos(q_2)\sec^2(q_1)\sin(\rho)}{\sin^2(\rho) + \left(\sin(q_2)\cos(\rho) - \cos(q_2)\tan(q_1)\right)^2}, \tag{A.9}$$

$$V = \frac{\sin(\rho)\left(\cos(q_2)\cos(\rho) + \sin(q_2)\tan(q_1)\right)}{\sin^2(\rho) + \left(\sin(q_2)\cos(\rho) - \cos(q_2)\tan(q_1)\right)^2}. \tag{A.10}$$

$$n_x = \sin(t_4)\big(\sin(t_1)\sin(\sigma) - \cos(t_1)\cos(\sigma)\sin(\rho/2)\big) + \cos(t_4)\begin{pmatrix}\cos(t_2)\cos(\sigma)\cos(\rho/2) - \\ \sin(t_2)\big(\cos(t_1)\sin(\sigma) + \sin(t_1)\cos(\sigma)\sin(\rho/2)\big)\end{pmatrix}, \tag{A.21}$$

$$o_x = \cos(t_4)\big(\sin(t_1)\sin(\sigma) - \cos(t_1)\cos(\sigma)\sin(\rho/2)\big) - \sin(t_4)\begin{pmatrix}\cos(t_2)\cos(\sigma)\cos(\rho/2) - \\ \sin(t_2)\big(\cos(t_1)\sin(\sigma) + \sin(t_1)\cos(\sigma)\sin(\rho/2)\big)\end{pmatrix}, \tag{A.22}$$

and

$$\frac{\partial a_x}{\partial t_1} = -\cos(t_2)\big(\sin(t_1)\sin(\sigma) - \cos(t_1)\cos(\sigma)\sin(\rho/2)\big), \tag{A.23}$$

$$\frac{\partial a_x}{\partial t_2} = -\sin(t_2)\big(\cos(t_1)\sin(\sigma) + \sin(t_1)\cos(\sigma)\sin(\rho/2)\big) + \cos(t_2)\cos(\sigma)\cos(\rho/2), \tag{A.24}$$

$$\frac{\partial a_y}{\partial t_1} = -\cos(t_1)\cos(t_2)\cos(\rho/2), \tag{A.25}$$

$$\frac{\partial a_y}{\partial t_2} = \cos(t_2)\sin(\rho/2) + \sin(t_1)\sin(t_2)\cos(\rho/2), \tag{A.26}$$

$$\frac{\partial a_z}{\partial t_1} = -\cos(t_2)\big(\sin(t_1)\cos(\sigma) + \cos(t_1)\sin(\sigma)\sin(\rho/2)\big), \tag{A.27}$$

$$\frac{\partial a_z}{\partial t_2} = -\sin(t_2)\big(\cos(t_1)\cos(\sigma) - \sin(t_1)\sin(\sigma)\sin(\rho/2)\big) - \cos(t_2)\sin(\sigma)\cos(\rho/2), \tag{A.28}$$

$$\frac{\partial n_x}{\partial t_1} = \sin(t_4)\big(\cos(t_1)\sin(\sigma) + \sin(t_1)\cos(\sigma)\sin(\rho/2)\big) + \cos(t_4)\big(\sin(t_2)\big(\sin(t_1)\sin(\sigma) - \cos(t_1)\cos(\sigma)\sin(\rho/2)\big)\big), \tag{A.29}$$

$$\frac{\partial n_x}{\partial t_2} = -\cos(t_4)\begin{pmatrix}\sin(t_2)\cos(\sigma)\cos(\rho/2) + \\ \cos(t_2)\big(\cos(t_1)\sin(\sigma) + \sin(t_1)\cos(\sigma)\sin(\rho/2)\big)\end{pmatrix}, \tag{A.30}$$

$$\frac{\partial o_x}{\partial t_1} = \cos(t_4)\big(\cos(t_1)\sin(\sigma) + \sin(t_1)\cos(\sigma)\sin(\rho/2)\big) - \sin(t_4)\big(\sin(t_2)\big(\sin(t_1)\sin(\sigma) - \cos(t_1)\cos(\sigma)\sin(\rho/2)\big)\big), \tag{A.31}$$

$$\frac{\partial o_x}{\partial t_2} = \sin(t_4)\begin{pmatrix}\sin(t_2)\cos(\sigma)\cos(\rho/2) + \\ \cos(t_2)\big(\cos(t_1)\sin(\sigma) + \sin(t_1)\cos(\sigma)\sin(\rho/2)\big)\end{pmatrix}. \tag{A.32}$$

B.2 Characteristics of escap® HPR 3N63-000-73 DC Motors

The characteristics of the escap® HPR 3N63-000-73 dc motors (Portescap, Inc., Switzerland), which have been investigated for actuation of the *PantoScope*'s pivoting degrees of freedom, are listed in table B.2. Note the particularly low mechanical time constant indicating a high bandwidth.

Voltage, nominal	42 V
Speed, nominal	3800 min^{-1}
Torque, nominal	0.23 Nm
Current, nominal	3.5 A
Power, nominal	90 W
Peak torque	2.05 Nm
Max. sustained torque (motor blocked)	0.225 Nm
Torque constant	0.076 Nm/A
Back emf	8.29 V / 1000 min^{-1}
Winding resistance	2.75 Ω (25°C), 4.15 Ω (155°C)
Winding inductance	0.4 mH
Inertia	$36.7 \cdot 10^{-7}$ kgm^2
Mechanical time constant	1.6 ms
Weight	1.36 kg
Volume	70 mm diameter, 87 mm length
Number of collector segments	13

Table B.2: Characteristics of escap® *HPR 3N63-000-73 iron-free dc motors [Portescap, 1995].*

B.3 Characteristics of escap® 35NT2R 82 DC Motor

The characteristics of the escap® 35NT2R82 dc motor with iron-free rotor from Portescap, Inc., Switzerland, are listed in table B.3. This motor is used for actuation of the instrument's translational degree of freedom.

B.4 Characteristics of MINIMOTOR 1724-012S-123 DC Motor and 16/7 Planetary Gear Reducer

Tables B.4 and B.5 show the characteristics of the MINIMOTOR conventional dc motor 1724-012S-123 and the MINIMOTOR 16/7 planetary gear reducer from Minimotor, Inc., Switzerland, used for actuation of the instrument's rotational degree of freedom.

B.5 Characteristics of Strain Gauge Torque and Force Sensors

Strain gauge torque and force sensors are installed on the *PantoScope*'s base drive axes after the cable transmission stages, and on the instrument shaft below the handle. These sensors are used for the compensation of friction and parasitic torques in the actuator-transmission stages. The torque sensors 1 and 2 (Schläpfer Messtechnik, Inc., Switzerland) are employed to measure base axes output torques, whereas a commercial six-axes force-torque sensor (Schunk Intec, Inc., Switzerland) is used to measure tension-compression forces in the instrument shaft. Figures B.1 - B.3 show the determined measurement errors of the strain gauge sensors over the working range of ±4 Nm and ±20 N, respectively. In order to exclude temperature drifting effects, the sensors were reset prior to each measurement.

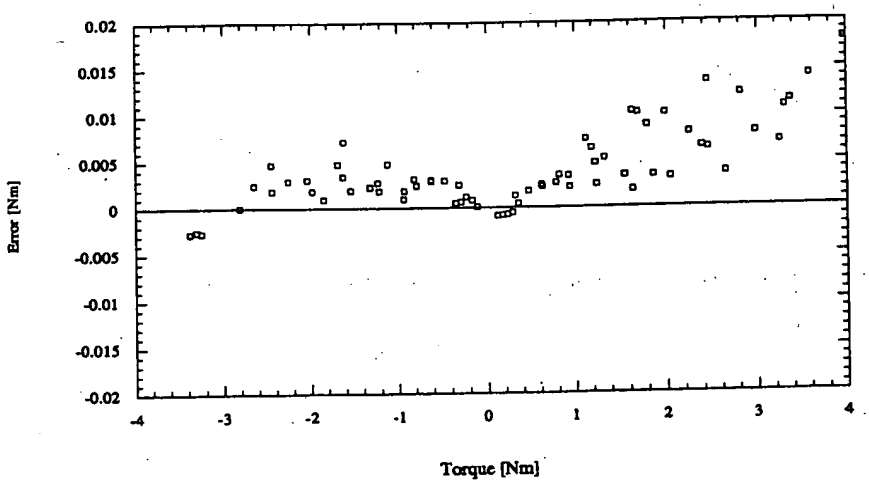

Figure B.1: Torque error of torque sensor 1 as function of reference torque.

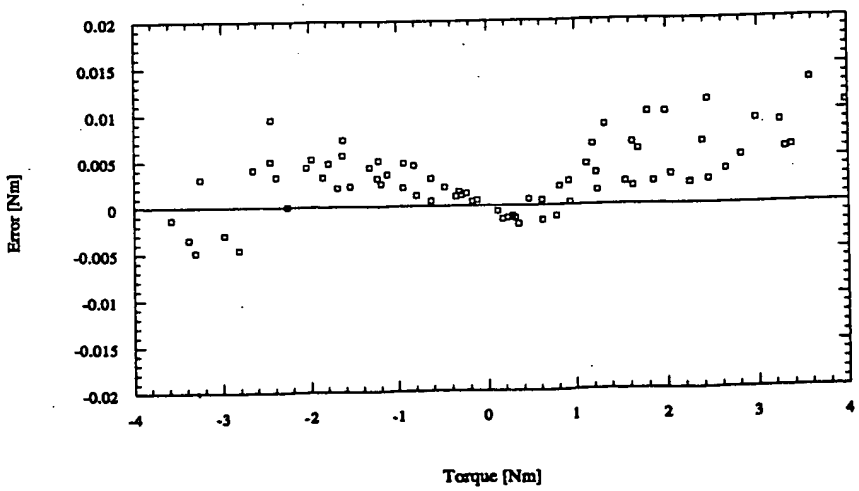

Figure B.2: Torque error of torque sensor 2 as function of reference torque.

Appendix C Gravity Compensation

As shown in section 6.2.3, the feedforward compensation of disturbing gravitational effects requires the computation of position dependent offset joint torques and forces $\mathbf{c}^*(\mathbf{q})$ that counterbalance the weight of the mechanical structure:

$$\mathbf{c}^*(\mathbf{q}) = [\tau_1 \; \tau_2 \; f_3 \; \tau_4]^T. \tag{C.1}$$

For this purpose we determine the weight m_i and center of mass $\mathbf{r}_i$ of each link i with respect to link fixed coordinate frames $(\mathbf{x}_i, \mathbf{y}_i, \mathbf{z}_i)$ as depicted in figure C.1. The link fixed reference frames are defined such that their origins all lie within the respective arm plane, this is the $\mathbf{x}_L$-$\mathbf{z}_L$ plane for all links belonging to the left drive chain, and the $\mathbf{x}_R$-$\mathbf{z}_R$ plane for all links belonging to the right drive chain. The trocar and instrument are counted to the right drive chain.

We then transform the position vectors of the centers of gravity of the left *PantoScope* drive arm into the frame $\mathcal{L}(\mathbf{x}_L, \mathbf{y}_L, \mathbf{z}_L)$ fixed to the left arm plane:

$$^L\mathbf{r}_1 = \mathrm{Trans}(^L\mathbf{r}_A)\, ^1\mathbf{r}_1, \tag{C.2}$$

$$^L\mathbf{r}_2 = \mathrm{Trans}(^L\mathbf{r}_A)\, \mathrm{Rot}(\mathbf{y}, t_2')\, ^2\mathbf{r}_2, \tag{C.3}$$

$$^L\mathbf{r}_3 = \mathrm{Trans}(^L\mathbf{r}_B)\, \mathrm{Rot}(\mathbf{y}, t_2')\, ^3\mathbf{r}_3, \tag{C.4}$$

$$^L\mathbf{r}_4 = \mathrm{Trans}(^L\mathbf{r}_D)\, \mathrm{Rot}(\mathbf{y}, -\varepsilon)\, ^4\mathbf{r}_4. \tag{C.5}$$

Similarly, the position vectors of the centers of gravity of the right drive arm are transformed into the frame $\mathcal{R}(\mathbf{x}_R, \mathbf{y}_R, \mathbf{z}_R)$ fixed to the right arm plane:

$$^{\mathcal{R}}\mathbf{r}_5 = \mathrm{Trans}\left(^{\mathcal{R}}\mathbf{r}_C\right)\,^5\mathbf{r}_5\,, \tag{C.6}$$

$$^{\mathcal{R}}\mathbf{r}_6 = \mathrm{Trans}\left(^{\mathcal{R}}\mathbf{r}_C\right)\mathrm{Rot}(\mathbf{y},t_2)\,^6\mathbf{r}_6\,, \tag{C.7}$$

$$^{\mathcal{R}}\mathbf{r}_7 = \mathrm{Trans}\left(^{\mathcal{R}}\mathbf{r}_D\right)\mathrm{Rot}(\mathbf{y},-\varepsilon)\,^7\mathbf{r}_7\,, \tag{C.8}$$

$$^{\mathcal{R}}\mathbf{r}_8 = \mathrm{Rot}(\mathbf{y},t_2)\,^8\mathbf{r}_8\,, \tag{C.9}$$

$$^{\mathcal{R}}\mathbf{r}_9 = \mathrm{Rot}(\mathbf{y},t_2)\,\mathrm{Trans}(0,0,q_3)\,^9\mathbf{r}_9\,, \tag{C.10}$$

where (from section 5.3.2)

$$t_2 = \mathrm{atan2}\left(\cos(\rho)\sin(q_2)-\cos(q_2)\tan(q_1),\sin(\rho)\right), \tag{C.11}$$

$$t_2' = \mathrm{atan2}\left(-\cos(\rho)\sin(q_1)+\cos(q_1)\tan(q_2),\sin(\rho)\right). \tag{C.12}$$

The gravity disturbance torques about the $\mathbf{x}_{\mathcal{L}}$ and $\mathbf{y}_{\mathcal{L}}$ axes, and the $\mathbf{x}_{\mathcal{R}}$ and $\mathbf{y}_{\mathcal{R}}$ axes[40] are then computed to

$$^{\mathcal{L}}\tau_{x_{\mathcal{L}}} = \left(\sum_{i=1}^{4} {}^{\mathcal{L}}\mathbf{r}_i \times \left(m_i\,{}^{\mathcal{L}}\mathbf{g}\right)\right)_x, \tag{C.13}$$

$$^{\mathcal{L}}\tau_{y_{\mathcal{L}}} = \left(\left({}^{\mathcal{L}}\mathbf{r}_2 - {}^{\mathcal{L}}\mathbf{r}_A\right)\times\left(m_2\,{}^{\mathcal{L}}\mathbf{g}\right)+\left({}^{\mathcal{L}}\mathbf{r}_3 - {}^{\mathcal{L}}\mathbf{r}_B\right)\times\left(m_3\,{}^{\mathcal{L}}\mathbf{g}\right)+{}^{\mathcal{L}}\mathbf{r}_D\times\left(m_4\,{}^{\mathcal{L}}\mathbf{g}\right)\right)_y, \tag{C.14}$$

and

$$^{\mathcal{R}}\tau_{x_{\mathcal{R}}} = \left(\sum_{i=5}^{9} {}^{\mathcal{R}}\mathbf{r}_i \times \left(m_i\,{}^{\mathcal{R}}\mathbf{g}\right)\right)_x, \tag{C.15}$$

$$^{\mathcal{R}}\tau_{y_{\mathcal{R}}} = \left(\left({}^{\mathcal{R}}\mathbf{r}_6 - {}^{\mathcal{R}}\mathbf{r}_C\right)\times\left(m_6\,{}^{\mathcal{R}}\mathbf{g}\right)+{}^{\mathcal{R}}\mathbf{r}_D\times\left(m_7\,{}^{\mathcal{R}}\mathbf{g}\right)+{}^{\mathcal{R}}\mathbf{r}_8\times\left(m_8\,{}^{\mathcal{R}}\mathbf{g}\right)+{}^{\mathcal{R}}\mathbf{r}_9\times\left(m_9\,{}^{\mathcal{R}}\mathbf{g}\right)\right)_y, \tag{C.16}$$

where $^{\mathcal{L}}\mathbf{g}$ and $^{\mathcal{R}}\mathbf{g}$ are the gravity vector $^{o}\mathbf{g} = [0,0,-g]^{\mathrm{T}}$ expressed in the $\mathcal{L}$ and $\mathcal{R}$ frames, respectively:

$$^{\mathcal{L}}\mathbf{g} = \mathrm{Rot}(\mathbf{x},-q_1)\,\mathrm{Rot}(\mathbf{z},\rho/2)\,\mathrm{Rot}(\mathbf{y},-\sigma)\,^{o}\mathbf{g}\,, \tag{C.17}$$

$$^{\mathcal{R}}\mathbf{g} = \mathrm{Rot}(\mathbf{x},-q_2)\,\mathrm{Rot}(\mathbf{z},-\rho/2)\,\mathrm{Rot}(\mathbf{y},-\sigma)\,^{o}\mathbf{g}\,, \tag{C.18}$$

---

[40]Note that the gravity torques about the $\mathbf{z}_{\mathcal{L}}$ and $\mathbf{z}_{\mathcal{R}}$ axes are resisted entirely by the mechanical structure and do not contribute to the torques seen at the actuators.

Link	Designation	Weight m_i [g]	G'Center r_i [mm]	Comment
1	Base axis left	93.17	x = -9.06 y = 0.00 z = -1.29	Includes 2 axes and 4 bearings.
2	Vertical link left (back)	34.86	x = 1.89 y = 0.00 z = -27.04	
3	Vertical link left (front)	37.31	x = -2.12 y = 0.00 z = -24.19	
4	Forearm left	117.27	x = 43.03 y = -10.38 z = -14.94	Includes 3 axes and 6 bearings.
5	Base axis right	45.95	x = 0.09 y = 0.00 z = 0.20	Includes 1 axis and 2 bearings.
6	Vertical link right	40.85	x = 0.45 y = 0.00 z = -26.26	
7	Forearm right	107.10	x = 50.80 y = 14.04 z = -15.06	Includes 2 axes and 4 bearings.
8	Trocar	545.57	x = 0.00 y = -1.25 z = -24.50	
9	Instrument	366.43	x = 0.00 y = 0.00 z = 72.49	Instrument without scissor handles.

Table C.1: Link masses and centers of gravity of the PantoScope prototype.

Parameter	Value	Comment
${}^{L}\mathbf{r}_{A}$	$[77.35 \quad 0 \quad -2.17]^{T}$ mm	Position vector of point A with respect to the left arm frame.
${}^{L}\mathbf{r}_{B}$	$[57.85 \quad 0 \quad -5.63]^{T}$ mm	Position vector of point B with respect to the left arm frame.
${}^{R}\mathbf{r}_{C}$	$[77.35 \quad 0 \quad -2.17]^{T}$ mm	Position vector of point C with respect to the right arm frame.
${}^{T}\mathbf{r}_{D}$	$[0 \quad 0 \quad -45.0]^{T}$ mm	Position vector of point D with respect to the trocar frame.
ε	10°	Base axes inclination angle with respect to the horizontal.
ρ	60°	Angle between the base axes.

Table C.2: Geometric parameters of the PantoScope prototype.

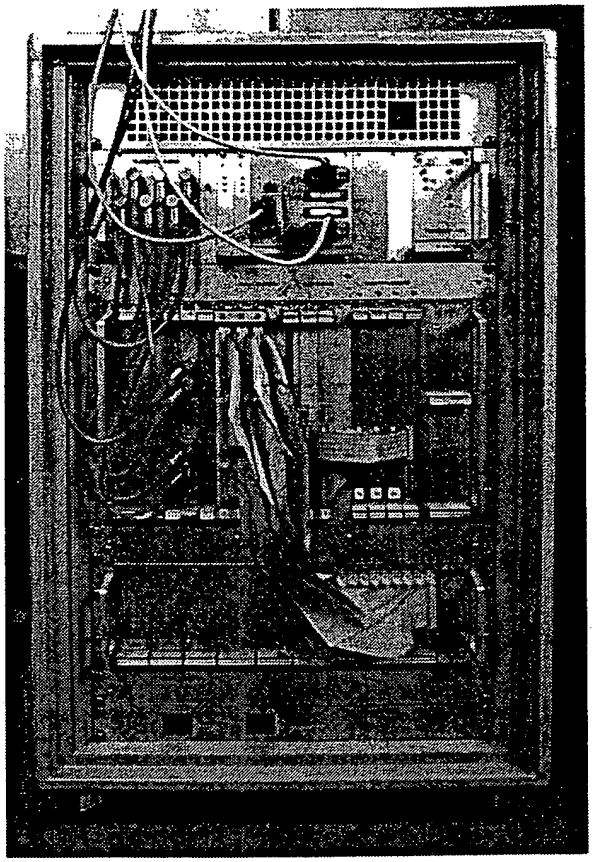

Figure D.1: Force feedback controller.

When data is passed between two processes, the output process does not proceed until the input process is ready and vice versa. Thus, channel communication is synchronous and a separate method for synchronization is not required.

Channels may be used independent of the actual physical location of the communicating processes. If two processes are executing on the same transputer, channel communication is achieved by means of memory to memory data transfer. If two processes are executing on different transputers, one of the transputer's serial links is employed for channel communication. During code development, external and internal channels can be treated identically. Knowledge of the specific hardware configuration is only needed at runtime when the processes are allocated to specific processors.

For further information on the T805 transputer and the employed MTM-2-11, TPM-IO, and BBK-V2 transputer boards from Parsytec, Inc., Germany, the reader is referred to the respective user manuals and technical documentations [Inmos, 1989] [Parsytec, 1988, 1989, 1991a].

D.2 Graphic Workstation

All experiments including external organ impedance computations and graphical simulations have been performed on a Silicon Graphics Indigo2™ workstation (100MHz, 32MB RAM, IRIX 5.3) equipped with a GU1 Extreme™ graphics board. The graphics programs have been built upon the graphics application library PTK 2.0, developed in-house [Nguyen, 1995a, 1995b][Mattei, 1996], and the Performer™ 2.0 graphics library of Silicon Graphics, Inc. [1994a, 1994b].

Baumann R., J.-F. Cuttat, 1995, "Cahier des charges d'un système de retour de force pour simulateur de chirurgie laparoscopique", Internal report, Institut de Microtechnique, Ecole Polytechnique Fédérale de Lausanne EPFL, Switzerland.

Baumann R., D. Glauser, D. Tappy, C. Baur, R. Clavel, 1996a, "Force Feedback for Virtual Reality Based Minimally Invasive Surgery Simulator", in S.J. Weghorst, H.B. Sieburg, K.S. Morgan (Eds.), *Medicine Meets Virtual Reality - Health Care in the Information Age*, IOS Press, Amsterdam, pp. 564-579.

Baumann R., C. Baur, D. Glauser, R. Clavel, 1996b, "The EPFL Laparoscopic Surgery Simulator", *Proceedings Journées de Microtechnique*, Lausanne, Switzerland, Bulletin ASMT, No. 20, pp. 60-68.

Baumann R., W. Maeder, D. Glauser, R. Clavel, 1997, "The *PantoScope*: A Spherical Remote-Center-of-Motion Parallel Manipulator for Force Reflection", *Proceedings IEEE International Conference on Robotics and Automation*, Albuquerque, NM, pp. 718-723.

Basso A., O. Verscheure, R. Noro, J.P. Hubaux, R. Meuli, R. Laurini, P. Patthéy, 1996, "A Multimedia Architecture for Medical Tele-Imaging over ATM", *Proceedings CAR'96*, Paris, France.

Bédat C., 1996, "Patient simulé PATSI", Diploma project, Ecole Cantonale d'Art, Bussigny, Switzerland.

Bejczy A.K., 1980, "Sensors, Controls, and Man-Machine Interface for Advanced Teleoperation", *Science*, Vol. 208, No. 4450, pp. 1327-1335.

Bejczy A.K., J.K. Salisbury, Jr., 1980, "Kinesthetic Coupling Between Operator and Remote Manipulator", *Advances in Computer Technology*, Vol. 1, pp. 197-211.

Bergamasco M., 1992, "Design of Hand Force Feedback Systems for Glove-like Advanced Interfaces", *Proceedings IEEE International Workshop on Robot and Human Communication, RoMan'92*, pp. 286-293.

Bergamasco M., B. Allotta, L. Bosio, L. Ferretti, G. Parrini, G.M. Prisco, F. Salsedo, G. Sartini, 1994, "An Arm Exoskeleton System for Teleoperation and Virtual Environment Applications", *Proceedings IEEE International Conference on Robotics and Automation*, San Diego, CA, pp. 1449-1455.

Bergamasco M., G.M. Prisco, 1995, "An Experimental Approach to Virtual Surfaces Exploration Exploiting an Arm Exoskeleton as Haptic Interface, *Telemanipulator and Telepresence Technologies*, SPIE, Vol. 2590, pp. 172-182.

Bergamasco M., 1997, "Virtual Environments and Telepresence", Oral presentation, Mechatronik Seminar, Eidgenössische Technische Hochschule ETH, Zurich, Switzerland, January.

Bolanowsky S.J., Jr., G.A. Gescheider, R.T. Verrillo, C.M. Checkosky, 1988, "Four Channels Mediate the Mechanical Aspects of Touch", *Journal of the Acoustical Society of America*, Vol. 84, No. 5, pp. 1680-1694.

Boston Dynamics, Inc., 1996, "VR Anastomosis Simulation", Company brochure, Cambridge, MA.

Brooks F.P., Jr., 1988, "Grasping Reality Through Illusion - Interactive Graphics Serving Science", *Proceedings Fifth Conference on Human Factors in Computing Systems*, Washington, DC, pp. 1-11.

Brooks F.P., Jr., M. Ouh-Young, J.J. Batter, P.J. Kilpatrick, 1990, "Project GROPE - Haptic Displays for Scientific Visualization", *Computer Graphics*, Vol. 24, No. 4, pp. 177-185.

Brooks T.L., 1990, "Telerobotic Response Requirements", *Proceedings IEEE International Conference on Systems, Man, and Cybernetics*, Los Angeles, CA, pp. 113-120.

Colgate J.E., J.M. Brown, 1994, "Factors Affecting the Z-Width of a Haptic Display", *Proceedings IEEE International Conference on Robotics and Automation*, San Diego, CA, pp. 3205-3210.

Colgate J.E., G. Schenkel, 1994, "Passivity of a Class of Sampled-Data Systems: Application to Haptic Interfaces", *Proceedings American Control Conference*, Baltimore, MD, pp. 3236-3240.

Colombi S., T. Raimondi, 1992, "Improvement of Brushless DC Motor Actuators", *Proceedings 23rd International Symposium on Industrial Robots*, Barcelona, Spain.

Colombi S., T. Raimondi, G. Costi, 1993, "Improvement of Transparency of Bilateral Master-Slave Force Reflecting Servomanipulators", *Proceedings 5th Topical Meeting on Robotics and Remote Handling*, Knoxville, TE.

Cotin S., H. Delingette, M. Bro-Nielsen, N. Ayache, J.M. Clément, V. Tassetti, J. Marescaux, 1996, "Geometric and Physical Representations for a Simulator of Hepatic Surgery", in S.J. Weghorst, H.B. Sieburg, K.S. Morgan (Eds.), *Medicine Meets Virtual Reality - Health Care in the Information Age*, IOS Press, Amsterdam, pp. 139-151.

Cover S.A., N.F. Ezquerra, J.F. O'Brien, R. Rowe, T. Gadacz, E. Palm, 1993, "Interactively Deformable Models for Surgery Simulation", *IEEE Computer Graphics and Applications*, Vol. 13, pp. 68-75.

Craig J.J., 1989, *Introduction to Robotics*, Addison-Wesley, Menlo Park, 2nd Edition.

Craver W.M., D. Tesar, 1990, "Force and Deflection Determination for a Parallel 3 DoF Robotic Shoulder Module", *Proceedings ASME Design Technical Conference*, Chicago, IL, pp. 473-479.

Cuschieri A., G. Buess, G. Perissat, 1992, *Operative Manual of Endoscopic Surgery*, Springer-Verlag, Berlin.

Cuttat J.-F., 1994, Personal communication, Centre Hospitalier Universitaire Vaudois, Lausanne, Switzerland, December.

Cuttat, J.-F., 1997, Personal communication, Centre Hospitalier Universitaire Vaudois, Lausanne, Switzerland, April.

Cybernet Systems, Inc., 1995, Company brochure, Ann Arbor, MI.

Da Lan D., 1997, "Simulateur de chirurgie laparoscopique", Diploma project, Département de Microtechnique, Ecole Polytechnique Fédérale de Lausanne EPFL, Lausanne, Switzerland.

Eberhardt S.P., L.E. Bernstein, D. Barac-Cikoja, D.C. Coulter, J. Jordan, 1994, "Including Dynamic Haptic Perception by the Hand: System Description and Some Results", in C.J. Radcliffe (Ed.), *Dynamic Systems and Control*, ASME, DSC-55, Vol. 1, pp. 345-351.

Ellis R.E., O.M. Ismaeil, M.G. Lipsett, 1993, "Design and Evaluation of a High-Performance Prototype Planar Haptic Interface", in H. Kazerooni, J.E. Colgate, B.D. Adelstein (Eds.), *Advances in Robotics, Mechatronics, and Haptic Interfaces*, ASME, DSC-49, pp. 55-64.

Eppinger S.D., W.P. Seering, 1987, "Understanding Bandwidth Limitations in Robot Force Control", *Proceedings IEEE International Conference on Robotics and Automation*, Raleigh, NC, Vol. 1, pp. 904-909.

Fischer P., R. Daniel, K.V. Siva, 1990, "Specification and Design of Input Devices for Teleoperation", *Proceedings IEEE International Conference on Robotics and Automation*, Cincinnatti, OH, pp. 540-545.

Gayed M.B., A. Guerrouad, C. Diaz, B. Lepers, P. Vidal, 1987, "An Advanced Control Micromanipulator for Surgical Applications", *Systems Science*, Vol. 13, No. 1-2, pp. 123-134.

Hon D., 1996, "Medical Reality and Virtual Reality", in S.J. Weghorst, H.B. Sieburg, K.S. Morgan (Eds.), *Medicine Meets Virtual Reality - Health Care in the Information Age*, IOS Press, Amsterdam, pp. 327-341.

Howe R.D., D.A. Kontarinis, 1993, "High-Frequency Force Information in Teleoperated Manipulation", in T. Yoshikawa, F. Miyazaki (Eds.), *International Symposium on Experimental Robotics III*, Kyoto, Japan, Springer-Verlag, pp. 343-352.

Hunt K.H., 1978, *Kinematic Geometry of Mechanisms*, Oxford University Press, New York.

Hunt K.H., 1983, "Structural Kinematics of In-Parallel-Actuated Robot Arms", *Journal of Mechanisms, Transmissions, and Automation in Design*, ASME, Vol. 105, pp. 705-712.

Hunter I.W., S. Lafontaine, P.M.F. Nielsen, P.J. Hunter, J.M. Hollerbach, 1989, "A Tele-Microrobot for Manipulation and Dynamic Mechanical Testing of Single Living Cells", *Proceedings IEEE Conference on Micro Electro Mechanical Systems*, Salt Lake City, UT, pp. 102-106.

Hunter I.W., T.D. Doukoglou, S.R. Lafontaine, P.G. Charette, L.A. Jones, M.A. Sagar, G.D. Mallinson, P.J. Hunter, 1993, "A Teleoperated Microsurgical Robot and Associated Virtual Environment for Eye Surgery", *Presence*, Vol. 2, No. 4, pp. 265-280.

Immersion, Inc., 1995, "Laparoscopic Impulse Engine", Company brochure, Santa Clara, CA.

Inmos, Ltd., 1989, "The Transputer Databook", Bristol, UK.

Ishii M., M. Sato, 1993, "A 3D Interface Device with Force Feedback: A Virtual Workspace for Pick-and-Place Tasks", *Proceedings IEEE Virtual Reality International Symposium*, Seattle, WA, pp. 331-335.

Ishii M., M. Sato, 1994a, "Force Sensations in Pick-and-Place Tasks", in C.J. Radcliffe (Ed.), *Dynamic Systems and Control*, ASME, DSC-55, Vol. 1, pp. 339-344.

Ishii M., M. Sato, 1994b, "A 3D Spatial Interface Device Using Tensed Strings", *Presence*, Vol. 3, No. 1, pp. 81-86.

Iwata H., 1990, "Artificial Reality with Force-Feedback: Development of Desktop Virtual Space with Compact Master Manipulator", *Computer Graphics*, Vol. 24, No. 4, pp. 165-170.

Iwata H., 1993, "Pen-Based Haptic Virtual Environment", *Proceedings IEEE Virtual Reality Annual International Symposium*, Seattle, WA, pp. 287-292.

Jandura L., M.A. Srinivasan, 1994, "Experiments on Human Performance in Torque Discrimination and Control", in C.J. Radcliffe (Ed.), *Dynamic Systems and Control*, ASME, DSC-55, Vol. 1, pp. 369-375.

Janocha H., 1992, *Aktoren - Grundlagen und Anwendungen*, Springer-Verlag, Berlin.

Kawamura S., M. Ida, T. Wada, J.L. Wu, 1995, "Development of a Virtual Sports Machine using a Wire Drive System - A Trial of Virtual Tennis", *Proceedings IEEE/RSJ International Conference on Intelligent Robotics and Systems*, Pittsburgh, PA, pp. 111-116.

Khatib O., B. Roth, 1991, "New Robot Mechanisms for New Robot Capabilities", *Proceedings IEEE/RSJ International Workshop on Intelligent Robots and Systems*, Osaka, Japan, pp. 44-49.

Klaiber C., A. Metzger, J. Petelin, 1993, *Manual of Laparoscopic Surgery*, Hogrefe & Huber Publishers.

Kokjer K., 1987, "The Information Capacity of the Human Fingertip", *IEEE Transactions on Systems, Man, and Cybernetics*, Vol. 17, No. 1, pp. 100-102.

Millman P.A., M. Stanley, P. Grafing, J.E. Colgate, 1992, "A System for the Implementation and Kinesthetic Display of Virtual Environments", *Telemanipulator Technology*, SPIE, Vol. 1833, pp. 49-56.

Millman P.A., M. Stanley, J.E. Colgate, 1993, "Design of a High Performance Haptic Interface to Virtual Environments", *Proceedings IEEE Virtual Reality Annual International Symposium*, Seattle, WA, pp. 216-222.

Minimotor, Inc., 1996, Company brochure, Croglio, Switzerland.

Minsky M., M. Ouh-young, O. Steele, F.P. Brooks, M. Behensky, 1990, "Feeling and Seeing: Issues in Force Display", *Computer Graphics*, Vol. 24, No. 2, pp. 235-243.

Morizono T., K. Kurahashi, S. Kawamura, 1997, "Realization of a Virtual Sports Training System with Parallel Wire Mechanism", *Proceedings IEEE International Conference on Robotics and Automation*, Albuquerque, NM, pp. 3025-3030.

Mosher R.S., 1985, U.S. Patent 4551058, "Low Cost Articulating/Articulating and Rotating Wrist Mechanism for Automatic Machine Tool and Automatic Machine Tool Employing the Same", filed July 20, 1983 and issued November 5, 1985.

Nevins J.L., D.E. Whitney, 1973, "The Force Vector Assembler Concept", *Proceedings 1st CSIM-IFToMM Symposium on Theory and Practice of Robots and Manipulators*, Italy, pp. 273-288.

Nguyen, 1995a, "A Toolkit Based on Performer", Internal report, Institut de Microtechnique, Ecole Polytechnique Fédérale de Lausanne EPFL, Lausanne, Switzerland.

Nguyen, 1995b, "Libptk - A Summary", Internal report, Institut de Microtechnique, Ecole Polytechnique Fédérale de Lausanne EPFL, Lausanne, Switzerland.

Nissho Electronics, Inc., 1995, "Haptic Master", Company brochure, Tokyo, Japan.

Ouerfelli M., V. Kumar, 1994, "Optimization of a Spherical Five-Bar Parallel Drive Linkage", *Journal of Mechanical Design*, ASME, Vol. 116, pp. 166-173.

Ouh-Young M., M. Pique, J. Hughes, N. Srinivasan, F.P. Brooks, Jr., 1988, "Using a Manipulator for Force Display in Molecular Docking", *Proceedings IEEE Conference on Robotics and Automation*, Philadelphia, PA, Vol. 3, pp. 1824-1829.

Parsytec, Inc., 1988, "BBK-V2 Transputer-Bus-Bridgehead for Interfacing VME-Systems to Megaframe Transputer Modules", Technical documentation, version 2.4, Aachen, Germany.

Parsytec, Inc., 1989, "TPM-IO Transputer Motherboard for I/O Daughterboards", Technical documentation, version 1.2, Aachen, Germany.

Parsytec, Inc., 1991a, "MTM-2-11/12/13 Multi-Transputer Module", Technical documentation", version 1.4, Aachen, Germany.

Parsytec, Inc., 1991b, "DBI-1 Quad RS232 Serial Interface Daughterboard", Technical documentation", version 1.2, Aachen, Germany.

Paul R.P., 1981, *Robot Manipulators: Mathematics, Programming, and Control*, MIT Press, Cambridge, MA.

Peifer J., M. Sinclair, R. Haleblian, M. Luxenberg, K. Green, D. Hull, 1994, "Virtual Environment for Eye Surgery Simulation", *Proceedings Medicine Meets Virtual Reality 2*, San Diego, CA, pp. 166-169.

Peifer J.W., W.D. Curtis, M.J. Sinclair, 1996, "Applied Virtual Reality for Simulation of Endoscopic Retrograde Cholangio-Pancreatography (ERCP)", in S.J. Weghorst, H.B. Sieburg, K.S. Morgan (Eds.), *Medicine Meets Virtual Reality - Health Care in the Information Age*, IOS Press, Amsterdam, pp. 36-42.

Pentland Systems, Ltd., 1990, "MPV-907 Analog Input VMEbus Board", Technical documentation, Livingston, UK.

Salisbury J.K., 1980, "Active Stiffness Control of a Manipulator in Cartesian Coordinates", *Proceedings IEEE Decision and Control Conference*, Vol. 1, pp. 95-100.

Sato T., J. Ichikawa, M. Mitsuishi, Y. Hatamura, 1993, "Micro Teleoperation System Concentrating Visual and Force Information at Operator's Hand", *3rd International Symposium on Experimental Robotics*, Kyoto, Japan, pp. 353-365.

Sato T., J. Ichikawa, M. Mitsuishi, Y. Hatamura, 1994, "A New Micro-Teleoperation System Employing a Hand-Held Force-Feedback Pencil", *Proceedings IEEE International Conference on Robotics and Automation*, San Diego, CA, Vol. 2, pp. 1728-1733.

Schmult B., R. Jebens, 1993, "Application Areas for a Force-Feedback Joystick", in H. Kazerooni, J.E. Colgate, B.D. Adelstein (Eds.), *Advances in Robotics, Mechatronics, and Haptic Interfaces*, ASME, DSC-49, pp. 47-54.

SCT Servo Control Technology, Inc., 1996, "ISA 10/100 amplifier", Technical documentation, Luzern, Switzerland.

SensAble Devices, Inc., 1996, "PHANToM", Company brochure, Cambridge, MA.

Shahidi R., J. Feller, C. Beaulieu, S. Napel, G. Fanton, G. Rubin, P. Tirman, 1997, "Virtual Arthroscopy: Techniques and Applications", *Proceedings Medicine Meets Virtual Reality 5*, San Diego, CA.

Sharpe J.E.E., 1988, "Technical and Human Operational Requirements for Skill Transfer in Teleoperations", *Proceedings International Symposium on Teleoperation and Control*, Bristol, UK, pp. 175-187.

Sheridan T.B., 1992a, "Defining our Terms", *Presence*, Vol. 1, No. 2, pp. 272-274.

Sheridan T.B., 1992b, *Telerobotics, Automation, and Human Supervisory Control*, MIT Press, Cambridge, MA.

Shimoga K.B., 1992, "Finger Force and Touch Feedback Issues in Dexterous Telemanipulation", *Proceedings NASA-CIRSSE International Conference on Intelligent Robotic Systems for Space Exploration*, Greenbelt, MD, pp. 159-178.

Shimoga K., 1993a, "A Survey of Perceptual Feedback Issues in Dexterous Telemanipulation: Part I. Finger Force Feedback", *Proceedings IEEE Virtual Reality Annual International Symposium*, Seattle, WA, pp. 263-270.

Shimoga K., 1993b, "A Survey of Perceptual Feedback Issues in Dexterous Telemanipulation: Part II. Finger Touch Feedback", *Proceedings IEEE Virtual Reality Annual International Symposium*, Seattle, WA, pp. 271-279.

Silicon Graphics, Inc., 1994a, "IRIS Performer Programming Guide", Mountain View, CA.

Silicon Graphics, Inc., 1994b, "IRIS Perfomer Reference Pages", Mountain View, CA.

Singh S.K., M. Bostrom, D.O. Popa, C.W. Wiley, 1994, "Design of An Interactive Lumbar Puncture Simulator with Tactile Feedback", *Proceedings IEEE International Conference on Robotics and Automation*, San Diego, CA, Vol. 2, pp. 1734-1739.

Spinnler G., 1997, *Conception des machines - Principes et applications*, Vol. 1, Presses Polytechniques et Universitaires Romandes, Switzerland.

Srinivasan M.A., J. Chen, 1993, "Human Performance in Controlling Normal Forces of Contact With Rigid Objects", in H. Kazerooni, J.E. Colgate, B.D. Adelstein (Eds.), *Advances in Robotics, Mechatronics, and Haptic Interfaces*, ASME, DSC-49, pp. 119-125.

Steinmetz J., 1994, "Artificial Hands: Assembly Strategies and Nonholonomic Motion Planning", Ph.D. thesis, Département de Microtechnique, Ecole Polytechnique Fédérale de Lausanne EPFL, Lausanne, Switzerland.

VR News, 1995, "Force-Feedback Technology", Vol. 4, No. 6, pp. 23-29.

Wapler, M., 1995, "Medical Manipulators - Breakthrough with Virtual Reality", *Virtual Reality World '95*, Stuttgart, Germany, pp. 145-151.

Webster M., 1996, *Merriam Webster's Tenth Collegiate Dictionary*, Merriam-Webster, Inc., Springfield, MA.

Whitney D.E., 1977, "Force Feedback Control of Manipulator Fine Motions", *Journal of Dynamic Systems, Measurement and Control*, ASME, pp. 91-97.

Whitney D.E., 1985, "Historical Perspective and State of the Art in Robot Force Control", *Proceedings IEEE International Conference on Robotics and Automation*, St. Louis, MO, pp. 262-268.

Wolf GmbH, 1994, "Thoracoscopie opératoire", Company brochure, Knittlingen, Germany.

Wu C.H., R.P. Paul, 1980, "Manipulator Compliance Based on Joint Torque Control", *Proceedings IEEE Conference on Decision and Control*, Vol. 1, pp. 88-94.

Yagel R., D. Stredney, G.J. Wiet, P. Schmalbrock, L. Rosenberg, D.J. Sessanna, Y. Kurzion, S. King, 1996, "Multisensory Platform for Surgical Simulation", *Proceedings IEEE Virtual Reality Annual International Symposium*, pp. 72-78.

Yang A.T., S. Zhishang, 1983, "Dynamic Force and Torque Analysis of Spherical Four Link Mechanisms", *Journal of Mechanims, Transmissions, and Automation in Design*, ASME, Vol. 105, pp. 492-497.

Yokoi H., J. Yamashita, Y. Fukui, M. Shimojo, 1994, "Development of the Virtual Shape Manipulating System", *Proceedings Fourth International Conference on Artificial Reality and Tele-Existence*, Tokyo, Japan, pp. 43-48.

Yokokohji Y., R.L. Hollis, T. Kanade, 1996, "What You Can See is What You Can Feel - Development of a Visual/Haptic Interface to Virtual Environment", *Proceedings IEEE Virtual Reality Annual International Symposium*, pp. 46-53.

Yoshikawa T., A. Nagura, 1997, "A Touch and Force Display System for Haptic Interface", *Proceedings IEEE International Conference on Robotics and Automation*, Albuquerque, NM, pp. 3018-3024.

Ziegler R., W. Mueller, G. Fischer, M. Goebel, 1995, "A Virtual Reality Medical Training System", *Proceedings International Conference on Computer Vision, Virtual Reality, and Robotics in Medicine*, Nice, France, pp. 282-286.

Zucker K.A. (Ed.), 1993, *Surgical Laparoscopy Update*, Quality Medical Publishing, St. Louis, MO.

Publications / Presentations

R. Baumann, D. Glauser, D. Tappy, C. Baur, R. Clavel, "Force Feedback for Virtual Reality Based Minimally Invasive Surgery Simulator", *Proceedings Medicine Meets Virtual Reality 4*, pp. 564-579, San Diego, CA, January, 1996.

D. Tappy, C. Baur, R. Baumann, R. Clavel, "Minimally Invasive Surgery Program", Schweizerischer Nationalfonds, *Bulletin der Abteilung Mathematik, Natur- und Ingenieurwissenschaften*, Info 2, No. 6, pp. 19-24, January, 1996.

D. Glauser, C. Baur, J.F. Cuttat, R. Baumann, F. Mattei, D. Guzzoni, W. Maeder, R. Clavel, "Laparoscopic Training System with Virtual Reality and Force Feedback", *Proceedings Minimally Invasive Therapy and Allied Technologies*, MITAT, Vol. 5, Cernobbio, Italy, September, 1996.

R. Baumann, C. Baur, D. Glauser, R. Clavel, "The EPFL Laparoscopic Surgery Simulator", *Proceedings Journées de Microtechnique 1996*, Ecole Polytechnique Fédérale de Lausanne EPFL, Switzerland, Bulletin ASMT, No. 20, pp. 60-68, October, 1996.

R. Baumann, "Haptic Interface for Laparoscopic Surgery Simulator", oral presentation, Mechatronik Seminar, Eidgenössische Technische Hochschule ETH, Zürich, December, 1996.

R. Baumann, W. Maeder, D. Glauser, R. Clavel, "The *PantoScope*: A Spherical Remote-Center-of-Motion Parallel Manipulator for Force Reflection", *Proceedings IEEE International Conference on Robotics and Automation*, Albuquerque, NM, April, 1997.

R. Baumann, "Impedance Control of a Force Reflecting Man-Machine Interface", submitted to *SGA-Bulletin*, Swiss Society for Automatic Control, October, 1997.

Télévision Suisse Romande TSR, "Téléscope", February 14, 1996. Same program later on TV5 France, March 31, 1997.

Télévision Suisse Romande TSR, "Téléjournal", July 25, 1997.